NASA Contractor Report 3591

Hybrid State Vector Methods for Structural Dynamic and Aeroelastic Boundary Value Problems

Larry Lee Lehman

GRANT NGL-05-020-243
AUGUST 1982

NASA Contractor Report 3591

Hybrid State Vector Methods for Structural Dynamic and Aeroelastic Boundary Value Problems

Larry Lee Lehman
Stanford University
Stanford, California

Prepared for
Langley Research Center
under Grant NGL-05-020-243

NASA
National Aeronautics
and Space Administration

**Scientific and Technical
Information Branch**

1982

Contents

Tables

Figures

Nomenclature

a	nondimensional location, in semichords, of structural reference axis with respect to aerodynamic midchord, positive aft of midchord (nondimensionalized by b_R)
a_c	nondimensional location, in semichords, of aerodynamic center with respect to aerodynamic midchord, positive aft of midchord (nondimensionalized by b_R)
a_d	aerodynamic downwash point, (D.6)
a_0	lift curve slope
a_n	leading coefficient of orthonormal polynomial (coefficient of x^n)
$\mathbf{a}, \tilde{\mathbf{a}}$	local, global loads vector (**Jp**)
$\mathbf{a}_r, \tilde{\mathbf{a}}_r$	local, global vector containing nonhomogeneous load terms
$\mathbf{a}_r^+$	vector of nonhomogeneous concentrated load terms
A_{ij}, B_{ij}, D_{ij}	composite stiffness terms, $i, j = 1, 2, 3$, (C.15)
$\overline{A}^*_{ij}, \overline{B}^*_{ij}, \overline{D}^*_{ij}$	nondimensional composite plate compliance terms ($i, j = 1, 2, 3$), (2.32)
$\mathbf{A}, \tilde{\mathbf{A}}$	local, global matrix of displacement dependent load terms
$\tilde{\mathbf{A}}^+$	matrix of displacement dependent concentrated load terms, (E.6)
$\mathbf{A}^*, \mathbf{B}^*, \mathbf{D}^*$	dimensional composite plate compliance matrices
$b, \overline{b}$	dimensional, nondimensional aerodynamic semichord, $\overline{b} = b/b_R$
$\mathbf{b}_0, \mathbf{b}_n$	boundary condition vectors defined in (4.7–4.8)
$B_{j,k}, B^*_{j,k}$	matrix elements defined in (A.25) and (A.49), respectively, for interval j, collocation point k
$\mathbf{B}_0, \mathbf{B}_n$	homogeneous boundary condition matrices, (4.5–4.6)
$\tilde{\mathbf{B}}$	block diagonal global boundary condition matrix (for homogeneous boundary conditions)
$\tilde{\mathbf{B}}_{nh}$	matrix of nonhomogeneous boundary conditions

c	chord length of structural box normal to structural reference axis
$C(\bar{s})$	Theodorsen function
C_{ℓ_e}	elastic lift distribution
C_{ℓ_r}	rigid lift distribution
$\mathbf{C}, \mathbf{C}_{FD}$	damping matrices
d_j	end points of interpolation interval ($j = 1, 2$), (A.13)
$\mathbf{D}$	constant matrix defined in (2.6)
$\boldsymbol{D}$	differentiating matrix, (D.3–D.4)
e_m^n	product defined in (A.11)
EA	axial stiffness
EI	bending stiffness
$\overline{EI}$	nondimensional isotropic bending compliance, (5.48)
E_1, E_2	Young's modulus
$\mathbf{f}$	nonhomogeneous loads vector defined in (4.13)
F_t	nondimensional tension parameter, (5.93)
F_u	nondimensional axial force defined in (5.4)
$\mathcal{F}$	defined in (3.5)
$\overline{\mathcal{F}}$	defined in (3.9)
$\mathbf{F}$	matrix defined in (4.12) (contains boundary condition modified integrating matrices)
$\mathbf{F}^+$	matrix defined in (E.11) (contains boundary condition modified summing matrices)
g	function defined in (3.13)
GJ	torsional stiffness
G_{12}	shear modulus
$\mathbf{H}$	structural matrix defined in (4.11)
$\mathbf{H}^*$	$\mathbf{H}^{-1}$, see (4.18)
$\mathbf{I}$	identity matrix

$\mathbf{I}^*$	matrix defined in (5.35)
j	$\sqrt{-1}$
$\mathbf{J}$	antisymmetric matrix with unit elements $(\mathbf{D} - \mathbf{D}^T)$
$\overline{k}_s$	nondimensional restraint spring stiffness, (5.27)
$\tilde{\mathbf{k}}$	constant vector of integration
$\mathbf{K}$	symmetric matrix containing structural related terms
ℓ	specified length along x-coordinate
L_α, L_γ	nondimensional steady aerodynamic lift terms, (6.2)
$\hat{L}_i$	nondimensional Laplace transforms of unsteady aerodynamic lifts, $i = w, \alpha, \gamma, \tau$
$\mathbf{L}, \tilde{\mathbf{L}}$	local, global integrating matrix
$\mathbf{L}_i^*$	integrating matrix modified by boundary conditions (type i)
$m, \overline{m}$	dimensional, nondimensional running mass distribution, $\overline{m} = m/m_R$
$\overline{m}_i$	nondimensional mass terms defined in (7.4), $i = ww, w\alpha, \alpha\alpha$
$\overline{m}_n^+$	nondimensional concentrated tip mass, $m_n/m_R\ell$
$\mathbf{m}$	dimensional vector of moment resultants (moment/unit length)
$M_i, \overline{M}_i$	dimensional, nondimensional components of moment resultant vector $(i = x, y, xy)$, (2.31)
M_α, L_γ	nondimensional steady aerodynamic moment terms, (6.2)
$\hat{M}_i$	nondimensional Laplace transform of unsteady aerodynamic moments, $i = w, \alpha, \gamma, \tau$
$\mathbf{M}, \mathbf{M}_{FD}$	mass distribution matrices
$\mathbf{n}$	dimensional vector of stress resultants (force/unit length)
N	number of collocation intervals
$N_i, \overline{N}_i$	dimensional, nondimensional components of stress resultant vector $(i = x, y, xy)$, (2.31)
N	interpolation shape functions
NL	number of layers
NS	number of states in local state vector

$p, \overline{p}$	dimensional, nondimensional lateral loading per unit length, (5.99)
$p_i, \overline{p}_i$	dimensional, nondimensional running external loads ($i = u, \gamma, w, \alpha$), (2.31)
p_i^+	magnitude of concentrated load, (E.1)
$p_n^{(\alpha,\beta)}, P_n^{(\alpha,\beta)}$	normalized, unnormalized Jacobi polynomial
$\mathbf{p}$	vector of running external loads
q	dynamic pressure
$\mathbf{Q}, \mathbf{Q}_{FD}$	unsteady aerodynamic matrices
$\overline{r}_\alpha$	dimensionless radius of gyration of section, $\overline{r}_\alpha = r_\alpha / b_R$
R	ratio of compressible to incompressible Theodorsen function
s, s^*	dimensional, nondimensional Laplace variable, $s^* = s\ell^2\sqrt{m_R/(EI)_R}$
$\overline{s}$	nondimensional Laplace variable defined in (D.5)
$\overline{S}^*$	nondimensional transverse shear compliance, (2.33)
$\mathbf{S}, \tilde{\mathbf{S}}$	local, global lower triangular summing matrix, (3.8)
t	time variable
$\mathbf{T}$	structural matrix defined in (4.25) (performs the function of a structural flexibility matrix by operating on force distribution terms)
$\mathbf{T}^+$	structural matrix defined in (E.15)
u, v, w	displacement variables along x, y, z, respectively
$\overline{u}, \overline{v}, \overline{w}$	displacement variables nondimensionalized by ℓ
u_0, v_0, w_0	plate geometric midplane displacements
$\mathcal{U}$	functional appearing in (2.1)
$\mathbf{U}$	constraint and coordinate transformation matrix
V	freestream velocity
V^*	velocity normal to structural reference axis, $V \cos\Lambda$
$V_x, \overline{V}_x$	dimensional, nondimensional transverse shear resultant, (2.31)
$\mathcal{W}_n$	weighting matrix

x, y, z	spatial coordinates
$\overline{x}, \overline{y}, \overline{z}$	spatial coordinates nondimensionalized by ℓ
$\mathbf{y}, \tilde{\mathbf{y}}$	local, global state vector
$\mathbf{y}_D, \tilde{\mathbf{y}}_D$	local, global generalized displacement components of state vector
$\mathbf{y}_F, \tilde{\mathbf{y}}_F$	local, global generalized force components of state vector
$\hat{\mathbf{y}}$	Laplace transform of state vector (with respect to time)
$\mathbf{Z}, \tilde{\mathbf{Z}}$	local, global coefficient matrix containing structural terms (**JK**)

Greek Symbols

α	angle of twist (elastic angle of attack for aeroelastic problems)
α_e	effective angle of attack, (6.6)
α_{er}	effective angle of attack for a rigid wing
α_s	nondimensional hub radius, R_0/ℓ
β_s	dimensional shear compliance (often written as μ_s/EA, where μ_s is a cross section shape factor)
β_t	taper parameter in (5.23); taper ratio equals $(1-\beta_t)$
γ	rotation of the normal to the elastic axis
γ_{xy}	shear strain
$\overline{\gamma}$	axial stiffness ratio defined in (5.24)
Γ	gamma function
$\boldsymbol{\Gamma}_i$	selection matrix for ith point, (G.9)
δ	first variation operator
δ_n	square of normalizing factor for P_n
$\delta(x-x_i)$	unit delta function, (E.1)
$\boldsymbol{\epsilon}^0$	vector of plate midplane strains, (C.9)
θ	composite fiber orientation angle (with respect to structural reference axis)
$\overline{\theta}$	mass ratio defined in (5.24)

$\boldsymbol{\kappa}$	vector of plate bending curvatures, (C.9)
λ	nondimensional constant parameter (dynamic pressure parameter for aeroelastic problems and eigenvalue for vibration problems)
λ_{D_0}	reference divergence dynamic pressure parameter
λ_s	nondimensional spin parameter, (5.95)
Λ	wing sweep angle, positive aft (aerodynamic and structural reference axis sweep angles are assumed equal for a uniform wing)
μ	nondimensional mass ratio parameter, (D.5)
ν_{12}, ν_{21}	Poisson's ratio
$\boldsymbol{\Xi}$	selection matrix, (G.2)
$\prod$	product
ρ	air density
σ^*	real part of s^*, $s^* = \sigma^* + j\omega^*$
σ_i	inplane stresses, $i = 1, 2, x, y$
τ	nondimensional axial compliance, (5.2)
τ_{12}, τ_{xy}	shear stresses
$\boldsymbol{\Upsilon}$	matrix defined in (G.6–G.7)
$\boldsymbol{\Phi}$	transition matrix, Appendix G
$\overline{\chi}_\alpha$	nondimensional location in semichords of section mass center with respect to structural reference axis, positive aft, $\overline{\chi}_\alpha = \chi_\alpha / b_R$
ω	natural frequency of vibration
ω^*	imaginary part of s^*, $s^* = \sigma^* + j\omega^*$
ω_s	rotational speed of hub, (5.95)
Ω	nondimensional buckling speed, $\alpha_s^2 \sqrt{\lambda_s}$
ϑ	nonnegative integrable weighting function for Gaussian integration rules, (3.12)

Miscellaneous Symbols

$\vec{1}$	vector of unit elements

$(\,)'$	$\frac{\partial}{\partial x}$
$(\vec{\ })$	vector
$\grave{}(\,)$	diagonal matrix
$(\,)^T$	transpose
$(\,)^{-1}$	inverse
$(\,)_F$	force subset
$(\,)_D$	displacement subset
$(\,)_R$	reference value

Summary

A computational technique is developed that is suitable for performing preliminary design aeroelastic and structural dynamic analyses of large aspect ratio lifting surfaces. The method proves to be quite general and can be adapted to solving various two-point boundary value problems.

The solution method, which is applicable to both fixed and rotating wing configurations, is based upon a formulation of the structural equilibrium equations in terms of a hybrid state vector containing generalized force and displacement variables. A mixed variational formulation is presented that conveniently yields a useful form for these state vector differential equations. Solutions to these equations are obtained by employing an integrating matrix method. The application of an integrating matrix provides a discretization of the differential equations that only requires solutions of standard linear matrix systems. It is demonstrated that matrix partitioning can be used to reduce the order of the required solutions. Results are presented for several example problems in structural dynamics and aeroelasticity to verify the technique and to demonstrate its use. These problems examine various types of loading and boundary conditions and include aeroelastic analyses of lifting surfaces constructed from anisotropic composite materials.

Integrating matrices, which provide a powerful tool for solving differential equations, are discussed in detail, and methods are given for their calculation. A derivation and calculation procedure is presented for a new type of maximum accuracy integrating matrix based upon orthogonal polynomials.

Chapter 1

Introduction

AN EXPANDED UTILIZATION of laminated composite materials in aircraft structural design has led to a search for new ways to employ these relatively high specific strength and stiffness materials. One result of this search has been the development of the concept of aeroelastic tailoring of a lifting surface, in which the directional characteristics of the composite material are used to synthesize a structure with enhanced aeroelastic performance. But along with the possibility for innovative design with structural composites comes greater complexity in the preliminary design task. This increased complexity arises in part from the anisotropic nature of the composites materials and in part from the increased design freedom allowed by these materials. Because of the additional complexity of the design task, new analysis tools are needed to aid the preliminary designer in efficiently evaluating the sometimes large number of design concepts available to him. Therefore, the primary objective of this research has been to develop a simple and versatile analysis method compatible with the needs of preliminary aeroelastic and structural dynamic design.

The motivation for this research effort stemmed from a desire to investigate the performance enhancements that can be achieved by aeroelastically tailoring large aspect ratio composite lifting surfaces. Essentially, aeroelastic tailoring involves

designing a structure to take advantage of the elastic deformation during loading. For static aeroelastic problems, this means controlling the relative amounts of bending and torsional deflection of a wing or lifting surface. By maintaining a desirable wing deformation shape, or by passively controlling the distribution of aerodynamic loading, it is often possible to enhance aerodynamic performance and to extend the operating envelopes of a lifting surface. For dynamic aeroelastic problems, the coupling between bending and torsion of composite structures provides a way of maximizing the dynamic instability (flutter) speed of a lifting surface. Since the primary objective of this research is to develop a convenient method for analyzing such aeroelastic and dynamic behavior, the above mentioned problems provide some excellent, nontrivial examples for verification of the devised solution method. At the same time, these example solutions hopefully provide a firm foundation for other in-depth studies of the aeroelastic behavior of composite structures, including the investigation of optimized aeroelastic designs.

Historically, most aeroelastic analyses of composite structures have been carried out by very complex computer codes involving finite element structural methods coupled with lifting surface aerodynamics. Unfortunately, these complicated numerical approaches can tend to obscure a basic understanding of the important parameters appearing in the analysis and, owing to cost considerations, often preclude an extensive study involving numerous design variations. Recent developments, such as those of Gimmestad [1], offer a suitable alternative for preliminary design investigations.

A fundamental approach to performing the aeroelastic and dynamic analyses of a structure described by one independent spatial coordinate involves formulating the ordinary differential equations representing the aeroelastic or dynamic response and obtaining analytical solutions to the resulting boundary value problems. Although the coupled bending and torsion equations can be formulated, it is often difficult,

if not impossible, to obtain analytical solutions for the general case in which the coefficients of the equations are variable. Some useful solutions have been obtained, however, for cases in which the coefficients in the linear aeroelastic equations can be written as constants. For instance, solutions to the differential equations for divergence and load distribution have been obtained for isotropic metallic wings by Diederich and Budiansky [2] and Diederich and Foss [3], and more recently, divergence and load distribution solutions for composite swept forward wings have been obtained by Weisshaar [4,5]. But with the application of the hybrid state vector approach discussed herein, approximate solutions to the differential equations can be easily obtained for much more difficult cases involving variable coefficients. The hybrid state vector approach has been utilized by Lehman [6] to obtain a variety of aeroelastic solutions, including flutter of composite wings. This type of solution does not require an explicit calculation of structural influence coefficients and can utilize various forms of aerodynamic influence matrices.

A major requirement for a solution method to be used in preliminary design is that the method be reasonably flexible in allowing solution of different types of problems, and yet easily specialized so that computations can be carried out efficiently. Furthermore, it is desirable to have a numerical solution that is easily programmable and that makes use of standard numerical methods, thus requiring minimal investment in software. It has been found that these requirements are well satisfied by a mixed state vector formulation of the differential equations combined with an integrating matrix solution procedure—hence, one of the reasons for referring to the method as a hybrid approach.

Other investigators (see the introduction to Chapter 3) have provided initial formulations for the concept of the integrating matrix solution in structural mechanics and have applied this concept to solving a variety of problems. Compared to other numerical approaches, such as finite element and finite difference, relatively little

has been done to generalize the integrating matrix method. In order to bring some generality to the integrating matrix method, it has been found useful to incorporate some of the familiar concepts employed in finite element analysis.

Even though the solution method presented here is applied only to two-point boundary value problems arising in aeroelasticity and structural dynamics, the approach is, in fact, quite general and can be applied to initial value problems as well as to multipoint boundary value problems. The method can also be extended to handle systems described by more than one independent variable.

The compact matrix notation used in the development of the hybrid state vector method is intended to aid in the task of programming the solutions, regardless of the programming language employed. Solutions for dynamic flutter instabilities in Chapter 7, which are iterative by nature, operate quite efficiently in languages like *FORTRAN* or *Pascal*. The hybrid state vector solution formulations, however, are especially suited to the matrix oriented programming language *APL*. In fact, the hybrid state vector method presented here, when coupled with *APL*, forms an extremely powerful interactive problem solving tool. It is further anticipated that the hybrid state vector solutions, since they are formulated in terms of simultaneous matrix operations, will be readily adaptable to parallel processing techniques.

In Chapter 2, a mixed variational formulation is presented for obtaining the linear state vector differential equations of structural equilibrium. This formulation is given for structures that can be described by one independent spatial variable. By casting the aerodynamic and inertial loads acting on a structure in terms of the displacement state variables, the state vector equations can be expanded into the equations suitable for aeroelastic and structural dynamic analyses. A detailed form of the state vector equations is then presented to describe an anisotropic plate-beam that is constructed from laminated composite materials. These equations are reserved for later use in the example solutions of Chapters 6 and 7.

Chapter 3 gives a general derivation of integrating matrices and describes how they are applied to the integration of either continuous or discontinuous integrands. Several different types of integrating matrices are discussed, including maximum precision integrating matrices based upon orthogonal polynomial approximations. The concept of a differentiating matrix is also introduced.

Chapter 4 describes how integrating matrices are used to formulate solutions for the discretized versions of the state vector equations derived in Chapter 2. By using matrix partitioning techniques, it is then shown that reduced order matrix equations for the displacement variables can be obtained by eliminating the force variables.

In Chapter 5, sample solutions are presented for simple beam and rod problems. These examples illustrate the application of the hybrid state vector method to the solution of two-point boundary value problems. Continuous and discontinuous parameter problems are demonstrated along with various types of boundary and loading conditions. Numerical results are compared with analytical results to evaluate the accuracy of the integrating matrix solutions.

Chapter 6 presents sample solutions for divergence and elastic lift distribution of composite wings. For the composite wings, solutions are given for the case of forward aerodynamic sweep. Brief comparisons are made with alternate solutions available for these problems.

Chapter 7 demonstrates solutions for flutter instabilities of both isotropic and composite wings. The isotropic wing flutter solutions are compared with known analytical solutions.

A brief summary and recommendations for additional research are given in Chapter 8.

Chapter 2

Hybrid State Vector Equations

A GENERAL FORMULATION of the structural equations will be presented which casts them into a state vector form involving a coupled system of first order differential equations. The state vector that appears in the following derivations will be termed a ***hybrid*** state vector in the sense that it is derived from a so-called *mixed* formulation involving both stress and displacement variables. Although this formulation is not entirely new to structural mechanics, it has not seen extensive use, nor has it been included among the everyday tools of most engineers working in structures and structural dynamics. However, some very noteworthy developments of improved numerical procedures based on mixed formulations combined with finite-difference solutions have been reported by Noor, Stephens, and Fulton [7]. Additional work presented by Noor and Stephens [8,9] has further demonstrated both the simplicity and high accuracy of such mixed formulation procedures. Results obtained by Stroud and Mayers [10] indicate that a numerical solution based upon direct application of a mixed variational principle also offers superior accuracy and convergence, especially for bending-moment solutions. More recently, investigations by Steele [11], Steele *et al.* [12], and Steele and Barry [13] have indicated that mixed state vector formulations of the differential equations in conjunction with asymptotic solutions can be advantageous for both analytical

investigation and numerical calculation. The present investigation will demonstrate that a simple and highly accurate numerical solution procedure is obtained by combining the mixed state vector formulation of the structural differential equations with an integrating matrix solution approach. It is worth noting that the transfer matrix method of structural solution also employs a mixed state vector similar to the one used in the following formulations.

The derivations to be presented employ a mixed variational formulation that can be consistently applied to a broad class of structural problems. This formulation, which will be discussed in Section 2.1, involves terms that are expressible as a product of generalized stresses and strains in addition to other terms that can be related to the complementary energy. For systems with linear stress-strain behavior, the complementary energy is, of course, the same as the strain energy. Therefore, in the context of linear systems, this formulation is equivalent to the more usual stationary potential energy approach. As will be demonstrated, the mixed variational formulation provides a convenient way of expressing the energy functional and allows a direct determination of the state vector equations in a desirable form.

There are also many classical structural problems for which differential equations already exist. In these instances, it may be convenient to recast these equations into a matrix form directly and dispense with the formality of rederiving them. As many readers are well aware, it is possible to take higher order differential equations and convert them to an equivalent system of first order equations. But this process becomes increasingly difficult as the complexity of the system increases. Regardless of how one chooses to obtain the differential equations describing a structural problem, there is a preferred way to write the state vector equivalent. The preferred state vector form will be shown to arise naturally from a mixed variational formulation. As will be discussed in more detail in later sections, the mixed (hybrid) state vector form of the equations, with fundamental unknowns consisting of both

generalized force and displacement parameters, will possesses a natural decomposition that proves quite useful for numerical solutions.

The equation derivations that follow will be presented in matrix notation. The primary advantage of matrix notation is that it allows a consistent treatment of problems with differing size and complexity. Furthermore, it is anticipated that the equation formulation will lead directly to a numerical algorithm that must necessarily deal with the matrix terminology of discretized systems. An additional reason for adhering to matrix notation is that several intermediate points exist at which further analytical formulation and simplification can be put aside in favor of numerical computation. If a matrix formulation is used throughout, it is easy to begin numerical calculations at these intermediate points.

2.1 Variational Formulation of State Vector Equations

A mixed variational formulation is presented here for the hybrid state vector equations that describe structural equilibrium. For the interested reader, some rather general examples of mixed variational statements can be found, for instance, in Nemat-Nasser [14]. Also, brief historical accounts of mixed variational methods in solid mechanics appear in both Nemat-Nasser [15] and Reissner [16]. In these accounts, the work of a number of investigators is cited, including the work of authors such as Hellinger, Reissner, and Washizu. In the literature in general, the mixed variational formulation involving independent variation of both stress and displacement variables is usually referred to as a Reissner (or sometimes Hellinger-Reissner) formulation, whereas the principle involving independent variation of stress, displacement, and strain is often referred to as a Hellinger-Reissner-Washizu formulation. In the work presented here, the development of the mixed state vector equations is based upon the formulation of Reissner [17] in which stress and displacement variables are independently varied to yield the appropriate equations

and boundary conditions. A similar development of mixed state vector equations from the Reissner formulation is given in Ref. [11].

Although the Reissner formulation is applicable to either linear or nonlinear problems, the following presentation will restrict consideration to the solution of linear aeroelastic and structural dynamic equations. From nonlinear equations, it is often feasible to obtain a set of linearized equations by perturbing about an appropriate nonlinear solution. This might be useful, for example, when considering problems with geometric nonlinearities. The linear perturbation equations obtained by such an approach fall within the scope of the following linear analyses. When considering future extensions of the present work to nonlinear analyses, it is anticipated that the Reissner principle should prove valuable for problems with nonlinear material behavior. Some important illustrations of the application of the Reissner principle to problems involving nonlinear material behavior are given by Nimmer and Mayers [18] and Anderson and Mayers [19].

For those problems that can be described by a single spatial variable, x, the mixed variational formulation can be written in general terms as

$$\delta \int_0^{\ell} U(x, t, \mathbf{y}(x,t), \mathbf{y}'(x,t))\, dx = 0 \tag{2.1}$$

where the prime on $\mathbf{y}$ indicates partial differentiation with respect to x only. The Euler-Lagrange equations resulting from variation on x are

$$-\frac{d}{dx}\frac{\partial U}{\partial \mathbf{y}'} + \frac{\partial U}{\partial \mathbf{y}} = 0. \tag{2.2}$$

Since the variation is being taken only with respect to the spatial variable, the time variable simply follows along as a parameter. For static problems, time disappears from the previous equations.

The next step in the formulation is to give an appropriate form of the functional appearing in Eqs. (2.1–2.2). When linearity is invoked, it is then possible to express

the functional in the following convenient form:

$$\mathcal{U} = \mathbf{y}'^T \mathbf{D}\mathbf{y} - \frac{1}{2}\mathbf{y}^T \mathbf{K}\mathbf{y} + \mathbf{p}^T \mathbf{y} \tag{2.3}$$

where $\mathbf{K}$ is a spatially variable symmetric matrix containing structural relations, $\mathbf{p}$ contains the external loads, and $\mathbf{D}$ is defined such that $(\mathbf{D} - \mathbf{D}^T)$ is a constant skew-symmetric matrix with unit elements.

The state vector, $\mathbf{y}$, is specified in the form

$$\mathbf{y} = \{\mathbf{y}_F \quad \mathbf{y}_D\}^T \tag{2.4}$$

where $\mathbf{y}_F$ are generalized forces and $\mathbf{y}_D$ are generalized displacements. This form for $\mathbf{y}$ is the same as would appear in a transfer matrix structural solution based upon a "mixed" finite element force-displacement relationship. The precise nature of the matrix terms appearing in the above representation of the functional will be clarified with specific examples.

Next, substituting Eq. (2.3) into Eq. (2.2) and performing the indicated differentiation yields the equilibrium equations

$$-\mathbf{J}\mathbf{y}' - \mathbf{K}\mathbf{y} + \mathbf{p} = 0 \tag{2.5}$$

in which

$$\mathbf{J} = \mathbf{D} - \mathbf{D}^T = \begin{bmatrix} \mathbf{0} & -\mathbf{I} \\ \mathbf{I} & \mathbf{0} \end{bmatrix}. \tag{2.6}$$

Noticing that

$$\mathbf{J}^{-1} = \mathbf{J}^T = -\mathbf{J} \quad \text{and hence} \quad \mathbf{J}^T\mathbf{J} = \mathbf{I}, \tag{2.7}$$

Eq. (2.5) can be rewritten in the standard state vector form

$$\mathbf{y}' = \mathbf{Z}\mathbf{y} - \mathbf{a} \tag{2.8}$$

where

$$\mathbf{Z} = \mathbf{JK} \quad \text{and} \quad \mathbf{a} = \mathbf{Jp}. \tag{2.9}$$

Eq. (2.8) will be the starting point for analyses to be presented in later chapters.

Rather than using the procedure demonstrated above, Eq. (2.5) and corresponding boundary conditions can also be obtained by substituting Eq. (2.3) into Eq. (2.1) and applying integration by parts. The consistent boundary conditions obtained with this approach are one of the key advantages of a variational development. Corresponding to the state vector equations in Eq. (2.8), the boundary conditions are obtained as

$$\mathbf{y}^T\mathbf{D}^T(\delta\mathbf{y})\Big|_0^\ell = 0. \tag{2.10}$$

Fortunately, in the state vector formulation, these boundary conditions always remain quite simple. This will prove to be especially advantageous when dealing with anisotropic structures, for which other formulations can yield coupled and considerably more complicated forms of the boundary conditions.

At this point, a simple example describing the lateral bending deflection of a beam will help to clarify the nature of the matrix terms appearing in the foregoing derivation. The example presented here follows an example given by Steele [11] for a Timoshenko beam. In the notation used in this study, the functional in Eq. (2.3) can be written for a Timoshenko beam in the form

$$U = M_x\left(\gamma' - \frac{1}{2}(EI)^{-1}M_x\right) + V_x\left(\gamma + w' - \frac{1}{2}\beta_s V_x\right) - pw \tag{2.11}$$

where the moment resultant is M_x; the transverse shear resultant is V_x; the rotation of the normal is γ; the normal displacement is w; the shear compliance is β_s; and the load per unit length is p. Prime, of course, denotes differentiation with respect

to x. In order to obtain a resemblance to the expression in Eq. (2.3), Eq. (2.11) can be rewritten as

$$U = M_x\gamma' + V_x w' - \frac{1}{2}\Big((EI)^{-1}M_x^2 + \beta_s V_x^2 - 2V_x\gamma\Big) - pw. \tag{2.12}$$

For linear systems, this functional can be constructed by subtracting the complementary energy from the product of stresses and strains, after which a slight rearrangement yields Eq. (2.12). Also note that the nature of U, as used in this presentation, implies that it has been obtained by integrating an energy density functional over the cross section of the beam.

If the state vector is now defined as

$$\mathbf{y} = \{M_x \quad V_x \quad \gamma \quad w\}^T \tag{2.13}$$

then $\mathbf{p}$, $\mathbf{D}$, and $\mathbf{K}$ in Eq. (2.3) take on the forms

$$\mathbf{p} = \{0 \quad 0 \quad 0 \quad -p\}^T \tag{2.14}$$

$$\mathbf{D} = \begin{bmatrix} 0 & 0 & 0 & 0 \\ 0 & 0 & 0 & 0 \\ 1 & 0 & 0 & 0 \\ 0 & 1 & 0 & 0 \end{bmatrix} \tag{2.15}$$

$$\mathbf{K} = \begin{bmatrix} (EI)^{-1} & 0 & 0 & 0 \\ 0 & \beta_s & -1 & 0 \\ 0 & -1 & 0 & 0 \\ 0 & 0 & 0 & 0 \end{bmatrix} \tag{2.16}$$

The procedure for arriving at this form of the matrix equations first involves specifying the state vector, $\mathbf{y}$, which is taken to be the same vector as would be

obtained in a *mixed*, or *hybrid* force-displacement formulation of the equilibrium equations. Such a formulation is discussed, for example, in Chapter 2 of McGuire and Gallagher [20]. This state vector form is also the same as that used in the *transfer matrix* format of structural analysis. It is assumed here, as shown in Eq. (2.4), that **y** will always be partitioned into two sets; one set contains generalized forces and the other contains generalized displacements. Once the state vector is specified in this way, then **p** is chosen so that one obtains the proper potential of the external loads.

After choosing the state vector, then **D** must be determined such that the derivative terms in the functional are given by the first group on the right hand side of Eq. (2.3). This requirement is met by specifying that **D** always be a square matrix having the same form as that given in Eq. (2.15); that is, it should have the same structure as Eq. (2.15) and should always contain only zero and unit terms. One can refer to Eq. (2.6) to see that **D** must be specified in this way to insure that **J** be an antisymmetric matrix with unit elements. If **J** is as shown in Eq. (2.6), then Eq. (2.5) and Eq. (2.8) are said to have a *symplectic* character. The symplectic nature of these equations means that an especially simple relationship will exist between the fundamental solution of the system in Eq. (2.8) and its adjoint (see Eq. (G.17) in Appendix G). For a description of this useful property of symplectic systems, refer to page 157 of Bryson and Ho [21].

Other remaining terms in the functional are now determined by specifying **K**, which is restricted to be a symmetric matrix. The elements of **K** contain spatially dependent constitutive terms and fixed structural kinematic relationships. It is usually easy to determine the elements of **K** by simple observation.

Having determined **y**, **p**, **D**, and **K** as just discussed, it is then clear that **a** and **Z** in Eq. (2.9) become

$$\mathbf{a} = \{0 \quad p \quad 0 \quad 0\}^T, \tag{2.17}$$

$$\mathbf{Z} = \begin{bmatrix} 0 & 1 & 0 & 0 \\ 0 & 0 & 0 & 0 \\ (EI)^{-1} & 0 & 0 & 0 \\ 0 & \beta_s & -1 & 0 \end{bmatrix}. \tag{2.18}$$

It should be noted that the right hand side of Eq. (2.18) displays a particular form that will show up again, even for much more complicated problems than the one discussed above. As mentioned in the introduction to this chapter, for many simple problems it is not necessary to follow through the complete equation derivation as just presented. In fact, once one becomes familiar with the matrix formulation given here, it is usually easy to write down Eq. (2.18) directly, at least for relatively simple systems. However, for considerably more complicated situations, the variational approach provides a consistent method for formulating equilibrium equations and boundary conditions. In addition, the mixed variational formulation also demonstrates a "natural" form of the state vector equations. Later, Section 4.2 will show that this natural form, when coupled with an integrating matrix solution procedure, provides significant savings in the numerical solution by allowing convenient analytical simplification. One should also keep in mind that with knowledge of the natural form of the equations it is possible to recast equations derived by other methods. To give one example, the nonlinear equations of an initially bent and twisted rod derived in Chapter 18 of Love [22] and examined by Ojalvo and Newman [23] can be linearized and recast into the desired form. In fact, a similar approach has been followed by Nitzsche [24] to obtain hybrid state vector equations for the aeroelastic analysis of vertical axis wind turbines.

2.2 Aeroelastic and Structural Dynamic Equations

The general equations presented in the previous section can be specialized to both aeroelastic and structural dynamic problems by being more specific about the type of loading. For both aeroelastic and dynamic problems the loading can be related in some way to the displacements of the structure (i.e., the displacement states of the structural state vector). In static aeroelastic problems the airloads are directly determined by the deformed shape of the structure, whereas in dynamic problems, the inertial, aerodynamic, and structural damping loads are related to time rates of change of the structural deformation. The discussion in this section will focus on the way in which these loads appear in the structural equilibrium equations, and the form of the equations to be used in later analyses will be given.

First, static aeroelastic problems will be analyzed by the usual procedure of breaking the total external loads acting on the system into a summation of those loads that act on a rigid structure plus perturbation loads due to elastic deformation. Therefore, the loads vector $\mathbf{a}$, which first appeared in Eq. (2.8), can be rewritten as

$$\mathbf{a} = q\mathbf{A}\mathbf{y} + \mathbf{a}_r \tag{2.19}$$

where $\mathbf{a}_r$ is a vector of the nonhomogeneous loads acting on a rigid structure, q is the dynamic pressure, and $\mathbf{A}$ is developed from an aerodynamic influence relationship. In fact, for the discrete version of these equations, $\mathbf{A}$ contains terms from an inverse aerodynamic influence matrix. Additionally, if $\mathbf{A}$ is partitioned corresponding to the force and displacement subsets of the state vector, only one of its submatrices contains nonzero elements, namely, that submatrix providing forces due to displacement. Although one can make use of various aerodynamic theories to calculate $\mathbf{A}$, the analyses of Chapters 5–7 will primarily use aerodynamic strip theory.

The static aeroelastic equations are now obtained by substituting Eq. (2.19) into Eq. (2.8). The result is

$$\mathbf{y}' = \mathbf{Z}\mathbf{y} - q\mathbf{A}\mathbf{y} - \mathbf{a}_r , \tag{2.20}$$

with $\mathbf{y} = \mathbf{y}(x)$. When the dynamic pressure is specified, then Eq. (2.20) is simply a system of equations for $\mathbf{y}$. On the other hand, if the nonhomogeneous term $\mathbf{a}_r$ is set to zero and the dynamic pressure is left unspecified, then Eq. (2.20) leads to a divergence eigenvalue problem, with q being the divergence dynamic pressure.

Now consider a dynamic aeroelastic system. The airloads still depend in some way on the displacements, but now time has entered the equations. Furthermore, inertia loads, and possibly damping loads, must be included in the analysis; as mentioned earlier these are also related in some way to the displacement. The approach taken here will be to remove the differential time dependence of the dynamic equations by Laplace transformation on time, thereby obtaining equations with an algebraic dependence on the Laplace variable, s. This has an added advantage for unsteady aeroelastic problems since the unsteady aerodynamic terms for general motion are conveniently described in the Laplace domain.

After Laplace transformation, one finds that the homogeneous state vector equations suitable for aeroelastic stability analysis can be written in the form

$$\frac{d}{dx}\hat{\mathbf{y}} = \mathbf{Z}\hat{\mathbf{y}} + s^2\mathbf{M}\hat{\mathbf{y}} + s\mathbf{C}\hat{\mathbf{y}} - \mathbf{Q}(s,q)\hat{\mathbf{y}} \tag{2.21}$$

where $\hat{\mathbf{y}} = \hat{\mathbf{y}}(x,s)$ and the matrices $\mathbf{M}$, $\mathbf{C}$, and $\mathbf{Q}$ contain, respectively, the mass, damping, and unsteady aerodynamic terms. (The hat symbol denotes a Laplace transformed variable). As mentioned for the static aeroelastic problem in Eq. (2.20), the matrices expressing any form of displacement dependent loading (here, $\mathbf{M}$, $\mathbf{C}$, and $\mathbf{Q}$) have only one nonzero partition, namely, the partition that multiplies the displacements in the state vector.

In order to specialize Eq. (2.21) to free vibration analysis, neglect the damping and aerodynamic terms, $\mathbf{C}$ and $\mathbf{Q}$. For undamped vibration, the Laplace variable s is purely imaginary. Therefore, if one takes $s = j\omega$, then the free vibration counterpart of Eq. (2.21) is given by

$$\frac{d}{dx}\hat{\mathbf{y}} = \mathbf{Z}\hat{\mathbf{y}} - \omega^2\mathbf{M}\hat{\mathbf{y}}. \tag{2.22}$$

Clearly, dynamic response problems in the time domain can also be accommodated by including forcing terms on the right hand sides of the time domain versions of Eqs. (2.21) and (2.22).

2.3 Anisotropic Beam Equations

A simplified anisotropic plate-beam model is presented here for which the resulting equations are suitable for analyzing aeroelastic phenomena of large aspect ratio lifting surfaces. The purpose for developing these equations is twofold: first, they will help clarify the application of the foregoing general formulation and second, these equations will later be used in numerical examples of aeroelastic analyses. The assumptions used in developing the equations for the plate-beam model will be discussed briefly here, but it should be noted that they are similar to those employed by Weisshaar [4,5] to describe laminated composite box beam lifting surfaces. As a consequence, the following equations will be specialized somewhat to deal with structures whose anisotropic behavior arises due to laminated composite construction. A summary of composite plate lamination theory is presented in Appendix C; for a more detailed development, however, the reader can refer to Chapter 4 of the text by Jones [25].

With the aid of the cartesian coordinate system presented for the lifting surface model in Fig. 1, the aeroelastic equations will be developed for aerodynamic strip

sections taken normal to the structural reference axis. The structural reference axis is specified to be coincident with the x-axis, also shown in Fig. 1. Primarily for reasons of convenience, it will be assumed that this reference axis coincides with the geometric middle surface of the structural box. Although the reference axis location is arbitrary, this particular choice follows the conventions used for development of the composite plate constitutive relations. For this study, it is assumed that the structural reference axis is a straight line which, of course, will be swept accordingly as the wing aerodynamic sweep angle, Λ, changes. When considering aerodynamic surfaces with structural axis curvature, then the present approach should be adapted to take this curvature into account. It is further assumed that no appreciable chordwise deformation occurs in cross sections normal to the structural reference axis, so that wing deformation is only a function of the spanwise coordinate, x. Applying these assumptions means that the deformation of the plate-beam model can be represented in terms of a bending deflection $w(y)$, positive downward, of the reference axis, plus a rotation $\alpha(y)$, positive nose-up, about this axis. For problems dealing with rotating beams, an additional displacement variable u, along the x-axis, must be added to describe the deformation. In the presentation given here, bending deformation in the x–y plane is neglected. This lead-lag deformation can be easily added, however, in a more detailed analysis.

As the next step, the in-plane strains and curvatures can be written in terms of the foregoing displacement variables by applying the differential relationships that describe strain-displacement for a plate (see Appendix C). But first, an additional remark concerning shearing deformations should be made. Since standard lamination theory assumes no transverse shearing effects, this assumption will be adhered to here, but only for the composite laminate. That is, the shearing deformation of the laminated portion of the structure will be assumed negligible, but the gross shearing behavior of the overall structure can still be included. For instance,

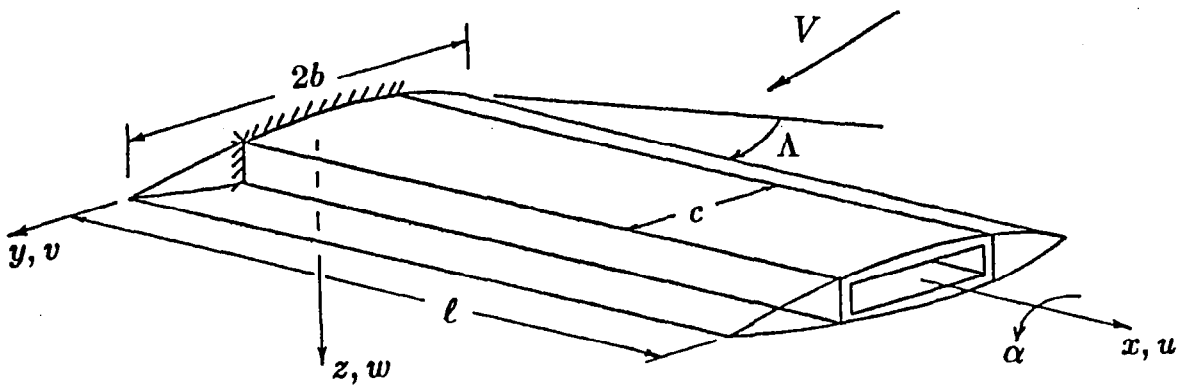

Fig. 1. Lifting Surface Model

standard composite structure fabrication quite often employs thin laminated face sheets placed over shear webs or a thick deformable core material. The transverse shearing effects induced by the webs or the core material can be included by adding a shearing energy to the energy functional. The transverse shear effects included here are assumed to arise in this manner. At the same time, it can reasonably be assumed that the composite cover sheets carry most of the bending stresses (and bending energy) of the structure.

Before introducing the preceding assumptions explicitly, the functional in the form specified by both Eq. (2.1) and Eq. (2.3) can be expressed in general terms for a composite plate as

$$U = \int_{-c/2}^{c/2} \Big[\mathbf{n}^T \boldsymbol{\epsilon}^0 + \mathbf{m}^T \boldsymbol{\kappa} - \frac{1}{2} (\mathbf{n}^T \mathbf{A}^* \mathbf{n} + \mathbf{n}^T \mathbf{B}^* \mathbf{m} + \mathbf{m}^T \mathbf{B}^* \mathbf{n} + \mathbf{m}^T \mathbf{D}^* \mathbf{m} + \beta_s V_x^2 - 2 V_x \gamma) \Big] dy - p_u u - p_\gamma \gamma - p_w w - p_\alpha \alpha \tag{2.23}$$

where an integration is to be performed over the chord length of the structural box. The composite plate compliance matrices $\mathbf{A}^*$, $\mathbf{B}^*$, and $\mathbf{D}^*$ are developed in Appendix C. Also found in the same appendix are descriptions of the resultant stress and moment vectors $\mathbf{n}$ and $\mathbf{m}$, respectively. Note that the transverse shear, V_x, has been included in Eq. (2.23) along with a transverse shear compliance term, β_s. The variable γ represents rotation of the normal to the neutral axis measured with respect to its initially undeformed position. In the absence of shearing deformation, it is assumed that normals remain normal so that γ is equal in magnitude to the slope of the neutral axis.

By introducing the assumption that the primary stresses are those that occur in the spanwise direction due to bending and axial stretching, the stress and moment resultants can be approximated as

$$\mathbf{n} = \{N_x \quad 0 \quad 0\}^T, \qquad \mathbf{m} = \{M_x \quad 0 \quad M_{xy}\}^T. \tag{2.24}$$

Furthermore, considering the deformation assumptions discussed earlier in this section, the midplane strains and bending curvatures can be approximated by

$$\boldsymbol{\epsilon}^0 = \{u_0' \quad 0 \quad 0\}^T, \qquad \boldsymbol{\kappa} = \{(\gamma' + y\alpha'') \quad 0 \quad 2\alpha'\}^T, \tag{2.25}$$

where the prime denotes differentiation with respect to x. All of the variables in Eq. (2.25) are assumed to be functions of x only. Next, substituting Eqs. (2.24–2.25) into Eq. (2.23) and performing the indicated integration yields an expression from which the state vector and other terms appearing in Eq. (2.3) can be readily defined.

The resulting state vector is

$$\mathbf{y} = \{\underline{N}_x \;\; \underline{M}_x \;\; \underline{V}_x \;\; 2\underline{M}_{xy} \;\; u \;\; \gamma \;\; w \;\; \alpha\}^T, \tag{2.26}$$

with

$$\underline{N}_x = cN_x, \quad \underline{M}_x = cM_x, \quad \underline{V}_x = cV_x, \quad \underline{M}_{xy} = cM_{xy}\,. \tag{2.27}$$

Having defined the state vector in this way, the differential equations can be determined by the approach laid down in Section 2.1.

It is convenient at this point to introduce a nondimensionalized version of the resulting anisotropic beam equations. The nondimensional differential equations, in the form of Eq. (2.8), can be written as

$$\frac{d}{d\overline{x}}\begin{Bmatrix} \overline{N}_x \\ \overline{M}_x \\ \overline{V}_x \\ 2\overline{M}_{xy} \\ \overline{u} \\ \gamma \\ \overline{w} \\ \alpha \end{Bmatrix} = \begin{bmatrix} 0 & 0 & 0 & 0 & 0 & 0 & 0 & 0 \\ 0 & 0 & 1 & 0 & 0 & 0 & 0 & 0 \\ 0 & 0 & 0 & 0 & 0 & 0 & 0 & 0 \\ 0 & 0 & 0 & 0 & 0 & 0 & 0 & 0 \\ \overline{A}^*_{11} & \overline{B}^*_{11} & 0 & \overline{B}^*_{13} & 0 & 0 & 0 & 0 \\ \overline{B}^*_{11} & \overline{D}^*_{11} & 0 & \overline{D}^*_{13} & 0 & 0 & 0 & 0 \\ 0 & 0 & \overline{S}^* & 0 & 0 & -1 & 0 & 0 \\ \overline{B}^*_{13} & \overline{D}^*_{13} & 0 & \overline{D}^*_{33} & 0 & 0 & 0 & 0 \end{bmatrix} \begin{Bmatrix} \overline{N}_x \\ \overline{M}_x \\ \overline{V}_x \\ 2\overline{M}_{xy} \\ \overline{u} \\ \gamma \\ \overline{w} \\ \alpha \end{Bmatrix} - \begin{Bmatrix} \overline{p}_u \\ \overline{p}_\gamma \\ \overline{p}_w \\ \overline{p}_\alpha \\ 0 \\ 0 \\ 0 \\ 0 \end{Bmatrix} \tag{2.28}$$

where the nondimensional coordinate and displacement variables are

$$\overline{x} = \frac{x}{\ell}, \qquad \overline{u} = \frac{u}{\ell}, \qquad \overline{w} = \frac{w}{\ell}. \tag{2.29}$$

It is also convenient to define

$$(EI)_R = c_R D_{11R}, \quad \text{and} \quad (GJ)_R = 4c_R D_{33R}, \tag{2.30}$$

which are the reference values of bending and torsional stiffness in terms of the appropriate composite stiffnesses derived in Appendix C. (The subscript R designates a reference value.) In terms of the reference bending stiffness, other nondimensional parameters appearing in Eq. (2.28) are the force and moment resultants and external loads

$$\begin{aligned} \overline{N}_x &= \frac{c\ell^2 N_x}{(EI)_R}, \qquad \overline{M}_x = \frac{c\ell M_x}{(EI)_R}, \qquad \overline{V}_x = \frac{c\ell^2 V_x}{(EI)_R}, \qquad \overline{M}_{xy} = \frac{c\ell M_{xy}}{(EI)_R}, \\ \overline{p}_u &= \frac{\ell^3 p_u}{(EI)_R}, \qquad \overline{p}_\gamma = \frac{\ell^2 p_\gamma}{(EI)_R}, \qquad \overline{p}_w = \frac{\ell^3 p_w}{(EI)_R}, \qquad \overline{p}_\alpha = \frac{\ell^2 p_\alpha}{(EI)_R}, \end{aligned} \tag{2.31}$$

and the nondimensional composite compliances

$$\begin{aligned} \overline{A}^*_{11} &= \frac{(EI)_R A^*_{11}}{c\ell^2}, \qquad \overline{B}^*_{11} = \frac{(EI)_R B^*_{11}}{c\ell}, \qquad \overline{B}^*_{13} = \frac{(EI)_R B^*_{13}}{2c\ell}, \\ \overline{D}^*_{11} &= \frac{(EI)_R D^*_{11}}{c}, \qquad \overline{D}^*_{13} = \frac{(EI)_R D^*_{13}}{2c}, \qquad \overline{D}^*_{33} = \frac{(EI)_R D^*_{33}}{4c}, \end{aligned} \tag{2.32}$$

and finally, the nondimensional shear compliance

$$\overline{S}^* = \frac{(EI)_R \beta_s}{\ell^2}. \tag{2.33}$$

It should be noted that the state vector equations presented in Eq. (2.28) are easily extended to both static and dynamic aeroelastic analyses by adopting the approach of Section 2.2 in which the load terms (i.e., inertia, damping, and aerodynamic) are expressed in terms of the displacement states of the structural state vector. The nondimensionalization of the load terms remains the same as that given in Eq. (2.31). Further use will be made of Eq. (2.28) when examining

aeroelastic behavior of composite lifting surfaces in Chapters 6 and 7. As a final observation about the anisotropic equations presented here, the equivalent equations representing isotropic structures can be obtained by simply replacing the composite compliance terms by isotropic compliances.

Chapter 3

Integrating and Differentiating Matrices

AN INTEGRATING MATRIX approach will now be developed to solve the state vector equations derived in Chapter 2. The solution of such equations can often be a difficult task since these equations, with their boundary conditions, take the form of two-point boundary value problems. Additional complexity is added for those equations that have nonconstant coefficients. By necessity, one is forced to consider numerical solutions since analytical approaches can be exceedingly difficult, if not impossible, for all but the simplest of cases. The primary objective of this chapter is to discuss the development of integrating matrices, which provide the basis for a simple and efficient concept for numerically solving two-point boundary value problems. Applications of the integrating matrix to the solution of differential equations will be considered in the next chapter. It is hoped that the discussions here will lend some perspective to the integrating matrix concept as a general numerical tool.

In Section 3.1, a general derivation is presented for integrating matrices that are suited to the integration of continuous functions. A new type of maximum precision integrating matrix that is developed from orthogonal polynomials will also be introduced. Some methods are discussed in Section 3.2 for applying continuous integrating matrices to the piecewise integration of discontinuous functions. Finally,

Section 3.3 discusses some of the aspects of a related topic, differentiating matrices.

Although numerical solution by an integrating matrix procedure is not an entirely new idea, this approach has seen relatively little attention and development compared to other well known numerical tools such as finite element and finite difference. In fact, only a handful of investigators have contributed to the integrating matrix method. One of the first applications of the integrating matrix method to problems in structural mechanics was presented in Russia by Vakhitov [26]. In this country, Hunter [27] is credited with much of the initial development of the integrating matrix procedure. As mentioned by Hunter, however, an integrating matrix was also used by Spector [28] to simply evaluate the integrals of an asymptotic "integral series" solution for nonuniform beam vibration. Other major contributions to the application of integrating matrices (including nonlinear problems) have been made by White and Malatino [29] and Kvaternik, White, and Kaza [30,31]. Most of their analyses were for vibration and stability of rotating beams. Vakhitov [32] has also employed integrating matrices for a circular plate analysis, while Levashov [33–35] has used integrating and differentiating matrices in the context of a generalized Ritz method. And recently, Lakin [36] has made useful contributions to the formulation of integrating matrices for arbitrarily spaced grid points.

Despite the fact that most of the applications in this work will be confined to structural mechanics, the developments in this chapter are quite general and can be applied to problems in other areas as well. It is interesting to note that the integrating matrix technique can often be closely related to discretization methods used in other areas of research. To pick a single example out of many, one could reexamine the spline series solutions used by Schneider and Reddy [37] to solve for optimal nonlinear thrust vector controls for guidance of an atmospheric interceptor. This problem can be solved in essentially the same manner with an integrating matrix formulation, where the integrating matrices are developed from the appropriate

spline approximations. Many parallels can also be drawn with the finite element method. In fact, the integrating matrix approach can be considered as a special type of collocation finite element method. The presentation given here, however, will differ from the formalism of the usual finite element approach.

As mentioned by Hunter [27], the integrating matrix also provides a useful tool for initial value calculations. Furthermore, the integrating matrix method is applicable in either linear or nonlinear situations. In the applications to be considered here, the focus will be on linear boundary value problems.

3.1 Integrating Matrices for Continuous Integrands

This section presents the basic development of the integrating matrix. As a preliminary requirement, it is assumed that the functions to be integrated are a continuous function of the spatial variable. More specifically, the integrating matrix development will be based upon integration of continuous polynomials that approximate the functional behavior of the structural state variables. The requirement of continuity, however, does not prove to be a restriction on the solution of more general problems. As will be shown in the next section, integrating matrices can be developed for piecewise continuous functions by extending the results presented here for continuous functions. With piecewise continuous functions, solutions are obtainable for almost any practical problem.

First, a review will be given of the fundamental theory of the integrating matrix. This review will be independent of a specific polynomial approximation. The viewpoint presented here will parallel the presentations given by both Hunter [27] and Lakin [36], in which it is assumed that the function to be integrated can be represented by a polynomial of given degree. Appendix A specializes this fundamental presentation to the case of integrating matrices based upon Jacobi

polynomials.

It should be noted that it is possible to derive many different types of integrating matrices, with each type dependent upon the form of approximation employed. One can easily formulate special purpose integrating matrices intended for a specific application. In this respect, the integrating matrix approach is very similar to finite element procedures that use element types suited to a given problem.

The primary objective of the integrating matrix approach is to develop a numerical procedure for performing indefinite integrations. In contrast with initial value integration schemes, which are commonly used for solving differential equations, the integrating matrix is formulated instead from a numerical quadrature. A quadrature is simply a numerical integration rule for integrating between fixed limits. An integrating matrix developed from such a quadrature rule is especially suited to solving boundary value problems since the region of integration is fixed by the boundaries. As pointed out by Hunter [27], however, the integrating matrix is just as easily applied to initial value problems.

To begin, let $f(x)$ be a continuous function on an interval $[a, b]$. In addition, suppose that a discrete set of $N+1$ grid points, $x_0, x_1, \ldots, x_N$, has been chosen on this interval such that

$$a = x_0 < x_1 < \ldots < x_N = b, \tag{3.1}$$

and let the function values at these points be given by

$$f_i = f(x_i). \tag{3.2}$$

In general, the points x_i can have either equal spacing or unequal spacing; ultimately, this will be determined by the nature of the approximations used for $f(x)$. Furthermore, the number of points chosen is somewhat arbitrary, but for an nth

degree polynomial approximation to $f(x)$ there must be at least $n+1$ grid points, where $n \leq N$. The $N+1$ grid points on $[a,b]$ determine N subintervals $[x_i, x_{i+1}]$ $(i = 0, \ldots, N-1)$. In general, a consecutive set of $n+1$ grid points will be designated by the sequence x_m, x_{m+1}, $\ldots$, x_{m+n}, where the subscript m denotes the starting grid point for the sequence.

Assuming that $f(x)$ can be approximated by an nth degree polynomial, then an approximation to $f(x)$ on any subinterval $[x_i, x_{i+1}]$ can be obtained in terms of the values $f_i = f(x_i)$ given for a consecutive set of $n+1$ grid points containing that subinterval. An appropriate approximation to $f(x)$ can be obtained by any of several different approaches, but the most useful methods include interpolation, spline fitting, and least-squares fitting. In the work presented here, only the interpolation method will be discussed in detail. If any type of approximate data is involved, however, a least-squares approximation would be preferable. Lakin [36] presents a nice discussion of the least-squares approach as applied to the determination of integrating matrices.

By integrating the approximation to $f(x)$ over any subinterval and arranging the result as a linear combination of the f_i's, one obtains a convenient numerical description of the integration. For a typical subinterval on $[a,b]$ this would appear as

$$\int_{x_i}^{x_{i+1}} f(x)\,dx \approx [\mathcal{W}_{im} f_m + \mathcal{W}_{im+1} f_{m+1} + \cdots + \mathcal{W}_{im+n} f_{m+n}] \tag{3.3}$$

where the $\mathcal{W}$'s are weighting terms that arise from integrating the approximation to $f(x)$. An approximation to $\int_a^b f(x)\,dx$ is now easily obtained by noting that $\int_a^b f(x)\,dx$ can be written as a sum of the integrations for each of the N subintervals. That is,

$$\int_a^b f(x)\,dx = \left\{ \int_{x_0}^{x_1} + \int_{x_1}^{x_2} + \cdots + \int_{x_{N-1}}^{x_N} \right\} f(x)\,dx. \tag{3.4}$$

The integrating matrix representation for the approximate integration of $f(x)$ contains the same information as expressed in Eqs. (3.3–3.4), but puts it in a compact matrix notation suitable for matrix manipulation. First, define the column vectors $\{\mathcal{F}\}$ and $\{f\}$ by

$$\{\mathcal{F}\} = \left(0, \int_{x_0}^{x_1} f(x)\,dx, \int_{x_1}^{x_2} f(x)\,dx, \ldots, \int_{x_{N-1}}^{x_N} f(x)\,dx\right)^T \tag{3.5}$$

and

$$\{f\} = (f_0, f_1, \ldots, f_N)^T. \tag{3.6}$$

With these definitions, the integral in Eq. (3.3) can be expressed for all subintervals in the matrix notation

$$\{\mathcal{F}\} = \mathcal{W}_n\{f\}, \tag{3.7}$$

where the subscript n indicates the degree of the polynomial used to approximate $f(x)$. $\mathcal{W}_n$ is an $(N+1)\times(N+1)$ weighting matrix. Since the first element of $\{\mathcal{F}\}$ is zero, the first row of $\mathcal{W}$ contains only zeros.

A summation of the subinterval integrations can now be formally obtained by premultiplying both sides of Eq. (3.7) by an $(N+1)\times(N+1)$ lower-triangular summing matrix,

$$\mathcal{S} = \begin{bmatrix} 1 & 0 & \ldots & 0 \\ 1 & 1 & \ldots & 0 \\ \vdots & \vdots & & \vdots \\ 1 & 1 & \ldots & 1 \end{bmatrix}, \tag{3.8}$$

for which $S_{ij} = 1$ when $i \geq j$ but $S_{ij} = 0$ if $i < j$. As a result of this summing operation, if $\{\overline{\mathcal{F}}\}$ is defined to be the the $N+1$ dimensional column vector,

$$\{\overline{\mathcal{F}}\} = \left(0, \int_{x_0}^{x_1} f(x)\,dx, \int_{x_0}^{x_2} f(x)\,dx, \ldots, \int_{x_0}^{x_N} f(x)\,dx\right)^T, \tag{3.9}$$

then the integrating matrix relationship can be written as

$$\{\overline{f}\} = \mathbf{L}\{f\} \tag{3.10}$$

where the integrating matrix $\mathbf{L}$ is defined by

$$\mathbf{L} = \mathcal{S}\mathcal{W}_n. \tag{3.11}$$

Incidentally, the summation indicated by $\mathcal{S}$ is most easily carried out in practice by simple summing, rather than by matrix multiplication.

As can be seen from Eq. (3.11), the derivation of the integrating matrix $\mathbf{L}$ relies primarily on the determination of $\mathcal{W}_n$ in Eq. (3.7) because the summing matrix $\mathcal{S}$ is known a priori. It is important to note that the integrating matrix depends on the polynomial approximation employed and on the number and spacing of the grid points, but it does not depend on the function values f_i at the grid points. Therefore, the integrating matrix has a separation of grid dependence and function dependence. Furthermore, the integrating matrix can now be viewed as a linear matrix operator that performs integrations via a simple matrix multiplication.

Although the foregoing discussion has presented the general procedure to be followed in deriving an integrating matrix, it is now worthwhile to focus a bit more closely on integrating matrices that can be derived from orthogonal polynomials. Traditionally, orthogonal polynomials have been used as a foundation for well-conditioned numerical procedures. The motivation for deriving integrating matrices based upon orthogonal polynomials actually stems from the fact that orthogonal polynomials form the basis for high accuracy quadrature rules of the Gaussian type (cf. Section 5.4 of the text by Conte and de Boor [38]). For these Gaussian integration rules, the function to be integrated can be written as a product of a sufficiently smooth function $g(x)$ and a nonnegative integrable weighting function

$\vartheta(x)$. That is, the integral of $f(x)$ over (a,b) is put into the form

$$\int_a^b f(x)\,dx = \int_a^b g(x)\vartheta(x)\,dx \tag{3.12}$$

where

$$g(x) = \frac{f(x)}{\vartheta(x)}. \tag{3.13}$$

As shown in Section 5.4 of Conte and de Boor [38] and Section 7.1 of Krylov [39], a quadrature of the highest possible precision for a given number of grid points is obtained when the polynomial approximation to $g(x)$ is orthogonal to the weight function $\vartheta(x)$ over the interval (a,b). In addition, the nodes (grid points) are specified to be the zeroes of the appropriate orthogonal polynomial. These nodes are nonevenly spaced and are all inside of the end points a and b.

But to be useful for the development of integrating matrices, the concept of an "optimal" quadrature must be extended one step further to allow nodes to be located exactly at the end points of an interval. The requirement for end point nodes becomes obvious when considering boundary value problems; these problems require that boundary conditions be satisfied precisely at the end points of the interval. The basic theory for the development of optimal quadratures having preassigned nodal locations is discussed in detail in Chapter 9 of Krylov [39], therefore, it will not be discussed in depth here. One point worth noting, however, is that fixed nodes at the end points give rise to a special weighting function, $\vartheta(x)$. This natural weighting function is a result of end point terms that appear in the interpolation of $f(x)$.

Because of the form of the weighting function that arises when end points of an interval are included, certain members of the Jacobi polynomial family turn out to be the appropriate orthogonal polynomials to use in deriving optimal quadratures. For this reason, the resulting integrating matrices will be referred to simply as "Jacobi" integrating matrices. Appendix A contains a detailed discussion of the

calculation procedure for Jacobi integrating matrices and Appendix B tabulates the corresponding weighting matrices up to $n+1 = 10$. To give an idea of the accuracy of the quadrature on which these integrating matrices are based, all polynomials of degree $\leq 2n-1$ will be integrated exactly.

For convenient use in later calculations, weighting matrices tabulated originally by Hunter [27] are also repeated in Appendix B. The corresponding integrating matrices are referred to as "Newton" integrating matrices since they are developed from Newton forward difference interpolating formulas. Some additional Lagrange and least-squares integrating matrices not listed here are tabulated by Lakin [36].

The Lagrange integrating matrices discussed by Lakin are somewhat related to the Jacobi matrices described above since both originate from Lagrange interpolations, which are valid for unequal grid point intervals. As noted by Lakin, however, the Lagrange integrating matrices are somewhat cumbersome to numerically compute for grid spacings chosen on an ad hoc basis. In contrast, however, the computation of Jacobi matrices is a much simpler numerical task. It turns out that Jacobi integrating matrices can be calculated by a procedure that is in many respects similar to the procedure presented by Lakin for least-squares fitting based on orthogonal polynomials. In fact, if the least-squares fit procedure is applied to the Jacobi grid points for an approximating polynomial of the maximum degree (i.e., the same degree used for an interpolation), then the least-squares procedure yields the Jacobi integrating matrix. A nice feature of the Jacobi integrating matrices is that optimal grid point locations are determined automatically by the underlying quadrature rule.

There are some other features of Jacobi integrating matrices that differ from Newton and Lagrange integrating matrices. The first of these differences arises because of the unequal grid point spacing. In the calculation of Newton matrices

for instance, the interpolations over a subinterval $[x_i, x_{i+1}]$ are performed by roving polynomials. That is, a polynomial of degree n, which makes use of $n+1$ consecutive grid points, can be shifted along the interval of $N+1$ grid points, one point at a time. This is possible, of course, because the Newton matrices are based on equal grid point spacings. For the interpolations required by the Jacobi integrating matrices, however, the unequal subinterval lengths mandate the use of a stationary polynomial. Because of the use of stationary polynomials, the Jacobi integrating matrices are in some respects analogous to high order, polynomial-based finite elements. That is, a Jacobi "element" corresponds to $n+1$ consecutive grid points and has $n-1$ unequally spaced internal nodes. The complete interval $[a, b]$ can be constructed by placing so-called Jacobi "elements" end to end. Experimentation with the Jacobi matrices reveals that the highest numerical efficiency is obtained by using a small number of "elements" of high order. This is in accord with results for finite element and other numerical approximation techniques.

A second aspect of a Jacobi integrating matrix (or any other type of integrating matrix with unequal intervals) is that interpolation may be required if one desires solution results at points other than the grid points. This is a fairly simple process, however, since interpolation shape functions are easily developed for the Jacobi polynomials. These shape functions are presented in Appendix A. Again, these shape functions are analogous to shape functions commonly used in finite element analysis.

Regardless of the type of integrating matrix, some very useful information can be obtained by investigating the quadrature rule on which the integrating matrix is based. The quadrature rule consists of the weighting terms that are applied to the integrand at each of the grid points. To be specific, the quadrature rule for the integral

$$\int_a^b f(x)\,dx \approx [\mathcal{W}_a f_a + \cdots + \mathcal{W}_b f_b] \tag{3.14}$$

simply consists of the $\mathcal{W}$'s and the corresponding x_i's. The $\mathcal{W}$'s, which are the primary values of interest, are contained in the last row of the integrating matrix. These quadrature weights, of course, can also be obtained by summing each of the terms in a column of the weighting matrix $\mathcal{W}$.

An examination of the underlying quadrature can often lead to a better understanding of the nature of a particular integrating matrix. For example, for the Jacobi weighting matrices given in Appendix B, the grid points are arranged symmetrically on the normalized interval $[-1, 1]$ and the quadrature weights (obtained by summing the columns) are all positive numbers that steadily increase in value as one approaches the midpoint of the interval. The values of the weight terms are also symmetric about the midpoint of the interval. But the important revelation is that the quadrature rule associated with Jacobi integrating matrices turns out to be the same as a well known numerical integration method, Lobatto quadrature. In fact, the numerical calculations for the Jacobi weighting matrices in Appendix B were verified by comparing the quadrature weights with those tabulated for Lobatto integration on page 920 of Abramowitz and Stegun [40].

An aspect of Newton integrating matrices that became apparent during this investigation was a possible asymmetry of the underlying quadrature. This phenomenon, which was also noted by Lakin [36], is referred to as "biasing." Biasing only arises when using interpolating polynomials for which the number of interpolation points, $n + 1$, is an odd number. The reason that biasing occurs for odd $n + 1$ is that away from the end points the interpolating polynomials cannot be centered on the subintervals $[x_i, x_{i+1}]$ that are being interpolated. When biasing is present, integrating matrices corresponding to Newton forward difference formulas differ from those derived from backward difference formulas. When $n + 1$ is even, there is

no biasing and both forward difference and backward difference formulations yield identical integrating matrices. When using the Newton integrating matrices, it is generally convenient to employ those matrices that are not biased (i.e., based upon $\mathcal{W}_n$ with $n+1$ even). It is interesting to note, however, that there is an easy way to symmetrize a biased Newton integrating matrix. Essentially, one develops a weighting matrix from one-half the sum of forward difference and backward difference weighting matrices. This is conveniently illustrated by taking a particular example that considers a quadratic Newton weighting matrix written for five grid points. By expressing the weighting matrix as a sum of forward and backward difference matrices, we have

$$\mathcal{W}_2 = \frac{1}{2}(\mathcal{W}_{2,f} + \mathcal{W}_{2,b}) \tag{3.15}$$

where the subscripts f and b refer, respectively, to forward and backward differencing. Equation (3.15) expands into (see Appendix B)

$$\begin{aligned}\mathcal{W}_2 &= \frac{1}{2}\left(\frac{h}{12}\right)\left\{\begin{bmatrix} 0 & 0 & 0 & 0 & 0 \\ 5 & 8 & -1 & 0 & 0 \\ 0 & 5 & 8 & -1 & 0 \\ 0 & 0 & 5 & 8 & -1 \\ \underline{0} & \underline{0} & \underline{-1} & \underline{8} & \underline{5} \\ 5 & 13 & 11 & 15 & 4 \end{bmatrix} + \begin{bmatrix} 0 & 0 & 0 & 0 & 0 \\ 5 & 8 & -1 & 0 & 0 \\ -1 & 8 & 5 & 0 & 0 \\ 0 & -1 & 8 & 5 & 0 \\ \underline{0} & \underline{0} & \underline{-1} & \underline{8} & \underline{5} \\ 4 & 15 & 11 & 13 & 5 \end{bmatrix}\right\} \\ &= \left(\frac{h}{24}\right)\begin{bmatrix} 0 & 0 & 0 & 0 & 0 \\ 10 & 16 & -2 & 0 & 0 \\ -1 & 13 & 13 & -1 & 0 \\ 0 & -1 & 13 & 13 & -1 \\ \underline{0} & \underline{0} & \underline{-2} & \underline{16} & \underline{10} \\ 9 & 28 & 22 & 28 & 9 \end{bmatrix}\end{aligned} \tag{3.16}$$

where the values below the horizontal bar in each matrix represent the quadrature weights. As can be seen, the final weighting matrix in Eq. (3.16) yields a symmetric quadrature. An interesting comparison can be made with the equivalent nonbiased

cubic Newton weighting matrix. It appears as

$$\mathcal{W}_3 = \left(\frac{h}{24}\right)\begin{bmatrix} 0 & 0 & 0 & 0 & 0 \\ 9 & 19 & -5 & 1 & 0 \\ -1 & 13 & 13 & -1 & 0 \\ 0 & -1 & 13 & 13 & -1 \\ 0 & 1 & -5 & 19 & 9 \\ \hline 8 & 32 & 16 & 32 & 8 \end{bmatrix} . \tag{3.17}$$

The similarity of the interior matrix elements between Eq. (3.17) and the last expression in Eq. (3.16) indicates that the symmetrized, nonbiased quadratic matrix will approach the accuracy of the cubic matrix. Obviously, error cancellation inherent in the summing of forward and backward difference formulations is responsible for the accuracy increase.

Also, rough comparisons between integrating matrices can be made based upon the quadrature rules. For instance, the Newton integrating matrices, in contrast with Jacobi integrating matrices, have quadrature weights that can oscillate considerably as one proceeds along the interval of integration. This oscillation tends to increase somewhat for the higher order Newton integrating matrices. This basic difference between the underlying quadratures for Newton and Jacobi integrating matrices can manifest itself in both accuracy and convergence properties. This will be discussed again in later chapters when comparisons are made between Newton and Jacobi solutions. It should be noted, however, that Newton and Jacobi matrices are identical for the quadratic approximation. For higher order approximations, their properties and relative accuracies differ. Although both types of integrating matrices provide very good solution accuracies, it has been found that Jacobi matrices are capable of offering faster, more predictable convergence and higher accuracy with fewer grid points.

3.2 Integrating Matrices for Discontinuous Integrands

Aided by the developments of the previous section, it is now straight forward to determine appropriate weighting matrices and integrating matrices for systems with discontinuous parameters. Basically, there are two types of discontinuities that occur often in static structural analysis and structural vibration. The first of these discontinuities stems from stepwise changes in coefficient terms of the differential equations. Such stepwise discontinuities could easily be the result of changes in stiffness or mass parameters. Appropriately, these discontinuities are best described by step functions. Methods for handling this type of discontinuity will be considered in this section. The methods discussed here for treating stepwise discontinuous systems are similar in some respects to the methods described by Vakhitov [26].

A second type of discontinuity results from point loading. Point loads can arise from either applied external loads or inertia loads associated with point masses. Point loads are most easily handled by introducing impulse functions. Since impulse functions are to be treated by an approach different from that for step functions, the methods for including concentrated loads in an analysis are taken up in Appendix E rather than this section.

The treatment of a problem with stepwise discontinuities is straightforward. The solution interval is simply divided up into analytic regions by breaking the integration at points of discontinuity. For each of these separate regions a different (or the same) weighting matrix can be used. An integrating matrix for the complete solution interval is then obtained in the normal way by summing the weighting matrix terms for each of the piecewise regions. This summation procedure is identical with the one carried out by the summing matrix $\boldsymbol{S}$ in Eq. (3.11). The only difference in forming the integrating matrix for stepwise discontinuous systems is that the weighting matrix $\mathcal{W}$ for the complete solution interval has a block matrix

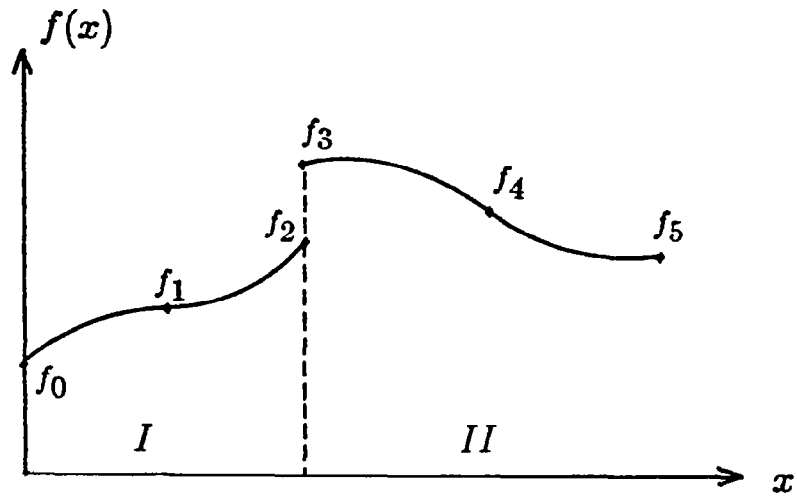

Fig. 2. Typical integration regions for a discontinuous function

structure, where each of the blocks corresponds to a normal weighting matrix written for one of the analytic regions.

Perhaps a simple example best explains the procedure to be applied to discontinuous functions. Consider integrating a function that has a single point of discontinuity, as shown in Fig. 2. The integration of the discontinuous function can clearly be broken into the two distinct integrations indicated by the regions *I* and *II*. For this particular example, which assumes weighting matrices with end point nodes, the equivalent of Eq. (3.7) can be written as

$$\{\mathcal{I}\} = \begin{bmatrix} \mathcal{W}_I & 0 \\ 0 & \mathcal{W}_{II} \end{bmatrix} \begin{Bmatrix} f_I \\ f_{II} \end{Bmatrix} = \mathcal{W}_{I+II} f . \tag{3.18}$$

Here, as in Eq. (3.11), the resulting integrating matrix can be calculated from

$$\mathsf{L} = S\mathcal{W}_{I+II} . \tag{3.19}$$

In Eq. (3.18), it should be noted that the "merged" weighting matrix has no overlap of rows or columns between the individual matrices for each region.

Note in Fig. 2 that two distinct function values have been defined at the discontinuous point, each corresponding to the appropriate function value an infinitesimal distance away from the discontinuity. These identically located points occur for the case in which the weighting matrices on either side of the discontinuity make use of grid points located at the end points of an interval. Strictly speaking, it is not mandatory that one have grid points at the discontinuity, unless, of course, boundary conditions or loads must be applied at such a point. For instance, an interior region of a multiple region integration might make use of weighting matrices based on Gauss-Legendre quadrature, which does not require grid points at the ends of an interval (see Appendix B). Regardless of whether or not grid points are located at discontinuities in the integrand, the continuity of the integration assures that solutions will be continuous.

Another feature that can be accommodated in much the same fashion as a stepwise discontinuity in integration is either a change in step size or a change in integrating matrix type within a solution interval. Grid points are fixed, of course, for weighting matrices based on orthogonal polynomials, but can be variable for constant step size matrices like the Newton integrating matrices. It is quite easy to switch to different types of integrating matrices to satisfy particular solution requirements for portions of a solution interval. The method for handling a discontinuous integration arising from integrating matrix changes or step size changes is very much similar to the method employed for discontinuous system parameters.

When compared to the discontinuous problem in Eq. (3.18), changes in either step size or integrating matrix type lead to a slightly different way of adding the *local* weighting matrices into the *global* weighting matrix. If weighting matrices with different step sizes (or even with the same step sizes) are merged to integrate a larger region, there will be some "overlap" between weighting values for the merged matrices. This is true for weighting matrices that use end point nodes as well as

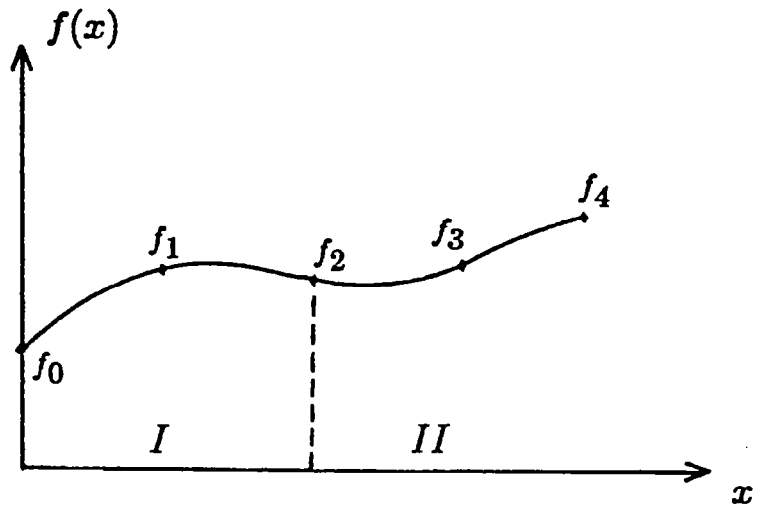

Fig. 3. Typical regions for piecewise integration of a continuous function

those that do not. The "overlap" shows up in the global weighting matrix as an overlapping of some of the rows and columns of adjoining matrix blocks. Again, a specific example easily demonstrates the procedure. Consider the five grid point, two region integration shown in Fig. 3. For the sake of illustration, second degree Newton weighting matrices having equal step sizes will be employed in both regions *I* and *II*. Furthermore, the the step size is conveniently chosen such that the constant step size factor $h/12$ has the value of unity. (See Appendix B.) With these specifications, the equivalent of Eq. (3.7) becomes

$$\{\mathcal{F}\} = \begin{bmatrix} 0 & 0 & 0 & & \\ 5 & 8 & -1 & & \\ -1 & 8 & 5 & 0 & 0 \\ & & 5 & 8 & -1 \\ & & -1 & 8 & 5 \end{bmatrix} \begin{Bmatrix} f_0 \\ f_1 \\ f_2 \\ f_3 \\ f_4 \end{Bmatrix} \tag{3.20}$$

For this specific example, it can be seen that the region *I* and region *II* submatrices overlap by one row and one column.

In the integrating matrix method, the process of merging weighting matrices is analogous to the merging of stiffness matrices in the finite element method. In fact, by considering the different situations that can arise in connection with discontinuous integrations, it is possible to write down a simple set of rules describing how weighting matrices should be merged. To be able to give a consistent set of rules for weighting matrices with and without end point nodes, one basic requirement must be met. This requirement simply stipulates that weighting matrices without end point nodes must conform to weighting matrices with end point nodes. An example of a conforming Gauss-Legendre weighting matrix is given in Appendix B. It should be noted too that the merging process is carried out by starting at one boundary of the solution interval and proceeding with consecutive piecewise regions in the direction of integration.

The rules for merging weighting matrices at points of continuous or discontinuous system coefficients can be considered separately. First, for discontinuous parameter systems we have the following requirements for merging at a point of discontinuity:

1. If both adjacent matrices have end point nodes, there will be no row or column overlap (e.g., Eq. (3.18)).
2. If one of the adjacent matrices has end point nodes and the other does not, there will be one row and one column of overlap.
3. If neither of the adjacent matrices have end point nodes, there will be one row of overlap and two columns of overlap.

For continuous parameter systems, the following rules for merging apply at any point within the solution interval:

1. If either or both of the adjacent matrices have end point nodes, there will be one row and one column of overlap (e.g., Eq. (3.20)).
2. If neither of the adjacent matrices have end points, there will be two rows and two columns of overlap.

Any of the above merging rules can be easily checked by taking a sample problem and examining the subinterval integrations, as demonstrated, for example, in Eq. (3.20). Since the merged weighting matrices only specify the subinterval integrations, the logical conclusion of the merging process is in the determination of the corresponding integrating matrix from Eq. (3.11). From the standpoint of numerical calculation, the merging rules can be applied during the summing process that forms the integrating matrix from the weighting matrix.

3.3 Differentiating Matrices

Similar to the idea of an integrating matrix, there is also a differentiating matrix. The differentiating matrix expresses the derivative of a function in terms of the function values at a discrete set of points. Usually, a differentiating matrix is determined by differentiating an interpolating polynomial, just as the integrating matrix is determined by integrating that same polynomial. It is also feasible to use simple differencing to calculate a differentiating matrix.

Differentiating matrices, in fact, are quite common in finite element applications. For instance, the strain-displacement relationships in a finite element analysis are usually written in terms of a differentiating matrix determined by differentiating the displacement shape functions. The papers by Levashov [33–35] show how a combination of both differentiating matrix and integrating matrix concepts can be used to solve structural problems by the displacement method. For the integrating matrix approach as presented here, one rarely has to resort to using differentiating matrices. Nonetheless, the differentiating matrix proves to be a useful tool in certain circumstances and is worthy of mention.

With the state vector formulation of the aeroelastic equations given in Chapter 2, it is normally possible to write the structural portion of the equations without

need for a differentiating matrix. To express certain descriptions of the aerodynamic loads, however, higher derivatives of some of the structural state variables may be required. In such a situation, the differentiating matrix provides a convenient way of writing these higher derivatives in terms of existing state variables. A similar situation can exist when writing the "preload" terms for a structure with initial curvature. In this latter case though, it appears that it's usually possible to rewrite the equations in such a way that the use of a differentiating matrix is avoided.

A variety of differentiating matrices can be calculated depending on the type of interpolating polynomial assumed. Methods for calculating differentiating matrices are quite straight forward since one simply determines derivative expressions for the approximating polynomials. Detailed calculations will not be presented here for differentiating matrices; however, some precalculated formulas do exist for derivatives of certain types of interpolations. For example, expressions for the derivatives of Newton forward difference interpolation formulas, which form the basis for the Newton integrating matrices, can be found on page 883 of Abramowitz and Stegun [40]. Also tabulated there are similar expressions for the derivatives of Lagrange's interpolation formula, which is useful for approximating functions with nonuniform grid spacings. And finally, differentiating matrices corresponding to Jacobi integrating matrices can be calculated by differentiating the shape functions presented in Appendix A. The finite series expansion for the Jacobi polynomials presented in that appendix should prove useful in obtaining the proper derivative expressions.

Chapter 4

Integrating Matrix Solution of State Vector Equations

INTEGRATING MATRICES PROVIDE a convenient and efficient method for solving two-point boundary value problems. The prime concern is the solution of the aeroelastic and structural dynamic equations presented in Chapter 2. The major focus of this chapter is on the formulation of discrete solutions for these equations when they are represented in state vector form. Other important issues that are discussed include methods for manipulating and reducing the discrete state vector equations to a suitable form for numerical solution.

A direct approach that does not require the calculation of influence matrices will be presented for formulating linear systems of equations and eigenvalue problems. It also turns out that the integrating matrix solutions to be discussed are closely related to alternate solutions in terms of transition matrices. In fact, the integrating matrix provides one of the easiest means for numerically calculating transition matrices. Furthermore, with the aid of a transition matrix, one can in turn calculate symmetric stiffness influence matrices for the types of problems considered in this chapter. Although the transition matrix approach will not be discussed here, it is presented briefly in Appendix G. Many of the ideas contained in this chapter can be used in connection with transition matrix calculations.

As will be evident to those familiar with approximate solution techniques, the integrating matrix approach belongs to a class of collocation solution methods. Since collocation solutions belong to the more general family of methods know as weighted residual methods, it is possible, in fact, to formalize the integrating matrix approach in much the same way that finite element methods are formalized. For the sake of simplicity, however, the following presentations will employ a more intuitive approach.

Collocation solutions are conveniently classified by Collatz [41] (also, Meĭrovitch [42]) according to the nature of the approximating functions. Within this classification scheme, the integrating matrix approach presented here falls into the category of a mixed method. That is, the approximating functions initially satisfy neither the differential equations nor the boundary conditions of the problem. (Other categories stipulate that the functions must initially satisfy either the boundary conditions or the differential equations.) Solutions with the mixed method are obtained by insisting that at selected collocation grid points the boundary conditions, or differential equations, as appropriate, are satisfied exactly. From the discussions of chapter 3, it should be clear that the arrangement of collocation grid points, as well as the approximating functions, are specified by the choice of integrating matrix.

A general advantage that collocation methods have over some other methods lies in the ease with which coefficient matrices can be generated for the approximate equations. As will be shown, the integrating matrix approach provides a very simple way of obtaining the matrix equations that describe a particular set of differential equations. In addition, if these differential equations are in state vector form, it is often possible, at least for linear problems, to take advantage of the structure of the state vector equations to further simplify the corresponding matrix equations.

There is, however, a disadvantage to collocation type approaches. Namely, the matrices involved are always nonsymmetric, thereby requiring less efficient

solution routines. But in many instances, this disadvantage is entirely offset by the simplicity of the approach. Furthermore, since the integrating matrix method easily accommodates very high order approximating functions, one often finds a considerable reduction in problem size for a required solution accuracy.

4.1 Discretized State Vector Equations

To obtain a discretized form of the state vector equations, it is convenient to consider a particular example problem. A suitable choice is Eq. (2.20), which can be used to describe aeroelastic response for a one dimensional structure. Although this equation is intended primarily for static aeroelastic response, with appropriate generalization it encompasses other types of equations, including dynamic equations like Eq. (2.21) and Eq. (2.22). To make the results generally applicable, it is assumed that Eq. (2.20) can be expressed in a nondimensional form so that it appears as

$$\mathbf{y}' = \mathbf{Z}\mathbf{y} - \lambda\mathbf{A}\mathbf{y} - \mathbf{a}_r \tag{4.1}$$

where λ represents a nondimensional parameter. For homogeneous problems, which are obtained by dropping the nonhomogeneous term $\mathbf{a}_r$, the parameter λ is to be taken as an eigenvalue. In the sample problems to be presented later, more precise definitions will be given for the terms appearing in Eq. (4.1), but for now it is convenient to use them simply as generic terms. In what follows, the state vector $\mathbf{y}$ in Eq. (4.1) will be referred to as a *local* state vector.

Since Eq. (4.1) must be valid for any value of the spatial coordinate, it can be written at a discrete set of $N+1$ points along the desired solution interval. In this discrete form it can be expressed as

$$\tilde{\mathbf{y}}' = \tilde{\mathbf{Z}}\tilde{\mathbf{y}} - \lambda\tilde{\mathbf{A}}\tilde{\mathbf{y}} - \tilde{\mathbf{a}}_r. \tag{4.2}$$

The discrete version of the state vector, $\tilde{\mathbf{y}}$, will be referred to as a *global* state vector. Note that the dimension of $\tilde{\mathbf{y}}$ will be NS$(N+1)$, where NS refers to the number of states in the local state vector. The ordering of components in the global state vector is actually arbitrary, but it turns out to be very useful in what follows to specify a particular ordering. It will be assumed that the global state vector is ordered such that its structure is the same as that of $\mathbf{y}$. More precisely, it is partitioned into generalized force and generalized displacement subsets as was done for the local vector $\mathbf{y}$ in Eq. (2.4), and furthermore, the discrete set of values for a particular state variable are grouped together. This will be clearly demonstrated in the sample problems of Chapter 5.

With the aforementioned ordering in mind, a global version of the integrating matrix, $\tilde{\mathbf{L}}$, can now be applied as a matrix operator to both sides of Eq. (4.2). The result is

$$\tilde{\mathbf{y}} = \tilde{\mathbf{L}}\tilde{\mathbf{Z}}\tilde{\mathbf{y}} - \lambda\tilde{\mathbf{L}}\tilde{\mathbf{A}}\tilde{\mathbf{y}} - \tilde{\mathbf{L}}\tilde{\mathbf{a}}_r + \tilde{\mathbf{k}} \tag{4.3}$$

where $\tilde{\mathbf{k}}$ is a constant vector of integration to be determined from boundary conditions. Note that the effect of applying the integrating matrix to the isolated derivative term on the left-hand side of Eq. (4.2) was simply to integrate that term and thus remove the derivative. Integrating matrices on the right-hand side of Eq. (4.3) perform their integration function through a matrix multiplication.

The global integrating matrix in Eq. (4.3) is a block diagonal matrix that appears as

$$\tilde{\mathbf{L}} = \begin{bmatrix} \mathbf{L} & & \\ & \ddots & \\ & & \mathbf{L} \end{bmatrix} \tag{4.4}$$

with each block being a standard $(N+1) \times (N+1)$ integrating matrix as derived in the previous chapter. The appropriate number of matrix blocks on the diagonal

is determined by the number of state variables, NS, in the local state vector. In essence, the integrating matrix allows one to proceed in much the same manner as solving a simple integrable equation by analytical methods. But with the numerical integration properties of the integrating matrix, it is now possible to deal with otherwise difficult integrations in a very simple manner.

At this point, Eq. (4.3) provides a matrix equation from which one can obtain a solution of the state vector differential equations. The only remaining step is to determine $\tilde{\mathbf{k}}$ from specified boundary conditions. And once $\tilde{\mathbf{k}}$ is known, there remains only a linear systems solution if considering the nonhomogeneous problem, or a matrix eigenvalue solution if considering the related homogeneous problem.

For two-point boundary value problems, it is useful to introduce the boundary condition matrices $\mathbf{B}_0$ and $\mathbf{B}_n$. These boundary condition matrices, which relate to homogeneous boundary conditions, will aid in solving for $\tilde{\mathbf{k}}$. $\mathbf{B}_0$ and $\mathbf{B}_n$ can be written as

$$\mathbf{B}_0 = \vec{\mathbf{1}}\mathbf{b}_0^T \tag{4.5}$$

and

$$\mathbf{B}_n = \vec{\mathbf{1}}\mathbf{b}_n^T \tag{4.6}$$

where $\vec{\mathbf{1}}$ is a column vector containing all unit terms. The vectors $\mathbf{b}_0$ and $\mathbf{b}_n$ can be expressed as

$$\mathbf{b}_0^T = \{1, 0, \ldots, 0\} \tag{4.7}$$

and

$$\mathbf{b}_n^T = \{0, \ldots, 0, 1\}. \tag{4.8}$$

The dimensions of $\mathbf{B}_0$ and $\mathbf{B}_n$ are $(N+1)\times(N+1)$, the same as a normal integrating matrix. Also, since the first row of the integrating matrix contains only zeroes, one has that $\mathbf{B}_0\mathbf{L} = \mathbf{0}$.

Corresponding to the global block diagonal integrating matrix $\tilde{\mathbf{L}}$, there is a similar block diagonal boundary condition matrix, $\tilde{\mathbf{B}}$. For a two-point boundary value problem, each matrix block on the diagonal of $\tilde{\mathbf{B}}$ is specified by applying either $\mathbf{B}_0$ or $\mathbf{B}_n$ (or equivalently, $\mathbf{b}_0^T$ or $\mathbf{b}_n^T$) to the corresponding state variable and solving for its constant vector of integration. This process will be clearly demonstrated in the examples of Chapter 5. Since $\mathbf{b}_0^T$ and $\mathbf{b}_n^T$ contain mostly zero elements, along with a strategically located unit term, their operational effect on a discrete state vector is to select the "degree of freedom" at which a boundary condition is to be applied.

In addition to the homogeneous boundary condition matrix $\tilde{\mathbf{B}}$, one can define $\tilde{\mathbf{B}}_{nh}$ to account for nonhomogeneous boundary conditions that can be written in terms of the state variables. The specific form of $\tilde{\mathbf{B}}_{nh}$ has to be determined for each particular problem, but one should note that for many common problems it is simply zero. When $\tilde{\mathbf{B}}_{nh}$ does need to be determined, it is defined in such a way that when it premultiplies the global state vector, it produces the required nonhomogeneous boundary terms. Similar to the situation for $\tilde{\mathbf{B}}$, $\tilde{\mathbf{B}}_{nh}$ will consist mainly of zeroes, but will have a few strategically located nonzero terms. The nonzero terms in $\tilde{\mathbf{B}}_{nh}$, however, are not usually unit terms as was required for $\tilde{\mathbf{B}}$.

With the foregoing definition of boundary condition matrices, a general expression can be obtained for the solution of $\tilde{\mathbf{k}}$. To obtain this expression, Eq. (4.3) is first multiplied through by $\tilde{\mathbf{B}}$. Since $\tilde{\mathbf{B}}$ has been defined for homogeneous boundary conditions, we have that $\tilde{\mathbf{B}}\tilde{\mathbf{y}} = 0$. Furthermore, the form of $\tilde{\mathbf{k}}$ is specified to be such that $\tilde{\mathbf{B}}\tilde{\mathbf{k}} = \tilde{\mathbf{k}}$. With these two identities, and with the aid of the nonhomogeneous boundary term $\tilde{\mathbf{B}}_{nh}\tilde{\mathbf{y}}$, one obtains from Eq. (4.3) the general result

$$\tilde{\mathbf{k}} = -\tilde{\mathbf{B}}\tilde{\mathbf{L}}(\tilde{\mathbf{Z}}\tilde{\mathbf{y}} - \lambda\tilde{\mathbf{A}}\tilde{\mathbf{y}} - \tilde{\mathbf{a}}_r) - \tilde{\mathbf{B}}_{nh}\tilde{\mathbf{y}} \tag{4.9}$$

where it can be noted that $\tilde{\mathbf{k}}$ consists of both homogeneous and nonhomogeneous components. For nonhomogeneous boundary terms that express displacement dependent loads, it is often possible to rewrite these terms is such a way that they can be included in $\tilde{\mathbf{A}}$ rather than $\tilde{\mathbf{B}}_{nh}$. The advantage in doing this will be discussed in the next section.

Having now determined a general expression for $\tilde{\mathbf{k}}$, the next step is to obtain a suitable matrix equation that can be solved by standard methods. This is easily achieved by substituting the expression for $\tilde{\mathbf{k}}$ from Eq. (4.9) into Eq. (4.3). Grouping similar terms and then rearranging leads to

$$[\mathbf{H} - \lambda\mathbf{F}\tilde{\mathbf{A}}]\tilde{\mathbf{y}} = \mathbf{f} \tag{4.10}$$

where

$$\mathbf{H} = \mathbf{I} + \tilde{\mathbf{B}}_{nh} + \mathbf{F}\tilde{\mathbf{Z}} \tag{4.11}$$

$$\mathbf{F} = [\tilde{\mathbf{B}} - \mathbf{I}]\tilde{\mathbf{L}} \tag{4.12}$$

$$\mathbf{f} = \mathbf{F}\tilde{\mathbf{a}}_r\,, \tag{4.13}$$

with $\mathbf{I}$ being an identity matrix with appropriate dimensions. It is obvious that Eq. (4.10) represents a system of linear equations when λ is specified and when the nonhomogeneous external load term, $\mathbf{f}$, is nonzero. If $\mathbf{f}$ is zero, then Eq. (4.10) provides a matrix eigenvalue problem. Furthermore, if one chooses to give different interpretations to $\lambda\tilde{\mathbf{A}}$, then Eq. (4.10) encompasses a broad range of aeroelastic, vibration, and structural problems. For instance, the free vibration and unsteady aeroelastic problems described by Eqs. (2.21–2.22) are manipulated into similar forms after application of the integrating matrix. More precise definitions for several

types of problems will be given in the following sections and in the example solutions of Chapters 5, 6, and 7.

It is possible to stop at this point and numerically solve Eq. (4.10) with standard methods. To do so, however, requires the solution of matrix equations with twice the number of necessary variables. As mentioned previously, the global state vector, $\tilde{\mathbf{y}}$, is partitioned into both force and displacement variables, $\tilde{\mathbf{y}}_F$ and $\tilde{\mathbf{y}}_D$, similar to Eq. (2.4). The next section will show that by applying matrix partitioning techniques one can conveniently reduce the solution of Eq. (4.10) to an equivalent problem written solely in terms of the displacement variables $\tilde{\mathbf{y}}_D$.

4.2 State Vector Equation Reduction

By partitioning the matrices in Eq. (4.10) according to the force and displacement states of the global state vector, it is possible to achieve an analytical reduction of the matrix equations such that only displacement variables are involved in the final solution. As will be shown, the reduction task is greatly simplified due to the structure of the state vector equations developed in Section 2.1.

Writing out the partitioned form of the matrices appearing in Eq. (4.10) reveals that

$$\mathbf{H} = \begin{bmatrix} \mathbf{H}_{FF} & \mathbf{H}_{FD} \\ \mathbf{H}_{DF} & \mathbf{H}_{DD} \end{bmatrix} \tag{4.14}$$

$$\tilde{\mathbf{A}} = \begin{bmatrix} \mathbf{0} & \mathbf{A}_{FD} \\ \mathbf{0} & \mathbf{0} \end{bmatrix} \tag{4.15}$$

$$\mathbf{F} = \begin{bmatrix} \mathbf{F}_{FF} & \mathbf{0} \\ \mathbf{0} & \mathbf{F}_{DD} \end{bmatrix} \tag{4.16}$$

and

$$\mathbf{f} = \begin{Bmatrix} \mathbf{F}_{FF}\tilde{\mathbf{a}}_{r_F} \\ \mathbf{0} \end{Bmatrix} . \tag{4.17}$$

First of all, it should be noted that the $\mathbf{H}$ matrix contains structural related terms, including elastic restraint boundary terms that arise from $\tilde{\mathbf{B}}_{nh}$. The $\mathbf{H}_{FD}$ submatrix consists of these elastic restraint terms as well as "geometric stiffness" terms for problems involving initial structural curvature and deformation dependent "preloads." As mentioned in connection with nonhomogeneous boundary terms in the previous section, it is often possible to shift terms that appear in $\mathbf{H}_{FD}$ so that instead they can be included in $\mathbf{A}_{FD}$. This can be easily done, for example, for the centrifugal stiffening term that appears in rotating beam problems. The motivation for rearranging in this way is to zero out the $\mathbf{H}_{FD}$ submatrix. If $\mathbf{H}_{FD} = 0$, the reduction process is considerably simplified, as will be indicated in what follows. For problems without nonhomogeneous boundary terms and without geometric nonlinearities, $\mathbf{H}_{FD}$ is automatically zero.

Other matrices and vectors appearing in Eqs. (4.15–4.17), such as $\tilde{\mathbf{A}}$ and $\mathbf{f}$, have the indicated forms because of the natural structure of the state vector equations derived in Section 2.1. For instance, since $\tilde{\mathbf{A}}$ contains only displacement dependent load terms, the only nonzero partition is given by $\mathbf{A}_{FD}$, which is the submatrix that expresses loads in terms of the displacement variables. $\mathbf{F}$, on the other hand, is a block diagonal matrix simply because the matrices from which it is calculated are also block diagonal.

With the partitioned form of the matrices given by Eqs. (4.14–4.17), it is straight forward to write out the corresponding partitioned equations from Eq. (4.10) and use them to eliminate the the generalized force variables, $\tilde{\mathbf{y}}_F$. This elimination process yields the expressions to be used in solving for the force variables once the displacement variables $\tilde{\mathbf{y}}_D$ are obtained. The method to be used in reducing

the partitioned equations involves multiplying them through by the inverse of the **H** matrix, where this inverse is obtained from the partitioned form of **H**. Matrix inversion by partitioning is discussed, for example, in Appendix A of the text by Przemieniecki [43]. If the inverse of **H** is denoted by

$$\mathbf{H}^{-1} = \begin{bmatrix} \mathbf{H}^*_{FF} & \mathbf{H}^*_{FD} \\ \mathbf{H}^*_{DF} & \mathbf{H}^*_{DD} \end{bmatrix}, \tag{4.18}$$

then the inverted terms that will be needed in the following reductions are

$$\mathbf{H}^*_{FF} = \mathbf{H}^{-1}_{FF} + \mathbf{H}^{-1}_{FF}\mathbf{H}_{FD}\left(\mathbf{H}_{DD} - \mathbf{H}_{DF}\mathbf{H}^{-1}_{FF}\mathbf{H}_{FD}\right)^{-1}\mathbf{H}_{DF}\mathbf{H}^{-1}_{FF} \tag{4.19}$$

and

$$\mathbf{H}^*_{DF} = -\left(\mathbf{H}_{DD} - \mathbf{H}_{DF}\mathbf{H}^{-1}_{FF}\mathbf{H}_{FD}\right)^{-1}\mathbf{H}_{DF}\mathbf{H}^{-1}_{FF}. \tag{4.20}$$

The first set of reduced equations to be obtained are those for aeroelastic lift distribution and structural deflection problems. Beginning with the nonhomogeneous linear equations given in Eq. (4.10), their partitioned form appears as

$$\left[\begin{bmatrix} \mathbf{H}_{FF} & \mathbf{H}_{FD} \\ \mathbf{H}_{DF} & \mathbf{H}_{DD} \end{bmatrix} - \lambda \begin{bmatrix} \mathbf{0} & \mathbf{F}_{FF}\mathbf{A}_{FD} \\ \mathbf{0} & \mathbf{0} \end{bmatrix}\right] \begin{Bmatrix} \tilde{\mathbf{y}}_F \\ \tilde{\mathbf{y}}_D \end{Bmatrix} = \begin{Bmatrix} \mathbf{F}_{FF}\tilde{\mathbf{a}}_{r_F} \\ \mathbf{0} \end{Bmatrix}. \tag{4.21}$$

Multiplying Eq. (4.21) through by $\mathbf{H}^{-1}$ then yields

$$\begin{bmatrix} \mathbf{I} & -\lambda\mathbf{H}^*_{FF}\mathbf{F}_{FF}\mathbf{A}_{FD} \\ \mathbf{0} & \mathbf{I} - \lambda\mathbf{H}^*_{DF}\mathbf{F}_{FF}\mathbf{A}_{FD} \end{bmatrix} \begin{Bmatrix} \tilde{\mathbf{y}}_F \\ \tilde{\mathbf{y}}_D \end{Bmatrix} = \begin{Bmatrix} \mathbf{H}^*_{FF}\mathbf{F}_{FF}\tilde{\mathbf{a}}_{r_F} \\ \mathbf{H}^*_{DF}\mathbf{F}_{FF}\tilde{\mathbf{a}}_{r_F} \end{Bmatrix}. \tag{4.22}$$

By applying Eqs. (4.19–4.20), this can be simplified to give the generalized force equation

$$\tilde{\mathbf{y}}_F = -\mathbf{H}^{-1}_{FF}[\mathbf{H}_{FD} - \lambda\mathbf{F}_{FF}\mathbf{A}_{FD}]\tilde{\mathbf{y}}_D + \mathbf{H}^{-1}_{FF}\mathbf{F}_{FF}\tilde{\mathbf{a}}_{r_F} \tag{4.23}$$

and the reduced linear system

$$\left[\mathbf{I} - \lambda \mathbf{T}\mathbf{A}_{FD} - \mathbf{H}_{DD}^{-1}\mathbf{H}_{DF}\mathbf{H}_{FF}^{-1}\mathbf{H}_{FD}\right]\tilde{\mathbf{y}}_D = \mathbf{T}\tilde{\mathbf{a}}_{r_F} \tag{4.24}$$

where

$$\mathbf{T} = -\mathbf{H}_{DD}^{-1}\mathbf{H}_{DF}\mathbf{H}_{FF}^{-1}\mathbf{F}_{FF} \,. \tag{4.25}$$

If $\mathbf{H}_{FD} = 0$, then Eq. (4.24) simplifies to

$$[\mathbf{I} - \lambda \mathbf{T}\mathbf{A}_{FD}]\tilde{\mathbf{y}}_D = \mathbf{T}\tilde{\mathbf{a}}_{r_F} \,. \tag{4.26}$$

This simplified result provides the expression to be used in several examples that will be presented in later chapters. Note that λ must be specified before solutions can be obtained from Eqs. (4.24) and (4.26). In the absence of aerodynamic or inertial loading, λ will be equal to zero and Eq. (4.26) directly provides structural deflection solutions.

The next important result concerns the reduced eigenvalue equations for both aeroelastic divergence and free vibration problems. This result is easily reached by first setting the right-hand side of Eq. (4.21) to zero to obtain the homogeneous version of the partitioned equations. Then, by following an approach similar to that given above for the nonhomogeneous case, one obtains the reduced eigenvalue equations

$$[\mathbf{H}_{DF}^{*}\mathbf{F}_{FF}\mathbf{A}_{FD} - (1/\lambda)\mathbf{I}]\tilde{\mathbf{y}}_D = 0 \,. \tag{4.27}$$

The corresponding generalized forces, after solving for $\tilde{\mathbf{y}}_D$, are given by

$$\tilde{\mathbf{y}}_F = \lambda \mathbf{H}_{FF}^{*}\mathbf{F}_{FF}\mathbf{A}_{FD}\tilde{\mathbf{y}}_D \,. \tag{4.28}$$

Similar to Eq. (4.26), a useful form of the reduced eigenvalue problem in Eq. (4.27) is obtained by considering $\mathbf{H}_{FD} = 0$, which gives the result

$$[\mathbf{T}\mathbf{A}_{FD} - (1/\lambda)\mathbf{I}]\tilde{\mathbf{y}}_D = 0. \tag{4.29}$$

This form of the eigenvalue problem will be employed in later examples.

To complete the presentation of the reduced equations, it is useful for reference purposes to give the flutter eigenvalue problem that will be discussed in Chapter 7. The flutter equations, which will be written for the Laplace domain, are obtained in a manner similar to Eq. (4.29), except that they derive initially from Eq. (2.21) rather than Eq. (2.20). By taking $\mathbf{H}_{FD} = 0$, these equations can be written in the form

$$\left[\mathbf{I} + \mathbf{T}[\mathbf{M}_{FD}s^{*2} + \mathbf{C}_{FD}s^* - \mathbf{Q}_{FD}(s^*, \lambda)]\right]\hat{\mathbf{y}}_D = 0 \tag{4.30}$$

where $\mathbf{M}_{FD}$ is a mass matrix, $\mathbf{C}_{FD}$ is a damping matrix, and $\mathbf{Q}_{FD}$ is an unsteady aerodynamic matrix. The variables s^* and $\hat{\mathbf{y}}_D$ are, respectively, a nondimensional Laplace variable and a nondimensional complex eigenvector. The terms appearing in Eq. (4.30) will be defined in more detail in Chapter 7.

An important observation about the foregoing reductions is that although the required matrix inversions can be carried out numerically, they can often easily be avoided or simplified. This is possible because of the particularly simple block matrix structure of $\mathbf{H}$. For example, if $\mathbf{H}_{FD} = 0$, then the inversion of $\mathbf{H}$ is given by

$$\begin{bmatrix} \mathbf{H}_{FF} & \mathbf{0} \\ \mathbf{H}_{DF} & \mathbf{H}_{DD} \end{bmatrix}^{-1} = \begin{bmatrix} \mathbf{H}_{FF}^{-1} & \mathbf{0} \\ -\mathbf{H}_{DD}^{-1}\mathbf{H}_{DF}\mathbf{H}_{FF}^{-1} & \mathbf{H}_{DD}^{-1} \end{bmatrix}. \tag{4.31}$$

Furthermore, as a result of the structure of the hybrid state vector equations, inversions for $\mathbf{H}_{DD}$ and $\mathbf{H}_{FF}$ are trivially obtained. This is due in part to the

sparseness of these matrices. Further clarification of the inversion process will be offered in the examples of Chapter 5. As a final result, however, one will find it possible to write out the simple matrix expressions for the calculation of $\mathbf{T}$ and its product with other matrices.

Additional simplification of the reduced equations is possible for situations where constraint equations exist. The equations of constraint that will be applied in later chapters express simple relationships between solution variables. Such relationships between variables can be used to eliminate certain degrees of freedom by writing them in terms of other degrees of freedom. The methods for applying such constraints to the discrete state vector equations are presented in Appendix F.

Chapter 5

Solutions for Isotropic Beams and Rods

INTEGRATING MATRIX SOLUTIONS are most easily demonstrated with the aid of sample problems. This chapter, and the next two, present examples of how integrating matrix solutions can be used to solve a variety of problems in structural dynamics and aeroelasticity. These solutions are presented both to validate the methods discussed in Chapter 4, and to evaluate the accuracy and convergence trends of the integrating matrix solutions. Comparisons are made between the integrating matrix solutions and alternate analytical or numerical calculations. Among the items considered in the following examples are various types of boundary conditions and loading conditions, all of which commonly arise in performing practical vibration studies and aeroelastic analyses.

5.1 Axial Vibration of Cantilevered Rods

Axial vibration of a rod provides a simple example with which to study the integrating matrix solution process. Since axial rod vibration is described by a second order Sturm-Liouville differential equation, analytical solutions are available for comparison with numerical solutions. The integrating matrix solution properties presented for these simple Sturm-Liouville systems carry through to the much more complicated problems to be discussed later. Aeroelastic divergence of unswept

isotropic wings is also described by a similar Sturm-Liouville differential equation. Therefore, the fundamental eigenvalue of the following eigenvalue solutions can alternately be interpreted in terms of divergence dynamic pressure.

A nondimensional form of the second-order Sturm-Liouville problem describing axial rod vibration can be written as

$$\frac{d}{d\bar{x}}\left(\frac{1}{\tau}\frac{d\bar{u}}{d\bar{x}}\right) + \lambda \bar{m}\,\bar{u} = 0 \tag{5.1}$$

where

$$\begin{aligned} \bar{u}(\bar{x}) &= \frac{u}{\ell}, \qquad \bar{x} = \frac{x}{\ell}, \qquad \bar{m}(\bar{x}) = \frac{m}{m_R}, \\ \tau(\bar{x}) &= \frac{(EA)_R}{EA}, \\ \lambda &= \frac{\omega^2 m_R \ell^2}{(EA)_R}. \end{aligned} \tag{5.2}$$

For this simple differential equation, the dimensionless state vector form can be written down directly, yielding

$$\frac{d}{d\bar{x}}\begin{Bmatrix} F_u \\ \bar{u} \end{Bmatrix} = \begin{bmatrix} 0 & 0 \\ \tau & 0 \end{bmatrix}\begin{Bmatrix} F_u \\ \bar{u} \end{Bmatrix} - \lambda \begin{bmatrix} 0 & \bar{m} \\ 0 & 0 \end{bmatrix}\begin{Bmatrix} F_u \\ \bar{u} \end{Bmatrix} \tag{5.3}$$

where

$$F_u(\bar{x}) = \frac{1}{\tau}\frac{d\bar{u}}{d\bar{x}}. \tag{5.4}$$

If the rod is considered to be clamped at the end $\bar{x} = 0$, the cantilever boundary conditions for Eqs. (5.1) and (5.3) can also be specified as

$$\bar{u}(0) = 0, \qquad F_u(1) = 0. \tag{5.5}$$

The differential equations appearing in either Eq. (5.1) or Eq. (5.3) can be readily solved with an integrating matrix, as will be demonstrated next.

5.1.1 Rods with Continuous Mass and Stiffness

The first solution to be presented will consider axial vibration for a cantilevered rod that can have variable mass and stiffness parameters. Because of its simplicity, this problem serves as a good demonstration of the integrating matrix solution procedures. The integrating matrix will be applied first to the hybrid state vector equations given in Eq. (5.3). It is also instructive to demonstrate how the integrating matrix can be utilized to solve the differential equations given in the form of Eq. (5.1). Both types of solutions will be presented in detail to serve as models for other problems discussed in this chapter.

Beginning with the discretized form of the state vector equations in Eq. (5.3), the integrating matrix is applied as an operator to perform the necessary integrations. The next step is the application of boundary conditions to determine the boundary condition matrices $\tilde{\mathbf{B}}$ and $\tilde{\mathbf{B}}_{nh}$. From the boundary condition matrices follow the definitions for the other matrices appearing in Eqs. (4.10–4.13), which have the partitioned forms displayed in Eqs. (4.14–4.17). For example, in a homogeneous vibration problem, for which $\tilde{\mathbf{a}}_r = 0$, the $\mathbf{F}$ matrix is defined in terms of the given boundary condition matrices, followed by the determination of the $\mathbf{H}$ matrix.

For the axial vibration problem, an application of the global integrating matrix to the discretized version of Eq. (5.3) yields

$$\begin{Bmatrix} F_u \\ \overline{u} \end{Bmatrix} = \begin{bmatrix} \mathbf{L} & 0 \\ 0 & \mathbf{L} \end{bmatrix} \left\{ \begin{bmatrix} 0 & 0 \\ \grave{r} & 0 \end{bmatrix} \begin{Bmatrix} F_u \\ \overline{u} \end{Bmatrix} - \lambda \begin{bmatrix} 0 & \grave{\overline{m}} \\ 0 & 0 \end{bmatrix} \begin{Bmatrix} F_u \\ \overline{u} \end{Bmatrix} \right\} + \begin{Bmatrix} \mathbf{k}_F \\ \mathbf{k}_u \end{Bmatrix} \tag{5.6}$$

To make it convenient to solve for boundary conditions, Eq. (5.6) is easily expanded into the two sets of equations

$$\{F_u\} = -\lambda \mathbf{L}\grave{\overline{m}}\{\overline{u}\} + \mathbf{k}_F \tag{5.7}$$

$$\{\overline{u}\} = \mathbf{L}\grave{r}\{F_u\} + \mathbf{k}_u \,. \tag{5.8}$$

Applying the boundary condition $\overline{u}(0) = 0$ to Eq. (5.8) gives

$$\mathbf{b}_0^T\{\overline{u}\} = 0 = k_u \tag{5.9}$$

where use has been made of $\mathbf{b}_0^T\mathbf{L} = 0$ and $\mathbf{b}_0^T\mathbf{k}_u = k_u$. (Note, for example, that $\mathbf{k}_u = \vec{\mathbf{1}}k_u$, where $\vec{\mathbf{1}}$ is as defined in Eqs. (4.5) and (4.6).) In a similar manner, the boundary condition $F_u(1) = 0$ can be applied to Eq. (5.7), yielding the scalar solution

$$\mathbf{b}_n^T\{F_u\} = 0 = -\lambda\mathbf{b}_n^T\mathbf{L}\grave{}\,\overline{m}\{\overline{u}\} + k_F\,, \tag{5.10}$$

which can be converted to the vector form

$$\mathbf{k}_F = \lambda\mathbf{B}_n\mathbf{L}\grave{}\,\overline{m}\{\overline{u}\}\,. \tag{5.11}$$

From the results in Eqs. (5.9) and (5.11), the boundary condition matrix $\tilde{\mathbf{B}}$ appearing in Eq. (4.9) can be written as

$$\tilde{\mathbf{B}} = \begin{bmatrix} \mathbf{B}_n & 0 \\ 0 & 0 \end{bmatrix}. \tag{5.12}$$

For this problem, one also has that $\tilde{\mathbf{B}}_{nh} = 0$.

Having obtained expressions for the constant vector of integration, the partitioned matrices in Eqs. (4.14–4.16) are given, via Eqs. (4.10–4.12), as

$$\mathbf{H} = \begin{bmatrix} \mathbf{I} & 0 \\ -\mathbf{L}\grave{}\,\tau & \mathbf{I} \end{bmatrix} \tag{5.13}$$

$$\tilde{\mathbf{A}} = \begin{bmatrix} 0 & \grave{}\,\overline{m} \\ 0 & 0 \end{bmatrix} \tag{5.14}$$

$$\mathbf{F} = \begin{bmatrix} (\mathbf{B}_n - \mathbf{I})\mathbf{L} & 0 \\ 0 & -\mathbf{L} \end{bmatrix} = \begin{bmatrix} \mathbf{L}_1^* & 0 \\ 0 & -\mathbf{L} \end{bmatrix} \tag{5.15}$$

where $\mathbf{L}_1^*$ can be considered as a special type of integrating matrix. ($\mathbf{L}_1^*$ is actually the equivalent of what Vakhitov [26] refers to as a "type two" integrating matrix. To see the significance of this modified integrating matrix, one can write out the type of integration that it performs; namely,

$$\mathbf{B}_n\mathbf{L} - \mathbf{L} = \int_0^\ell - \int_0^x = \int_x^\ell . \tag{5.16}$$

Other such special integrating matrices will be defined for convenience sake in later problems. Each one will be assigned a different subscript that will serve to distinguish it.)

The matrices in Eqs. (5.13–5.15) can be used directly in Eq. (4.25) and Eq. (4.29) to obtain the reduced eigenvalue problem for free vibration. From Eq. (4.25), we obtain the result

$$\mathbf{T} = \mathbf{L}\grave{}\,\tau\mathbf{L}_1^* , \tag{5.17}$$

and from Eq. (4.29) the eigenvalue problem is

$$[\mathbf{L}\grave{}\,\tau\mathbf{L}_1^*\grave{}\,\overline{m} - (1/\lambda)\mathbf{I}]\{\overline{u}\} = 0 . \tag{5.18}$$

This result provides the eigenvalue problem for a cantilevered axial rod with variable stiffness and mass parameters. As can be seen, the eigenvalue problem is formed by specifying the integrating matrix and the corresponding discrete values for the diagonal matrices $\grave{}\,\tau$ and $\grave{}\,\overline{m}$.

For simple problems, such as the one considered here, an alternate approach that often proves very convenient is to apply the integrating matrix to the form of the equations given in Eq. (5.1), rather than utilizing the state vector form. A discrete form of Eq. (5.1) can be written as

$$\frac{d}{d\overline{x}}\{F_u\} + \lambda\grave{}\,\overline{m}\{\overline{u}\} = 0 . \tag{5.19}$$

Applying the integrating matrix to Eq. (5.19) yields

$$\{F_u\} + \lambda \mathbf{L}\grave{}\,\overline{m}\{\overline{u}\} = \mathbf{k}_F. \tag{5.20}$$

Now multiplying this result through by the diagonal matrix $\grave{}\,\tau$ to isolate another derivative term gives

$$\frac{d}{d\overline{x}}\{\overline{u}\} + \lambda\grave{}\,\tau\mathbf{L}\grave{}\,\overline{m}\{\overline{u}\} = \grave{}\,\tau\mathbf{k}_F\,. \tag{5.21}$$

Another application of the integrating matrix then produces the result

$$\{\overline{u}\} + \lambda\mathbf{L}\grave{}\,\tau\mathbf{L}\grave{}\,\overline{m}\{\overline{u}\} = \mathbf{L}\grave{}\,\tau\mathbf{k}_F + \mathbf{k}_u. \tag{5.22}$$

If Eq. (5.22) is multiplied through by $\mathbf{b}_0^T$, then use of the boundary condition $\overline{u}(0) = 0$ gives, as before, $\mathbf{k}_u = 0$. Similarly, multiplying Eq. (5.20) by $\mathbf{b}_n^T$ and using $F_u(1) = 0$ leads to the result in Eq. (5.11). Substituting these results for the constant vectors into Eq. (5.22) and rearranging gives the eigenvalue problem presented in Eq. (5.18).

From the eigenvalue problem given by Eq. (5.18), results can be obtained for either uniform or variable property rods. For the case of a uniform rod, the matrices $\grave{}\,\tau$ and $\grave{}\,\overline{m}$ are simply identity matrices. The numerical calculation of the eigenvalues and eigenvectors can make use of standard eigenvalue routines. For the examples presented, the computations were carried out on an IBM 3033. The calculations that form the matrix for the eigenvalue problem were performed in single precision arithmetic, and the eigenvalues and eigenvectors of the resulting real, nonsymmetric matrix were calculated with a reliable double precision routine available in the EISPACK eigenvalue package (see Smith [44]). Calculations were performed for both Jacobi and Newton integrating matrices, with the number of discretization intervals N varying from two to five. For each level of discretization, the maximum order integrating matrix was used for the given number of collocation points $(N + 1)$.

The numerical solutions for axial vibration of both uniform and linearly tapered rods were compared with analytical solutions. For the uniform rod, analytical solutions for the constant coefficient Sturm-Liouville problem can be found in Section 3.5 of Bisplinghoff, Ashley, and Halfman [45]. For linearly tapered rods, useful analytical solutions for the eigenvalues of the homogeneous differential equation are are given in closed form by Hildebrand and Reissner [46]. (These solutions are also repeated in Ref. [45], pp. 432–434.)

In the case of the uniform rod, results for the axial frequencies obtained with both Newton and Jacobi integrating matrices are presented in Table 1 at the end of this chapter. Also presented in Table 1 are the percentage errors between the approximate integrating matrix results and the exact analytical solutions. Fig. 4 gives a display of these percentage errors for the first three vibrational modes. As can be seen by comparing the frequency errors, both Newton and Jacobi solutions provide highly accurate results despite the relatively crude discretization. It is also clear that for those frequencies that are nearing convergence, the Jacobi solutions are more accurate than those provided by the Newton solutions. For the uniform rod, the frequencies given by the Jacobi integrating matrices always converge from above to the exact frequencies, unlike the oscillatory convergence of the Newton solutions. Since all of the available frequencies are displayed for each discretization level, it is useful to note how the higher frequencies behave as the discretization level increases. For the Jacobi solutions, it is apparent that each newly introduced modal frequency is quite high compared to the exact result, but rapidly converges to the correct solution as new discretization intervals are introduced. In comparison, each newly introduced Newton solution frequency is not as high, but the convergence to the correct result tends to be somewhat oscillatory. These convergence trends for uniform parameter systems are also evident in additional solutions to be presented in the following sections. Aside from the finer details of convergence, however, both

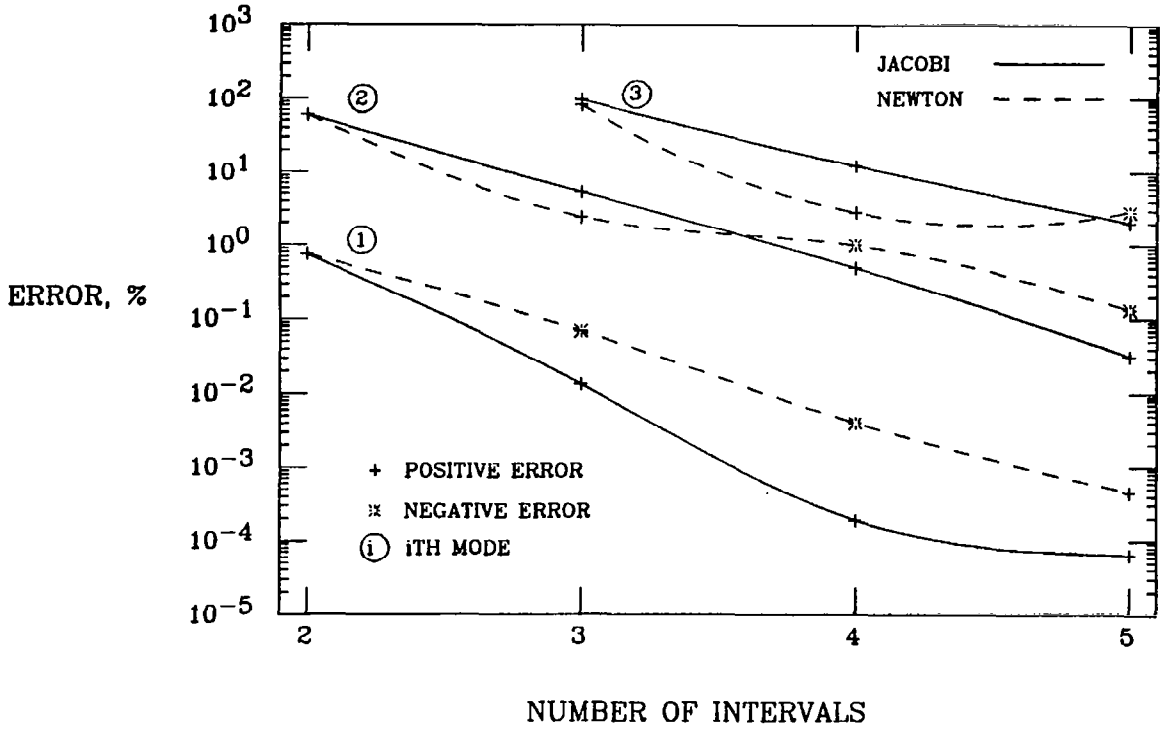

Fig. 4. Error in computed frequencies, compared to exact solutions, for the first three axial modes of a uniform cantilevered rod. The error for both Jacobi and Newton integrating matrix solutions is plotted vs. the number of collocation intervals N.

Newton and Jacobi solutions have the capability to provide accurate results for the lower frequencies without requiring a highly refined mesh of grid points.

For the uniform axial rod vibration just discussed, Table 2 gives the first three axial mode shapes. Results are shown for both Newton and Jacobi integrating matrix solutions based on five collocation intervals. Since the Newton solutions make use of evenly spaced collocation points, the Newton based mode shapes in Table 2 are simply presented for these collocation points without interpolation being required. On the other hand, the Jacobi solutions have been interpolated to these evenly spaced points with the same order Jacobi polynomial used in the solution. The results of performing such an interpolation are less than satisfactory since it appears that the Jacobi mode shapes in Table 2 are less accurate than the Newton results. But in fact, it is easily shown that the Jacobi mode shapes are quite accurate if evaluated at the Jacobi collocation points. This behavior emphasizes an important aspect of interpolation processes in general. Due to the fact that interpolation error is itself an oscillatory function, the highest accuracy for the interpolated displacement solutions can be expected to occur at the collocation points, and the largest error will occur between the collocation points. The same conclusion is reached if the Newton solutions are interpolated to the unevenly spaced Jacobi points. This all seems to suggest, not unexpectedly, that if mode shape results must be interpolated, it is probably better to use a localized least squares procedure based on a slightly lower order polynomial approximation.

Vibration frequencies for a linearly tapered rod can be easily determined from Eq. (5.18) after introducing the following variables to describe the taper. First, the taper ratio of the rod is defined to be $(1 - \beta_t)$, where β_t is the taper parameter. Each dimension in the cross section of the rod varies linearly as $(1 - \beta_t \bar{x})$. For this description of the taper, it follows that the mass and stiffness parameters m and EA appearing in Eq. (5.2) can be written as

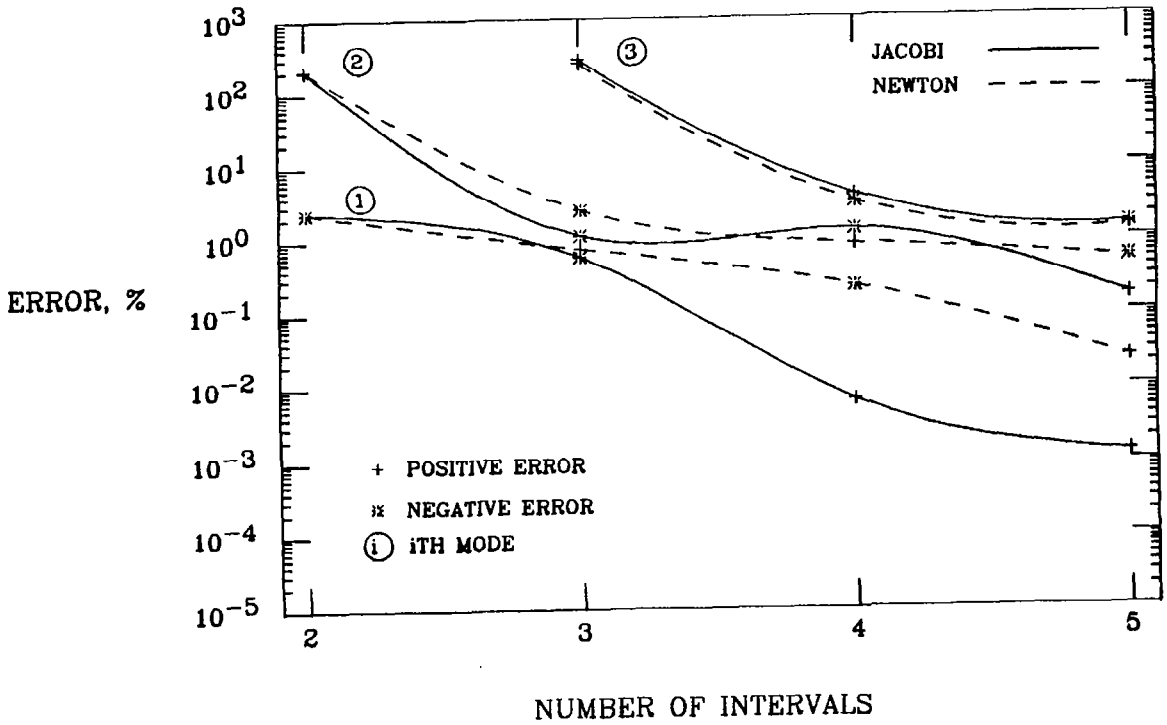

Fig. 5. Error in computed frequencies, compared to exact solutions, for the first three axial modes of a linearly tapered cantilevered rod with a taper ratio of one half ($\beta_t = 0.5$). The error for both Jacobi and Newton integrating matrix solutions is plotted vs. the number of collocation intervals N.

$$m = m_R(1 - \beta_t \bar{x})^2,$$
$$EA = (EA)_R(1 - \beta_t \bar{x})^4. \tag{5.23}$$

Using these definitions for the mass and stiffness, the frequencies of a linearly tapered rod with $\beta_t = 0.5$ are given in Table 3. The percentage errors between the exact solutions and the integrating matrix solutions are also displayed in Fig. 5 for the first three vibrational modes. As evident from the eigenvalue error results, neither the Jacobi nor the Newton solutions converge quite as rapidly as in the uniform rod case, which is to be expected. For this linearly tapered rod, the Jacobi results do not necessarily converge to the exact frequencies from above as they do for uniform parameter problems. Nonetheless, the convergence of the Jacobi solutions is quite predictable in that all modes, except the first, appear at a high frequency and only very slightly overshoot on the negative side enroute to converging. The Jacobi solutions still provide faster convergence to the lower modes. In contrast, the Newton solutions retain their oscillatory convergence character, with the frequency error changing sign for each added collocation interval. Aside from this oscillatory behavior, the magnitude of the Newton solution errors can be considered quite small. It is well known that one cannot always guarantee convergence from above for eigenvalues obtained from a collocation procedure. The fact that there are sign changes in the error of both Jacobi and Newton frequencies for this nonuniform parameter problem is indicative of the collocation nature of the integrating matrix solutions.

5.1.2 Rods with Discontinuous Mass and Stiffness

Because of the common occurrence of structural elements with parameter discontinuities, it is useful to examine the hybrid state vector technique as applied to axial vibration of rods having stepwise jumps in mass and stiffness. The eigenvalue

problem for a discontinuous rod is still given by Eq. (5.18), which was originally derived for continuous parameter rods. The only difference arises in the proper specification of the integrating matrix and the diagonal coefficient matrices $`\tau$ and $`\overline{m}$. The methods for specifying the integrating matrix and the corresponding function values for a discontinuous integrand were discussed in Section 3.2.

To allow comparison with alternate solutions, the problem chosen for discontinuous axial rod vibration is the same as a problem discussed by Hodges [47], in which solutions were obtained by a Ritz method. The cantilevered rod, which is normalized to unit length and clamped at $\bar{x} = 0$, is divided into three segments. The first segment extends from $\bar{x} = 0$ to $\bar{x} = 0.25$, the second segment from 0.25 to 0.75, and the third segment from 0.75 to 1.0. Mass and stiffness parameters in the first and third segments are assigned the same values, and within each segment the parameters are assumed constant. The ratios between the parameters of the different segments are given by

$$\bar{\gamma} = \frac{(EA)_2}{(EA)_1} = \frac{\tau_1}{\tau_2}, \qquad \bar{\theta} = \frac{\overline{m}_2}{\overline{m}_1}, \tag{5.24}$$

where

$$\begin{aligned} \tau_1 = \tau_3 &= \frac{1+\bar{\gamma}}{2}, \\ \overline{m}_1 = \overline{m}_3 &= \frac{2}{1+\bar{\theta}}. \end{aligned} \tag{5.25}$$

Thus, when $\bar{\gamma} = 1$ and $\bar{\theta} = 1$ there is no discontinuity in the parameters.

Integrating matrix solutions are obtained for the discontinuous case by calculating an integrating matrix for the piecewise integration of the three segments. Maximum order weighting matrices are assumed in this calculation. An equal number of collocation intervals are used for each segment; thus, it is appropriate to describe the solution in terms of the number of intervals per segment.

For $\bar{\gamma} = 10$ and $\bar{\theta} = 100$ the results are presented in Table 4 for the axial frequencies obtained with both Jacobi and Newton integrating matrices. Fig. 6 displays for the first three vibrational modes the percentage error between the exact solutions (Ref. [47]) and the integrating matrix solutions. Similar to the earlier discovery for uniform axial rod vibration, the Jacobi solutions for a piecewise uniform rod offer the advantage of a rapid, monotonic convergence to the exact result from above. From a practical viewpoint, either the Jacobi or the Newton integrating matrix yields highly accurate results without requiring an extremely fine mesh of grid points.

An interesting point to notice in Fig. 6 is that the eigenvalue error for the fundamental mode bottoms out and then begins to rise slightly. The reason for this occurrence is that the numerical precision limit has been reached for the calculation of this eigenvalue. As a consequence, the last digits of the result change rather than remaining exactly at the converged value. D.H. Hodges (in a private communication) stated that this same phenomenon was encountered when obtaining similar high accuracy solutions with a variable order Ritz finite element method. The apparent cure for this is to increase the precision level of the computations.

Because integrating matrices with end points were used to solve this problem, one should note that two identically located collocation points are present at each discontinuity. Since the solution values will be identical for each of these points, a constraint is available that can be used to eliminate the solution degrees of freedom at one of the points. The rectangular transformation matrix resulting from this constraint can be applied as discussed in Appendix F. It turns out that this transformation matrix, which consists only of ones and zeroes, produces a diagonal matrix when premultiplied by its transpose. Therefore, the pseudoinverse mentioned in Appendix F can be obtained quite simply. It should be pointed out, however, that for small sized problems it is not necessary, and generally not worth

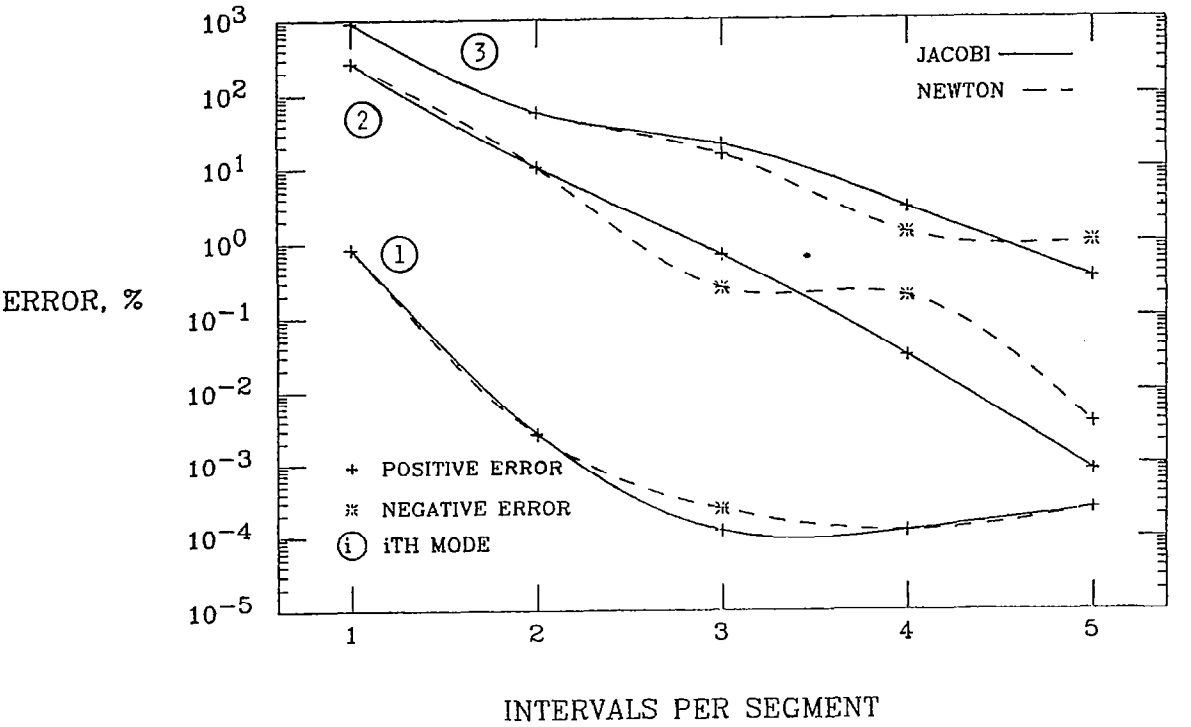

Fig. 6. Error in computed frequencies, compared to exact solutions, for the first three axial modes of a cantilevered rod with discontinuous stiffness and mass ($\overline{\gamma} = 10$; $\overline{\theta} = 100$). The rod has three uniform segments between the points $\overline{x} = 0, .25, .75, 1$. The error for the integrating matrix solutions is plotted vs. the number of collocation intervals per segment N.

the trouble, to apply this constraint. The exception would be a large sized problem. In that case one might expect a significant reduction in the number of degrees of freedom present in the solution.

A final note concerning axial vibration of a discontinuous rod is that solutions were also tried in which the discontinuities were ignored. That is, an integrating matrix was used which allowed the integrations (i.e., the interpolations) to proceed across the discontinuity boundaries. As expected, the eigenvalue solutions approached the exact results when enough collocation points were taken. Although a reasonably accurate solution for the fundamental mode could be obtained without too much effort, matching the accuracies of Table 4 for the higher modes required a somewhat larger number of collocation points. Furthermore, the convergence with this approach was highly oscillatory for some modes and seemed unpredictable for anything but the fundamental mode.

5.1.3 Rods with Elastic Restraint

A type of boundary condition that occurs quite often is that of elastic restraint. Methods for handling this type of boundary condition are easily demonstrated for a uniform axial rod. It will be assumed that the axial modes of vibration are to be found for a rod that is cantilevered at one end and has an axial spring restraint at the opposite end. Fig. 7 illustrates a rod with these boundary conditions. Since the axial restraining spring applies a force to the rod that is proportional to the displacement at the end of the rod, the boundary condition can be included as a displacement dependent loading in the $\mathbf{A}_{FD}$ submatrix of Eq. (4.15). In the present example, however, the restraint will be introduced instead through the nonhomogeneous boundary condition matrix $\tilde{\mathbf{B}}_{nh}$.

The nondimensional equations describing the rod are given by Eqs. (5.3–5.4)

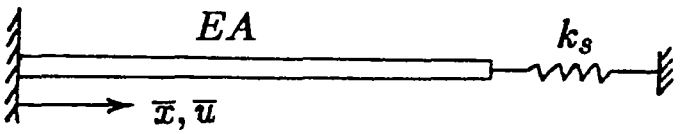

Fig. 7. A cantilevered axial rod with a spring restraint boundary condition

and Eqs. (5.6–5.8). Boundary conditions for the rod are

$$\bar{u}(0) = 0\,, \qquad F_u(1) = -\bar{k}_s \bar{u}(1)\,, \tag{5.26}$$

where

$$\bar{k}_s = \frac{k_s}{(EA)_R}\,. \tag{5.27}$$

As the nondimensional restraining spring stiffness $\bar{k}_s$ varies from zero to infinity, the boundary conditions for the rod vary from cantilevered to clamped-clamped.

Solutions for this problem are obtained by the same approach as presented in Section 5.1.1. In fact, the only changes to be made are to the boundary condition solution in Eqs. (5.10–5.11) and to the **H** matrix in Eq. (5.13). The boundary condition solution for the spring restrained end is given by

$$\mathbf{b}_n^T\{F_u\} = -\bar{k}_s \mathbf{b}_n^T\{\bar{u}\} = -\lambda \mathbf{b}_n^T \mathbf{L}^{\backprime} \bar{m}\{\bar{u}\} + k_F\,, \tag{5.28}$$

which yields the vector form

$$\mathbf{k}_F = \lambda \mathbf{B}_n \mathbf{L}^{\backprime} \bar{m}\{\bar{u}\} - \bar{k}_s \mathbf{B}_n\{\bar{u}\}\,. \tag{5.29}$$

From this result, one finds that the boundary condition matrix $\tilde{\mathbf{B}}$ is still given by Eq. (5.12), and the nonhomogeneous boundary condition matrix is now given by

$$\tilde{\mathbf{B}}_{nh} = \begin{bmatrix} 0 & \bar{k}_s \mathbf{B}_n \\ 0 & 0 \end{bmatrix}. \tag{5.30}$$

With the definition for $\mathbf{H}$ in Eq. (4.11), the replacement for Eq. (5.13) is found to be

$$\mathbf{H} = \begin{bmatrix} \mathbf{I} & \bar{k}_s \mathbf{B}_n \\ -\mathbf{L}`\tau & \mathbf{I} \end{bmatrix}. \tag{5.31}$$

If one now makes use of Eq. (4.27), along with Eqs. (5.14–5.15), the eigenvalue problem can be written as

$$[\mathbf{I}^* \mathbf{L}`\tau \mathbf{L}_1^{*}` \overline{m} - (1/\lambda)\mathbf{I}]\{\overline{u}\} = 0 \tag{5.32}$$

where

$$\mathbf{I}^* = [\mathbf{I} + \bar{k}_s \mathbf{L}`\tau \mathbf{B}_n]^{-1}. \tag{5.33}$$

The eigenvalue problem in Eq. (5.32) applies to vibration of a nonuniform rod and can be solved for any value of restraining spring stiffness.

Although it might appear to be a formidable task, it is actually quite easy to analytically invert the expression in Eq. (5.33), and thus obtain a simpler form for the eigenvalue problem. The reason that Eq. (5.33) can be easily simplified is that $\mathbf{B}_n$ contains unit terms only in the last row, and zeroes elsewhere. Thus, for all practical purposes, the second expression in the summation of Eq. (5.33) yields a vector. This allows easy inversion of the entire matrix when applying inversion by matrix partitioning. In general terms, one can write

$$[\mathbf{I} + \bar{k}_s \mathbf{L}`\tau \mathbf{B}_n] = \begin{bmatrix} \mathbf{I} & \vec{e}_1 \\ 0 & e_2 \end{bmatrix} \tag{5.34}$$

where the matrix has been partitioned such that e_2 is a scalar and $\vec{e}_1$ is a vector. The inverse of Eq. (5.34) is

$$\mathbf{I}^* = \begin{bmatrix} \mathbf{I} & -\vec{e}_1/e_2 \\ 0 & 1/e_2 \end{bmatrix}. \tag{5.35}$$

This result can be conveniently written in the form

$$\mathbf{I}^* = [\mathbf{I} - v\bar{k}_s \mathbf{L}\grave{}\, r\mathbf{B}_n] \tag{5.36}$$

where

$$v = \frac{1}{e_2} = \frac{1}{1 + \bar{k}_s \mathbf{b}_n^T \mathbf{L}\grave{}\, r\vec{\mathbf{1}}}. \tag{5.37}$$

For the case of a uniform rod ($\grave{}\, r = \grave{}\, \overline{m} = \mathbf{I}$), the eigenvalue problem given by Eq. (5.32), in conjunction with Eq. (5.36), can be written as

$$[\mathbf{I}^* \mathbf{L}\mathbf{L}_1^* - (1/\lambda)\mathbf{I}]\{\overline{u}\} = 0 \tag{5.38}$$

where

$$\mathbf{I}^* = \left[\mathbf{I} - \frac{\bar{k}_s}{1 + \bar{k}_s} \mathbf{L}\mathbf{B}_n\right]. \tag{5.39}$$

Note that in obtaining Eq. (5.39) from Eq. (5.37) a special identity was used; namely,

$$\mathbf{b}_n^T \mathbf{L}\vec{\mathbf{1}} = 1. \tag{5.40}$$

This identity applies when the integrating matrix has been written for a normalized interval of unit length. It is well worth remembering this identity since it appears often in solving for various types of boundary conditions.

Exact eigenvalues for the uniform cantilevered rod with spring restraint are easily found by analytically solving the differential equations. It can be shown that

the eigenvalues are given by the roots of the transcendental equation

$$\bar{k}_s \tan\sqrt{\lambda} + \sqrt{\lambda} = 0, \tag{5.41}$$

and the corresponding axial mode shapes are obtained from

$$\bar{u}(\bar{x}) = C \sin\sqrt{\lambda}\,\bar{x}. \tag{5.42}$$

For the exact solutions, as $\bar{k}_s \to 0$, $\sqrt{\lambda} \to n\pi/2$, with $n = 1,3,5,\ldots,\infty$. This is the result for a purely cantilevered rod. On the other hand, as $\bar{k}_s \to \infty$, $\sqrt{\lambda} \to n\pi$, with $n = 0,1,2,\ldots,\infty$, which is the solution for a rod clamped at both ends.

Presented in Table 5 for a uniform rod are nondimensional frequencies calculated from Eq. (5.38). Comparisons are made with the exact results of Eq. (5.41). The frequencies are presented for the first three modes and are calculated for several values of the restraint spring stiffness $\bar{k}_s$. These calculations make use of a Jacobi integrating matrix corresponding to six collocation points. The exact frequencies listed under $\bar{k}_s = 1 \times 10^6$ actually correspond to $\bar{k}_s = \infty$. This gives a valid comparison with the integrating matrix solutions since values of the spring stiffness larger than 1×10^6 produce no significant changes in the integrating matrix results when using single precision calculations.

5.1.4 Rods with Concentrated Mass

Another important example deals with the vibration of rods having concentrated mass points in addition to continuously distributed mass properties. The approach to solving problems with concentrated masses involves a simple extension of methods already presented for continuous parameter problems. This extension of the foregoing methods is presented in Appendix E, which discusses the treatment

of any type of concentrated loading. For the problem at hand, the point loads arise from concentrated masses.

The problem to be considered in this section is the axial vibration of a cantilevered rod with a tip mass. The method of solution will be that of Appendix E, but one should note that for this particular problem the mass provides a tip boundary condition that can also be handled with the approach given in the previous section. Since the solution turns out to be an extension of that presented in Section 5.1.1, the matrices defined in Eqs. (5.13–5.15) still apply. To account for the concentrated inertia loads, however, it is necessary to include from Eq. (E.11) the matrix

$$\mathbf{F}^{+} = \begin{bmatrix} (\mathbf{B}_n - \mathbf{I})\boldsymbol{S} & 0 \\ 0 & -\boldsymbol{S} \end{bmatrix} = \begin{bmatrix} \boldsymbol{S}_1^{*} & 0 \\ 0 & -\boldsymbol{S} \end{bmatrix}. \tag{5.43}$$

Notice that this matrix is the same as $\mathbf{F}$ in Eq. (5.15) with the summing matrix $\boldsymbol{S}$ substituted for the integrating matrix. A second matrix that must be added is the matrix containing the concentrated mass terms specified at the collocation points. For the problem under consideration this matrix is

$$\mathbf{A}_{FD}^{+} = \begin{bmatrix} 0 & & \\ & \ddots & \\ & & \overline{m}_n^{+} \end{bmatrix} = \grave{}\,\overline{m}_n^{+} \tag{5.44}$$

where $\overline{m}_n^{+} = m_n/m_R\ell$ is the tip mass nondimensionalized by the total mass of a reference rod (i.e., m_n is a total mass and m_R is a running mass). With the matrices defined in Eqs. (5.43–5.44), the eigenvalue problem given by Eq. (E.16) can be written as

$$[(\mathbf{L}\grave{}\,r\mathbf{L}_1^{*}\grave{}\,\overline{m} + \mathbf{L}\grave{}\,r\boldsymbol{S}_1^{*}\grave{}\,\overline{m}_n^{+}) - (1/\lambda)\mathbf{I}]\{\overline{u}\} = 0. \tag{5.45}$$

This eigenvalue problem is the extension of Eq. (5.18) to include point mass terms. For a uniform beam, Eq. (5.45) simplifies to

$$[(\mathbf{L}\mathbf{L}_1^* + \mathbf{L}\mathbf{S}_1^* \overline{m}_n^+) - (1/\lambda)\mathbf{I}]\{\overline{u}\} = 0 \tag{5.46}$$

where it should be noted that the lumped tip mass will only affect terms in the last column of the matrix from which the eigenvalues are found.

Exact solutions for the eigenvalues of a similar Sturm-Liouville problem can be found in Section 5.9 of Meirovitch [42]. The transcendental equation for the eigenvalues is given by

$$\sqrt{\lambda}\tan\sqrt{\lambda} - 1/\overline{m}_n^+ = 0. \tag{5.47}$$

Upon examining this equation, one finds that when $m_n \to 0$, then $\sqrt{\lambda} \to n\pi/2$, with $n = 1, 3, 5, \ldots, \infty$. Similarly, as $m_n \to \infty$, $\sqrt{\lambda} \to n\pi$, with $n = 0, 1, 2, \ldots, \infty$. In physical terms, as the tip mass tends to zero, the eigenvalue solution reduces to that for a simple cantilever rod. As the tip mass grows very large, the solution approaches that for a rod clamped at both ends.

Table 6 gives for a uniform rod the nondimensional frequencies calculated from Eq. (5.46). Comparisons are made with the exact results of Eq. (5.47). The frequencies are given for the first three modes and are calculated for several values of the tip mass ratio $\overline{m}_n^+$. Calculations are based on a Jacobi integrating matrix corresponding to six collocation points. The exact frequencies that are listed under $\overline{m}_n^+ = 1 \times 10^8$ actually correspond to $\overline{m}_n^+ = \infty$. This gives a valid comparison with the integrating matrix solutions since values of the tip mass ratio larger than 1×10^8 produce no further changes in the integrating matrix results when using single precision calculations.

5.2 Bending Vibration of Beams

Applications of the hybrid state vector approach are now examined for beam vibration problems. Since beam vibration analyses are so common in structural dynamics and aeroelasticity, it is useful to give them a separate treatment. The following problems demonstrate the application of hybrid state vector techniques to the lateral vibration of beams with various type of boundary conditions, including unrestrained beams possessing rigid body modes. Sample results are presented for uniform beams.

The differential equations that describe lateral vibration of isotropic beams are well known. Rather than rederiving the nondimensional state vector equations, they can be extracted from the anisotropic beam equations given in Section 2.3. After including inertia terms and neglecting transverse shear effects, the appropriate equations can be written as

$$\frac{d}{d\bar{x}}\begin{Bmatrix}\overline{M}\\ \overline{V}\\ \gamma\\ \overline{w}\end{Bmatrix}=\begin{bmatrix}0 & 1 & 0 & 0\\ 0 & 0 & 0 & 0\\ \overline{EI} & 0 & 0 & 0\\ 0 & 0 & -1 & 0\end{bmatrix}\begin{Bmatrix}\overline{M}\\ \overline{V}\\ \gamma\\ \overline{w}\end{Bmatrix}-\lambda\begin{bmatrix}0 & 0 & 0 & 0\\ 0 & 0 & 0 & \overline{m}\\ 0 & 0 & 0 & 0\\ 0 & 0 & 0 & 0\end{bmatrix}\begin{Bmatrix}\overline{M}\\ \overline{V}\\ \gamma\\ \overline{w}\end{Bmatrix} \tag{5.48}$$

where

$$\overline{EI}=\frac{(EI)_R}{EI}, \qquad \overline{m}=\frac{m}{m_R}, \tag{5.49}$$

and

$$\lambda=\frac{\omega^2 m_R \ell^4}{(EI)_R}. \tag{5.50}$$

Other nondimensional terms are as defined in Eq. (2.29) and Eq. (2.31), with c taken to have unit value for a beam.

Irrespective of boundary conditions, one can begin the solution of Eq. (5.48) by discretizing, multiplying through by the global integrating matrix, and adding the constant vector of integration. In a manner analogous to Eqs. (5.6–5.8), this result can be expanded into the set of equations

$$\{\overline{M}\} = \mathbf{L}\{\overline{V}\} + \mathbf{k}_m \tag{5.51}$$

$$\{\overline{V}\} = -\lambda \mathbf{L}\grave{}\,\overline{m}\{\overline{w}\} + \mathbf{k}_v \tag{5.52}$$

$$\{\gamma\} = \mathbf{L}\grave{}\,\overline{EI}\{\overline{M}\} + \mathbf{k}_\gamma \tag{5.53}$$

$$\{\overline{w}\} = -\mathbf{L}\{\gamma\} + \mathbf{k}_w\,. \tag{5.54}$$

Boundary conditions can be applied to these equations to solve for the constant vectors of integration.

The basic approach to be used in solving for the constants of integration of two-point boundary value problems is demonstrated in Section 5.1.1. Only the important aspects of boundary condition determination will be addressed in detail in the following problems. It is worth noting, however, that there is a recommended procedure to simplify the solution for boundary conditions. One should first apply any homogeneous or nonhomogeneous boundary conditions at the end $\overline{x} = 0$. It is assumed that this end is the starting point for the integrations performed by the integrating matrix. The second step is to apply boundary conditions at the point $\overline{x} = 1$ (assuming, of course, a normalized interval $\overline{x} = [0, 1]$). This second step often involves applying boundary conditions to state variables that were already used in the boundary conditions at $\overline{x} = 0$. When this occurs, one must express these variables in terms of the remaining unused variables to insure that all unknown constants are determined. An important requirement when solving for constants of integration is that the resulting boundary condition matrix $\tilde{\mathbf{B}}$ be block diagonal.

5.2.1 Cantilevered Beam

A cantilevered beam offers simple boundary conditions from which the constants of integration are readily determined from Eqs. (5.51–5.54). The boundary conditions to be satisfied are given by

$$\gamma(0) = 0, \qquad \overline{w}(0) = 0, \qquad \overline{M}(1) = 0, \qquad \overline{V}(1) = 0. \tag{5.55}$$

It is clear from the first two conditions that $\mathbf{k}_\gamma = \mathbf{k}_w = 0$. The boundary conditions at the free end of the beam yield

$$\mathbf{k}_m = -\mathbf{B}_n \mathbf{L}\{\overline{V}\} \tag{5.56}$$

$$\mathbf{k}_v = \lambda \mathbf{B}_n \mathbf{L}^{`} \overline{m}\{\overline{w}\}. \tag{5.57}$$

With these constants determined, one finds that

$$\mathbf{F} = \begin{bmatrix} (\mathbf{B}_n - \mathbf{I})\mathbf{L} & 0 & 0 & 0 \\ 0 & (\mathbf{B}_n - \mathbf{I})\mathbf{L} & 0 & 0 \\ 0 & 0 & -\mathbf{L} & 0 \\ 0 & 0 & 0 & -\mathbf{L} \end{bmatrix} = \begin{bmatrix} \mathbf{L}_1^* & 0 & 0 & 0 \\ 0 & \mathbf{L}_1^* & 0 & 0 \\ 0 & 0 & -\mathbf{L} & 0 \\ 0 & 0 & 0 & -\mathbf{L} \end{bmatrix} \tag{5.58}$$

and as a result,

$$\mathbf{H} = \begin{bmatrix} \mathbf{I} & \mathbf{L}_1^* & 0 & 0 \\ 0 & \mathbf{I} & 0 & 0 \\ -\mathbf{L}^{`}\overline{EI} & 0 & \mathbf{I} & 0 \\ 0 & 0 & \mathbf{L} & \mathbf{I} \end{bmatrix} \tag{5.59}$$

From Eq. (4.25), one then obtains

$$\mathbf{T} = \begin{bmatrix} \mathbf{L}^{`}\overline{EI}\mathbf{L}_1^* & -\mathbf{L}^{`}\overline{EI}\mathbf{L}_1^{*2} \\ -\mathbf{L}^{2`}\overline{EI}\mathbf{L}_1^* & \mathbf{L}^{2`}\overline{EI}\mathbf{L}_1^{*2} \end{bmatrix} \tag{5.60}$$

which, when substituted into Eq. (4.29), yields the eigenvalue problem

$$[\mathbf{L}^{2\backprime}\overline{EI}\mathbf{L}_1^{*2\backprime}\overline{m} - (1/\lambda)\mathbf{I}]\{\overline{w}\} = 0. \tag{5.61}$$

This simplifies for a uniform beam since $\backprime\overline{EI}$ and $\backprime\overline{m}$ are then identity matrices. It should be noted that the row and column of Eq. (5.61) corresponding to the constrained lateral displacement at the fixed end can be deleted before solving for the eigenvalues and eigenvectors.

Results are presented in Table 7 for the nondimensional frequencies of a uniform cantilevered beam. The numerically computed results are based on a Jacobi integrating matrix for five collocation intervals and are compared with exact results tabulated by Hunter [27]. One can also refer to Hunter for detailed Newton integrating matrix solutions of the cantilevered beam problem.

Mode shapes corresponding to the first three modes of the Jacobi solutions are given in Table 8. The accuracy of the higher modes can be improved further by adding rotary inertia and transverse shear terms to the analysis. The mode shapes in Table 8 were interpolated to the evenly spaced grid points with a Jacobi polynomial of the same order used in the integrating matrix solution. Some of the aspects of this type of interpolation are discussed in Section 5.1.1.

5.2.2 Simply Supported Beam

A simply supported beam requires boundary conditions to be applied to both moment and lateral displacement variables at both ends of the beam. The familiar boundary conditions for a simply supported beam are concisely stated as

$$\overline{M}(0) = 0, \qquad \overline{w}(0) = 0, \qquad \overline{M}(1) = 0, \qquad \overline{w}(1) = 0. \tag{5.62}$$

The boundary conditions at $\bar{x} = 0$ applied to Eqs. (5.51) and (5.54) yield immediately

$$\bar{k}_m = \bar{k}_w = 0. \tag{5.63}$$

To apply boundary conditions at $\bar{x} = 1$, it is necessary to write expressions for $\overline{M}$ and $\overline{w}$ in terms of the other unknown constants appearing in Eqs. (5.52) and (5.53). These expressions are

$$\{\overline{M}\} = \mathbf{L}(-\lambda \mathbf{L}\grave{}\,\overline{m})\{\overline{w}\} + \mathbf{L}\mathbf{k}_v \tag{5.64}$$

$$\{\overline{w}\} = -\mathbf{L}(\mathbf{L}\grave{}\,\overline{EI})\{\overline{M}\}w - \mathbf{L}\mathbf{k}_\gamma. \tag{5.65}$$

After applying the boundary conditions at $\bar{x} = 1$ and making use of the two identities $\mathbf{k}_j = \vec{\mathbf{1}}k_j$ and $\mathbf{b}_n^T\mathbf{L}\vec{\mathbf{1}} = 1$, one obtains the results

$$\begin{aligned} \mathbf{k}_v &= -\mathbf{B}_n\mathbf{L}(\lambda\mathbf{L}\grave{}\,\overline{m})\{\overline{w}\} \\ \mathbf{k}_\gamma &= -\mathbf{B}_n\mathbf{L}(\mathbf{L}\grave{}\,\overline{EI})\{\overline{M}\}, \end{aligned} \tag{5.66}$$

which leads to

$$\mathbf{F} = \begin{bmatrix} -\mathbf{L} & 0 & 0 & 0 \\ 0 & (\mathbf{B}_n\mathbf{L} - \mathbf{I})\mathbf{L} & 0 & 0 \\ 0 & 0 & (\mathbf{B}_n\mathbf{L} - \mathbf{I})\mathbf{L} & 0 \\ 0 & 0 & 0 & -\mathbf{L} \end{bmatrix} = \begin{bmatrix} -\mathbf{L} & 0 & 0 & 0 \\ 0 & \mathbf{L}_2^* & 0 & 0 \\ 0 & 0 & \mathbf{L}_2^* & 0 \\ 0 & 0 & 0 & -\mathbf{L} \end{bmatrix}. \tag{5.67}$$

From Eq. (5.67), one then obtains in the manner of Section 5.2.1 that

$$\mathbf{T} = \begin{bmatrix} \mathbf{L}_2^*\grave{}\,\overline{EI}\mathbf{L} & -\mathbf{L}_2^*\grave{}\,\overline{EI}\mathbf{L}\mathbf{L}_2^* \\ -\mathbf{L}\mathbf{L}_2^*\grave{}\,\overline{EI}\mathbf{L} & \mathbf{L}\mathbf{L}_2^*\grave{}\,\overline{EI}\mathbf{L}\mathbf{L}_2^* \end{bmatrix} \tag{5.68}$$

from which follows the reduced eigenvalue problem

$$[\mathbf{L}\mathbf{L}_2^*\grave{}\,\overline{EI}\mathbf{L}\mathbf{L}_2^*\grave{}\,\overline{m} - (1/\lambda)\mathbf{I}]\{\overline{w}\} = 0. \tag{5.69}$$

Results are presented in Table 9 for the nondimensional frequencies of a uniform simply supported beam. The numerically computed results are based on Jacobi integrating matrices and are compared with exact results given in Ref. [45].

5.2.3 Hinged-Free Beam

The hinged-free beam considered in the following analysis is assumed to be simply supported at $\bar{x} = 0$ and unrestrained at $\bar{x} = 1$; this leads to a single rigid body mode in rotation. Boundary conditions for this beam are specified by

$$\overline{M}(0) = 0, \qquad \overline{w}(0) = 0, \qquad \overline{M}(1) = 0, \qquad \overline{V}(1) = 0. \tag{5.70}$$

From the conditions at $\bar{x} = 0$ it is easily found that

$$\mathbf{k}_m = \mathbf{k}_w = 0, \tag{5.71}$$

and at $\bar{x} = 1$ one readily has

$$\mathbf{k}_v = \lambda \mathbf{B}_n \mathbf{L}^{-1} \overline{m}\{\overline{w}\}. \tag{5.72}$$

To complete the solution for the remaining constant of integration, it is necessary to write an expression for $\overline{M}$ in terms of $\mathbf{k}_\gamma$. After substituting Eqs. (5.71–5.72) into Eqs. (5.51–5.54), this expression can be obtained in the form

$$\{\overline{M}\} = -\lambda \mathbf{L}\mathbf{L}_1^{*-1} \overline{m}\mathbf{L}(\mathbf{L}^{-1} \overline{EI}\{\overline{M}\} + \mathbf{k}_\gamma). \tag{5.73}$$

From the boundary condition $\overline{M}(1) = 0$, one then obtains the result

$$\mathbf{k}_\gamma = -c_\gamma \mathbf{B}_n \mathbf{L}\mathbf{L}_1^{*-1} \overline{m}\mathbf{L}(\mathbf{L}^{-1} \overline{EI})\{\overline{M}\} \tag{5.74}$$

where

$$c_\gamma = \frac{1}{\mathbf{b}_n^T \mathbf{L}\mathbf{L}_1^{*-1} \overline{m}\mathbf{L}\vec{1}}. \tag{5.75}$$

The foregoing solutions for the constants of integration lead to the expressions

$$\mathbf{F} = \begin{bmatrix} -\mathbf{L} & 0 & 0 & 0 \\ 0 & (\mathbf{B}_n - \mathbf{I})\mathbf{L} & 0 & 0 \\ 0 & 0 & (c_\gamma \mathbf{B}_n \mathbf{L}\mathbf{L}_1^{*\backprime} \overline{m}\mathbf{L} - \mathbf{I})\mathbf{L} & 0 \\ 0 & 0 & 0 & -\mathbf{L} \end{bmatrix} = \begin{bmatrix} -\mathbf{L} & 0 & 0 & 0 \\ 0 & \mathbf{L}_1^* & 0 & 0 \\ 0 & 0 & \mathbf{L}_3^* & 0 \\ 0 & 0 & 0 & -\mathbf{L} \end{bmatrix} \tag{5.76}$$

and

$$\mathbf{T} = \begin{bmatrix} \mathbf{L}_3^{*\backprime} \overline{EI}\mathbf{L} & -\mathbf{L}_3^{*\backprime} \overline{EI}\mathbf{L}\mathbf{L}_1^* \\ -\mathbf{L}\mathbf{L}_3^{*\backprime} \overline{EI}\mathbf{L} & \mathbf{L}\mathbf{L}_3^{*\backprime} \overline{EI}\mathbf{L}\mathbf{L}_1^* \end{bmatrix}. \tag{5.77}$$

From Eq. (5.77) follows the reduced eigenvalue problem

$$[\mathbf{L}\mathbf{L}_3^{*\backprime} \overline{EI}\mathbf{L}\mathbf{L}_1^{*\backprime} \overline{m} - (1/\lambda)\mathbf{I}]\{\overline{w}\} = 0. \tag{5.78}$$

Results are presented in Table 10 for the nondimensional frequencies of a uniform hinged-free beam. The numerically computed results are based on Jacobi integrating matrices and are compared with exact results obtained from the expression $\tan\beta - \tanh\beta = 0$, where $\sqrt{\lambda} = \beta^2$ is the nondimensional frequency.

Solutions for the eigenvalues of Eq. (5.78) can be obtained without having to apply constraint equations. Constraint equations do exist, however, in problems with rigid body modes. The presence of constraints in an eigenvalue problem will be evident from the existence of zero eigenvalues. With finite precision calculations, the zero eigenvalues are not guaranteed to be exactly zero for nonsymmetric eigenvalue problems like that in Eq. (5.78). In practice, these zero eigenvalues can appear as very small positive or negative quantities, and in some cases, complex quantities with very small real parts. The appearance of these parasitic eigenvalues is not an indication that a solution has gone astray; parasitic eigenvalues can simply be

neglected. In Eq. (5.78) the eigenvalues are related to reciprocals of the vibration frequency; therefore, the parasitic eigenvalues will equivalently manifest themselves as very high frequencies.

For problems with rigid body modes, conservation of linear and angular momentum provide the constraints that can eliminate associated zero eigenvalues. The constraint arising from linear momentum conservation is

$$\int_0^\ell \ddot{w} m \, dx = 0, \tag{5.79}$$

which, for free vibration, leads to the discrete constraint equation

$$\mathbf{b}_n^T \mathbf{L}\{wm\} = 0. \tag{5.80}$$

Similarly, the constraint given by angular momentum conservation is

$$\int_0^\ell \ddot{w} m x \, dx = 0, \tag{5.81}$$

which results in

$$\mathbf{b}_n^T \mathbf{L}\{wmx\} = 0. \tag{5.82}$$

These constraint equations can be used to reduce an eigenvalue problem as discussed in Appendix F.

5.2.4 Free-Free Beam

A free-free beam possessing rigid body translation and rotation modes presents a slightly more complicated solution for the constants of integration. Nonetheless, the procedure to be followed is similar to that used in previous problems. The

boundary conditions for the free-free beam are given by

$$\overline{M}(0) = 0, \qquad \overline{V}(0) = 0, \qquad \overline{M}(1) = 0, \qquad \overline{V}(1) = 0. \tag{5.83}$$

The application of these boundary conditions to Eqs. (5.51–5.54) gives the constants of integration

$$\begin{aligned} \mathbf{k}_m &= 0 \\ \mathbf{k}_v &= 0 \\ \mathbf{k}_w &= -c_w \mathbf{B}_n \mathbf{L}^{`} \overline{m}(-\mathbf{L})\{\gamma\} \\ \mathbf{k}_\gamma &= -c_\gamma \mathbf{B}_n \mathbf{L}^{2`} \overline{m} \mathbf{L}_4^* (\mathbf{L}^{`} \overline{EI})\{\overline{M}\}, \end{aligned} \tag{5.84}$$

where

$$\begin{aligned} c_w &= \frac{1}{\mathbf{b}_n^T \mathbf{L}^{`} \overline{m} \vec{\mathbf{1}}} \\ c_\gamma &= \frac{1}{\mathbf{b}_n^T \mathbf{L}^{2`} \overline{m} \mathbf{L}_4^* \vec{\mathbf{1}}} \end{aligned} \tag{5.85}$$

and

$$\mathbf{L}_4^* = (c_w \mathbf{B}_n \mathbf{L}^{`} \overline{m} - \mathbf{I})\mathbf{L}. \tag{5.86}$$

These results then lead to the expressions

$$\mathbf{F} = \begin{bmatrix} -\mathbf{L} & 0 & 0 & 0 \\ 0 & -\mathbf{L} & 0 & 0 \\ 0 & 0 & (c_\gamma \mathbf{B}_n \mathbf{L}^{2`} \overline{m} \mathbf{L}_4^* - \mathbf{I})\mathbf{L} & 0 \\ 0 & 0 & 0 & (c_w \mathbf{B}_n \mathbf{L}^{`} \overline{m} - \mathbf{I})\mathbf{L} \end{bmatrix} = \begin{bmatrix} -\mathbf{L} & 0 & 0 & 0 \\ 0 & -\mathbf{L} & 0 & 0 \\ 0 & 0 & \mathbf{L}_5^* & 0 \\ 0 & 0 & 0 & \mathbf{L}_4^* \end{bmatrix} \tag{5.87}$$

and

$$\mathbf{T} = \begin{bmatrix} \mathbf{L}_5^{*`} \overline{EI} \mathbf{L} & \mathbf{L}_5^{*`} \overline{EI} \mathbf{L}^2 \\ \mathbf{L}_4^* \mathbf{L}_5^{*`} \overline{EI} \mathbf{L} & \mathbf{L}_4^* \mathbf{L}_5^{*`} \overline{EI} \mathbf{L}^2 \end{bmatrix}. \tag{5.88}$$

With the aid of Eq. (5.88), the reduced eigenvalue problem is given by

$$[\mathbf{L}_4^*\mathbf{L}_5^*\overline{EI}\mathbf{L}^2\overline{m} - (1/\lambda)\mathbf{I}]\{\overline{w}\} = 0. \tag{5.89}$$

For a uniform property beam the eigenvalue problem reduces to

$$[\mathbf{L}_2^*\mathbf{L}_5^*\mathbf{L}^2 - (1/\lambda)\mathbf{I}]\{\overline{w}\} = 0 \tag{5.90}$$

where

$$\mathbf{L}_5^* = (c_\gamma \mathbf{B}_n \mathbf{L}^2 \mathbf{L}_2^* - \mathbf{I})\mathbf{L} \tag{5.90}$$

and

$$c_\gamma = \frac{1}{\mathbf{b}_n^T \mathbf{L}^2 \mathbf{L}_2^* \vec{\mathbf{1}}}. \tag{5.91}$$

Note that $\mathbf{L}_2^*$ is the same as given in Section 5.2.2.

Table 11 gives the results for the nondimensional frequencies of a uniform free-free beam. The numerically computed results are based on Jacobi integrating matrices and are compared with exact results obtained from $(\cosh\beta)\cos\beta - 1 = 0$, where $\sqrt{\lambda} = \beta^2$ is the nondimensional frequency. If desired, constraint equations that reduce out the rigid body modes can be applied as discussed in the previous section.

5.3 Buckling of a Rotating Beam

In the following analysis, the state vector approach will be used to obtain solutions for buckling instabilities of the cantilevered, inward oriented rotating beam pictured in Fig. 8. Buckling is assumed to take place in the plane of rotation. Since this problem has been thoroughly examined by many investigators, results

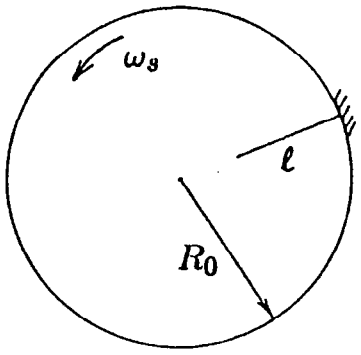

Fig. 8. Rotating beam geometry

are available with which to compare the integrating matrix solutions. This analysis demonstrates that solutions can be easily obtained for many problems involving aeroelasticity, buckling, or vibration of rotating machinery.

The state vector equations to be employed in the buckling analysis compare directly with the equations used by Steele and Barry [13]. Considering bending deformations in the plane of rotation, the nondimensional form of these equations is given by

$$\frac{d}{d\bar{x}}\begin{Bmatrix}\overline{M}\\ \overline{V}\\ \gamma\\ \overline{w}\end{Bmatrix} = \begin{bmatrix}0 & 1 & 0 & 0\\ 0 & 0 & 0 & 0\\ EI & 0 & 0 & 0\\ 0 & 0 & -1 & 0\end{bmatrix}\begin{Bmatrix}\overline{M}\\ \overline{V}\\ \gamma\\ \overline{w}\end{Bmatrix} - \lambda_s\begin{bmatrix}0 & 0 & -F_t & 0\\ 0 & 0 & 0 & \overline{m}\\ 0 & 0 & 0 & 0\\ 0 & 0 & 0 & 0\end{bmatrix}\begin{Bmatrix}\overline{M}\\ \overline{V}\\ \gamma\\ \overline{w}\end{Bmatrix} \tag{5.92}$$

where the nondimensional tension parameter F_t is given as

$$F_t(\bar{x}) = (1/2)\left[(\alpha_s - 1)^2 - (\alpha_s - \bar{x})^2\right] \tag{5.93}$$

with

$$\alpha_s = R_0/\ell\,. \tag{5.94}$$

The nondimensional spin parameter λ_s is given by

$$\lambda_s = \frac{\omega_s^2 m_R \ell^4}{(EI)_R}. \tag{5.95}$$

Except for the displacement dependent load terms, these equations are very similar to those presented in Eq. (5.48). The solution to Eq. (5.92) is readily obtained by using the $\mathbf{T}$ matrix presented in Eq. (5.60) for cantilever boundary conditions. The resulting buckling eigenvalue problem is given by

$$[\mathbf{TA}_{FD} - (1/\lambda_s)\mathbf{I}]\begin{Bmatrix}\gamma\\ \overline{w}\end{Bmatrix} = 0 \tag{5.96}$$

where

$$\mathbf{TA}_{FD} = \begin{bmatrix} -\mathbf{L}\overline{EI}\mathbf{L}_1^{*}F_t & -\mathbf{L}\overline{EI}\mathbf{L}_1^{*2}\overline{m} \\ \mathbf{L}^2\overline{EI}\mathbf{L}_1^{*}F_t & \mathbf{L}^2\overline{EI}\mathbf{L}_1^{*2}\overline{m} \end{bmatrix}. \tag{5.97}$$

Results are given in Table 12 for the nondimensional critical buckling speed Ω of a uniform beam, where $\Omega = \alpha_s^2\sqrt{\lambda_s}$. The buckling speeds, which are presented for varying values of the parameter α_s, are compared with numerical solutions given in Ref. [13]. These comparison solutions consist of results from an asymptotic iteration scheme as well as results from a high order Ritz finite element method due to Hodges [48]. Further elaboration on these critical buckling speed solutions is given by White, Kvaternik, and Kaza [31] and by Peters and Hodges [49].

5.4 Deflection of Beams

Static beam deflections and forces can be easily and accurately calculated with the hybrid state vector approach. The nondimensional state vector equations

describing lateral deflection of a beam under an applied loading p are

$$\frac{d}{d\bar{x}}\begin{Bmatrix}\overline{M}\\ \overline{V}\\ \gamma\\ \overline{w}\end{Bmatrix}=\begin{bmatrix}0 & 1 & 0 & 0\\ 0 & 0 & 0 & 0\\ \overline{EI} & 0 & 0 & 0\\ 0 & 0 & -1 & 0\end{bmatrix}\begin{Bmatrix}\overline{M}\\ \overline{V}\\ \gamma\\ \overline{w}\end{Bmatrix}-\begin{Bmatrix}0\\ \overline{p}\\ 0\\ 0\end{Bmatrix} \tag{5.98}$$

where

$$\overline{p}=\frac{p\ell^3}{(EI)_R}. \tag{5.99}$$

Solutions to Eq. (5.98) are given by Eqs. (4.23) and (4.24). If aerodynamic loads are not present, one must take $\lambda = 0$. Noting that $\mathbf{H}_{FD} = 0$, then for cantilever boundary conditions the deflection and force solutions are given by

$$\mathbf{y}_D = \mathbf{T}\tilde{\mathbf{a}}_{r_F}, \tag{5.100}$$

$$\mathbf{y}_F = \mathbf{H}_{FF}^{-1}\mathbf{L}_1^*\tilde{\mathbf{a}}_{r_F}. \tag{5.101}$$

By using the $\mathbf{T}$ matrix in Eq. (5.60), these solutions can be further refined to give

$$\mathbf{y}_D=\begin{Bmatrix}\gamma\\ \overline{w}\end{Bmatrix}=\begin{Bmatrix}-\mathbf{L}\,\overline{EI}\mathbf{L}_1^{*2}\overline{p}\\ \mathbf{L}^2\,\overline{EI}\mathbf{L}_1^{*2}\overline{p}\end{Bmatrix} \tag{5.102}$$

and

$$\mathbf{y}_F=\begin{Bmatrix}\overline{M}\\ \overline{V}\end{Bmatrix}=\begin{Bmatrix}-\mathbf{L}_1^{*2}\overline{p}\\ \mathbf{L}_1^*\overline{p}\end{Bmatrix}. \tag{5.103}$$

As an indicator of solution accuracy, one can easily verify with a sample calculation that a four interval Jacobi integrating matrix solution will provide the exact deflections for a uniform cantilevered beam having a constant load distribution.

It should be noted that matrix inversions are not required in solving for either forces or displacements. Deflection solutions similar to these are used to obtain static aeroelastic lift distributions in the next chapter.

Table 1

Nondimensional frequencies, $\lambda^{1/2}$, for the axial modes of a uniform cantilevered rod with N collocation intervals. ($\lambda = \omega^2 m_R \ell^2/(EA)_R$)

					% Error	
N	Mode	Jacobi	Newton	Exact	Jacobi	Newton
2	1	1.582576	1.582576	1.570796	.749938	.749938
	2	7.582580	7.582580	4.712389	60.9073	60.9073
3	1	1.571009	1.569703	1.570796	.013560	−.069583
	2	4.962687	4.826099	4.712389	5.31149	2.41300
	3	15.39166	14.25626	7.853982	95.9727	81.5163
4	1	1.570799	1.570732	1.570796	.000191	−.004074
	2	4.735692	4.665351	4.712389	.494505	−.998177
	3	8.807365	8.070704	7.853982	12.1388	2.75939
	4	25.64255	21.64282	10.99557	133.208	96.8321
5	1	1.570797	1.570803	1.570796	.000064	.000446
	2	4.713869	4.706141	4.712389	.031407	−.132587
	3	8.011505	7.631141	7.853982	2.00564	−2.83730
	4	13.27345	11.23810	10.99557	20.7163	2.20567
	5	38.40523	29.57599	14.13717	171.661	109.207

Table 2

Axial vibration mode shapes, $\{\bar{u}\}$, for a uniform cantilevered rod (Numerical solutions obtained with five collocation intervals)

$\bar{x}$	0.0	0.2	0.4	0.6	0.8	1.0
Mode 1						
Jacobi	0.00000	0.30903	0.58779	0.80902	0.95107	1.00000
Newton	0.00000	0.30902	0.58779	0.80902	0.95106	1.00000
Exact	0.00000	0.30902	0.58779	0.80902	0.95106	1.00000
Mode 2						
Jacobi	0.00000	−.81474	−.94453	−.30816	0.58191	1.00000
Newton	0.00000	−.81516	−.95512	−.31182	0.59050	1.00000
Exact	0.00000	−.80902	−.95106	−.30902	0.58779	1.00000
Mode 3						
Jacobi	0.00000	0.91354	−.01155	−.87489	−.09662	1.00000
Newton	0.00000	0.98697	−.03503	−.95027	−.08023	1.00000
Exact	0.00000	1.00000	0.00000	−1.0000	0.00000	1.00000

Table 3

Nondimensional frequencies, $\lambda^{1/2}$, for the axial modes of a linearly tapered cantilevered rod with N collocation intervals. ($\beta_t = 0.5$; $\lambda = \omega^2 m_R \ell^2/(EA)_R$)

					% Error	
N	Mode	Jacobi	Newton	Exact	Jacobi	Newton
2	1	1.613095	1.613095	1.652805	−2.40258	−2.40258
	2	11.15869	11.15869	3.627852	207.584	207.584
3	1	1.643238	1.665064	1.652805	−.578834	.741709
	2	3.587127	3.535655	3.627852	−1.12257	−2.54137
	3	22.39381	20.38371	5.807501	285.601	250.989
4	1	1.652913	1.649068	1.652805	.006534	−.226100
	2	3.580021	3.658788	3.627852	−1.31844	.852736
	3	6.040474	5.622661	5.807501	4.01159	−3.18278
	4	37.76820	30.95097	8.215935	359.694	276.719
5	1	1.652826	1.653185	1.652805	.001271	.022991
	2	3.633674	3.608995	3.627852	.160481	−.519784
	3	5.721657	5.887524	5.807501	−1.47816	1.37793
	4	9.001691	7.591113	8.215935	9.56381	−7.60500
	5	57.31683	42.52789	10.27790	457.671	313.780

Table 4

Nondimensional frequencies, $\lambda^{1/2}$, for the axial modes of a three segment cantilevered rod with discontinuous stiffness and mass. There are N collocation intervals per segment. ($\lambda = \omega^2 m_R \ell^2/(EA)_R$; $\overline{\gamma} = 10$, $\overline{\theta} = 100$; Error based on six significant figures)

					% Error	
N	Mode	Jacobi	Newton	Exact	Jacobi	Newton
1	1	.8336431	.8336431	.8267091	.838747	.838747
	2	22.20007	22.20007	6.097328	264.095	264.095
	3	121.7023	121.7023	11.98907	915.105	915.105
2	1	.8267307	.8267298	.8267091	.002661	.002540
	2	6.729430	6.729422	6.097328	10.3668	10.3667
	3	19.03003	19.03001	11.98907	58.7275	58.7275
	4	41.08241	41.08287	17.57944	133.696	133.699
	5	85.56076	85.56099	19.46456	339.571	339.572
3	1	.8267099	.8267071	.8267091	.000121	−.000242
	2	6.139068	6.082418	6.097328	.684562	−.244533
	3	14.52343	13.85007	11.98907	21.1384	15.5224
	4	19.45551	19.33504	17.57944	10.6722	9.98669
	5	38.17844	37.79570	19.46456	96.1427	94.1766
4	1	.8267105	.8267104	.8267091	.000121	.000121
	2	6.099150	6.085790	6.097328	.029849	−.189263
	3	12.34547	11.82625	11.98907	2.97270	−1.35790
	4	18.83118	18.54741	17.57944	7.12083	5.50645
	5	25.28983	22.48436	19.46456	29.9271	15.5143
5	1	.8267107	.8267107	.8267091	.000242	.000242
	2	6.097375	6.097551	6.097328	.000820	.003608
	3	12.03000	11.86734	11.98907	.341143	−1.01592
	4	18.17894	17.10370	17.57944	3.41024	−2.70601
	5	20.28574	19.38240	19.46456	4.21843	−.422331

Table 5

Nondimensional frequencies, $\lambda^{1/2}$, for the axial modes of a uniform cantilevered rod with variable stiffness elastic restraint at the free end. Results were obtained with a Jacobi integrating matrix using six collocation points. ($\overline{k}_s = k/(EA)_R$; $\lambda = \omega^2 m_R \ell^2/(EA)_R$)

Mode	$\overline{k}_s = 0.0$	$\overline{k}_s = 0.25$	$\overline{k}_s = 1.0\text{E}6$
1	1.57080	1.71551	3.14161
(exact)	(1.57080)	(1.71551)	(3.14159)
2	4.71387	4.76644	6.30594
(exact)	(4.71239)	(4.76481)	(6.28318)
3	8.01150	8.04779	10.1059
(exact)	(7.85398)	(7.88567)	(9.42478)

Table 6

Nondimensional frequencies, $\lambda^{1/2}$, for the axial modes of a uniform cantilevered rod with tip mass. Results were obtained with a Jacobi integrating matrix using six collocation points. ($\overline{m}_n^+ = m_n/m_R\ell$; $\lambda = \omega^2 m_R \ell^2/(EA)_R$)

Mode	$\overline{m}_n^+ = 0.0$	$\overline{m}_n^+ = 0.25$	$\overline{m}_n^+ = 1.0\text{E}8$
1	1.57080	1.26770	0.00010
(exact)	(1.57080)	(1.26459)	(0.00000)
2	4.71387	3.98864	3.24838
(exact)	(4.71239)	(3.93517)	(3.14159)
3	8.01150	7.00118	6.52342
(exact)	(7.85398)	(6.81401)	(6.28319)

Table 7

Nondimensional bending frequencies, $\lambda^{1/2}$, of a uniform cantilever beam for a Jacobi integrating matrix solution using five collocation intervals. ($\lambda = \omega^2 m_R \ell^4/(EI)_R$)

Mode	1	2	3	4	5
Calculated	3.516022	22.04884	64.15257	178.0921	1032.319
Exact	3.516015	22.03449	61.69721	120.9019	199.8595

Table 8

Lateral bending mode shapes, $\{\overline{w}\}$, of a uniform cantilever beam (Jacobi integrating matrix solution using five collocation intervals)

Mode\$\overline{x}$	0.0	0.2	0.4	0.6	0.8	1.0
1	0.00000	0.06386	0.22990	0.46114	0.72547	1.00000
(exact)	(0.00000)	(0.06387)	(0.22989)	(0.46114)	(0.72548)	(1.00000)
2	0.00000	−.30660	−.68022	−.58537	0.06418	1.00000
(exact)	(0.00000)	(−.30106)	(−.68347)	(−.58948)	(0.07004)	(1.00000)
3	0.00000	0.60087	0.45954	−.40455	−.41063	1.00000
(exact)	(0.00000)	(0.60450)	(0.52593)	(−.47377)	(−.39488)	(1.00000)

Table 9

Nondimensional bending frequencies, $\lambda^{1/2}$, of a uniform, simply supported beam with N collocation intervals; ($\lambda = \omega^2 m_R \ell^4/(EI)_R$)

N	Mode	Jacobi	Exact
2	1	12.00003	9.86960
3	1	10.00003	9.86960
	2	59.99989	39.4784
4	1	9.875132	9.86960
	2	41.99992	39.4784
	3	170.1317	88.8264
5	1	9.869781	9.86960
	2	39.76482	39.4784
	3	102.1309	88.8264
	4	380.2456	157.9137

Table 10

Nondimensional bending frequencies, $\lambda^{1/2}$, of a uniform, hinged-free beam with N collocation intervals; ($\lambda = \omega^2 m_R \ell^4/(EI)_R$)

N	Mode	Jacobi	Exact
2	1	24.00014	15.41821
3	1	16.07796	15.41821
	2	105.5557	49.96487
4	1	15.46149	15.41821
	2	56.60144	49.96487
	3	295.1689	104.2477
5	1	15.42012	15.41821
	2	50.88158	49.96487
	3	131.8585	104.2477
	4	628.4688	178.2697

Table 11

Nondimensional bending frequencies, $\lambda^{1/2}$, of a uniform, free-free beam with N collocation intervals; $(\lambda = \omega^2 m_R \ell^4/(EI)_R)$

N	Mode	Jacobi	Exact
3	1	24.49481	22.37332
4	1	22.61198	22.37332
	2	76.68076	61.68503
5	1	22.38678	22.37332
	2	64.21640	61.68503
	3	174.3449	120.9027

Table 12

Nondimensional buckling speeds, Ω, of a uniform, inward-oriented, rotating beam. Jacobi integrating matrix solutions with N collocation intervals. $(\Omega = \alpha_s^2\sqrt{\lambda_s})$

	WKB	Hodges	State Vector Method			
	Direct	Ritz				
α_s	Integration	FEM	$N=5$	$N=4$	$N=3$	$N=2$
.2	.35	.35	.35	.35	.35	.65
.5	1.13	1.13	1.13	1.13	1.13	1.19
1.0	2.96	2.99	2.99	2.99	2.99	3.05
1.5	5.35	5.38	5.38	5.38	5.38	5.46
2.0	8.27	8.19	8.19	8.19	8.19	8.30
3.0	14.91	14.87	14.87	14.87	14.89	15.05
4.0	22.70	22.77	22.77	22.77	22.81	23.03

Chapter 6

Divergence and Aeroelastic Lift of Composite Wings

STATIC AEROELASTIC BEHAVIOR, which includes both divergence instability and aeroelastic lift distribution, is an important consideration in the design of elastically flexible lifting surfaces. An innovative approach to aeroelastic design is provided by the concept of aeroelastic tailoring, which addresses the problem of designing a flexible lifting surface to take advantage of structural deformation. Essentially, one strives to control the deformation, and thus the load distribution, in a way that enhances aerodynamic performance. Because of their unique directional properties, advanced composite materials prove to be an important ingredient in many tailored designs.

Along with the increased design flexibility allowed by composite materials, there comes an additional complexity in the structural analysis. The hybrid state vector method discussed in previous chapters provides a simple, yet powerful tool for analyzing large aspect ratio composite lifting surfaces. The primary focus of this chapter is on applying the anisotropic beam equations developed in Section 2.3 to the static aeroelastic analysis of forward swept composite wings.

The potential benefits of aeroelastic tailoring applied to forward swept composite wings have been thoroughly examined by Weisshaar [4,5,50]. In order to

facilitate the verification of the hybrid state vector solutions, the problems considered in this chapter are similar in nature to those discussed by Weisshaar for uniform geometry wings. In the following analyses, aerodynamic loads will be calculated from modified strip theory aerodynamics.

6.1 Divergence of a Forward Swept Composite Wing

The cantilevered composite wing structure considered in the following analysis is identical to the lifting surface model presented in Fig. 1 of Chapter 2. The aeroelastic equations apply to aerodynamic sections taken normal to the swept structural reference axis. A detailed derivation of the differential equations for this plate-beam model, including important assumptions, is presented in Section 2.3. It should be noted that for static aeroelastic stability calculations, these equations are, in fact, perturbation equations, with the state vector containing perturbation quantities.

For the sake of simplifying the presentation, it is assumed that transverse shear terms can be neglected. Another important assumption to be used in the analysis is that the composite wing structure, which is modelled as an equivalent composite plate, can be considered as having the same properties as a midplane symmetric laminate. Primarily, this means that the $\overline{B}^*_{ij}$ coupling compliances in Eq. (2.28) will be taken as zero.

For fixed wing problems, it is clear that no appreciable external spanwise loads exist. In the event that $\overline{B}^*_{ij}$ coupling compliances are included in the analysis, there will be induced spanwise loads that arise from satisfying the fifth equation in Eq. (2.28). These coupling-induced spanwise loads can be directly calculated if one has solutions for the static spanwise midplane deformations u_0. If solutions for u_0 are not readily available, the coupling-induced loads can be approximately determined

by assuming that the spanwise strains and strain gradients are negligible.

By following the solution procedure described in Chapter 4, the **T** matrix corresponding to Eq. (2.28) can be easily determined for a cantilevered composite wing. When the $\overline{B}^*_{ij}$ terms are assumed to be zero, this matrix can be written as

$$\mathbf{T} = \begin{bmatrix} \mathrm{L}\grave{}\overline{A}^*_{11}\mathrm{L}^*_1 & 0 & 0 & 0 \\ 0 & \mathrm{L}\grave{}\overline{D}^*_{11}\mathrm{L}^*_1 & -\mathrm{L}\grave{}\overline{D}^*_{11}\mathrm{L}^{*2}_1 & \mathrm{L}\grave{}\overline{D}^*_{13}\mathrm{L}^*_1 \\ 0 & -\mathrm{L}^2\grave{}\overline{D}^*_{11}\mathrm{L}^*_1 & \mathrm{L}^2\grave{}\overline{D}^*_{11}\mathrm{L}^{*2}_1 & -\mathrm{L}^2\grave{}\overline{D}^*_{13}\mathrm{L}^*_1 \\ 0 & \mathrm{L}\grave{}\overline{D}^*_{13}\mathrm{L}^*_1 & -\mathrm{L}\grave{}\overline{D}^*_{13}\mathrm{L}^{*2}_1 & \mathrm{L}\grave{}\overline{D}^*_{33}\mathrm{L}^*_1 \end{bmatrix}. \tag{6.1}$$

A steady aerodynamics matrix based on strip theory can be extracted from the unsteady strip theory results in Appendix D by taking $s^* = 0$, C(0) = 1.0, and R = 1.0. The resulting aerodynamic matrix is given by

$$\mathbf{A}_{FD} = \begin{bmatrix} 0 & 0 & 0 & 0 \\ 0 & 0 & 0 & 0 \\ 0 & \grave{}\mathcal{L}_\gamma & 0 & \grave{}\mathcal{L}_\alpha \\ 0 & \grave{}\mathrm{M}_\gamma & 0 & \grave{}\mathrm{M}_\alpha \end{bmatrix} \tag{6.2}$$

where the terms in $\mathbf{A}_{FD}$ are obtained from the corresponding terms of Eqs. (D.1–D.2) in Appendix D. For example, $\lambda\grave{}\mathcal{L}_\gamma = \grave{}\hat{\mathcal{L}}_\gamma(s^* = 0, \lambda)$, where λ is a nondimensional dynamic pressure parameter (see Appendix D). For large aspect ratio and moderate sweep angles, the terms in Eqs. (D.3–D.4) involving $\grave{}\mathcal{L}_\tau$ and $\grave{}\mathrm{M}_\tau$ are negligible.

Substituting Eqs. (6.1–6.2) into Eq. (4.29) leads to the divergence eigenvalue problem

$$\left[\begin{bmatrix} \mathbf{G}_{11} & \mathbf{G}_{12} \\ \mathbf{G}_{21} & \mathbf{G}_{22} \end{bmatrix} - \frac{1}{\lambda}\begin{bmatrix} \mathbf{I} & 0 \\ 0 & \mathbf{I} \end{bmatrix}\right]\begin{Bmatrix} \gamma \\ \alpha \end{Bmatrix} = 0, \tag{6.3}$$

where

$$
\begin{aligned}
\mathbf{G}_{11} &= -\mathbf{L}\overline{D}_{11}^{*}\mathbf{L}_1^{*2}\mathcal{L}_\gamma + \mathbf{L}\overline{D}_{13}^{*}\mathbf{L}_1^{*}\mathcal{M}_\gamma \\
\mathbf{G}_{12} &= -\mathbf{L}\overline{D}_{11}^{*}\mathbf{L}_1^{*2}\mathcal{L}_\alpha + \mathbf{L}\overline{D}_{13}^{*}\mathbf{L}_1^{*}\mathcal{M}_\alpha \\
\mathbf{G}_{21} &= -\mathbf{L}\overline{D}_{13}^{*}\mathbf{L}_1^{*2}\mathcal{L}_\gamma + \mathbf{L}\overline{D}_{33}^{*}\mathbf{L}_1^{*}\mathcal{M}_\gamma \\
\mathbf{G}_{22} &= -\mathbf{L}\overline{D}_{13}^{*}\mathbf{L}_1^{*2}\mathcal{L}_\alpha + \mathbf{L}\overline{D}_{33}^{*}\mathbf{L}_1^{*}\mathcal{M}_\alpha .
\end{aligned}
\tag{6.4}
$$

Since the divergence problem being considered involves neither axial loading nor constitutive terms that couple axial deformations with other degrees of freedom, one might expect that the use of simple strip theory aerodynamics, as given above, should allow representation of the eigenvalue problem in Eq. (6.3) in terms of an effective angle of attack. This is indeed the situation.

In order to carry out the reduction to effective angle of attack, first note that because of the nature of the aerodynamic terms one can write

$$
\begin{bmatrix} \mathbf{G}_{11} & \mathbf{G}_{12} \\ \mathbf{G}_{21} & \mathbf{G}_{22} \end{bmatrix} = \begin{bmatrix} -\mathbf{G}_{12} & \mathbf{G}_{12} \\ -\mathbf{G}_{22} & \mathbf{G}_{22} \end{bmatrix} \begin{bmatrix} \tan\Lambda & 0 \\ 0 & \mathbf{I} \end{bmatrix}. \tag{6.5}
$$

Second, note that a constraint equation involving the effective angle of attack α_e can be written as

$$
\alpha_e = \alpha - \gamma \tan\Lambda . \tag{6.6}
$$

This constraint equation expresses the fact that the effective angle of attack for a swept wing consists of the actual twist of the wing plus an induced angle of attack that arises from lateral bending. From this constraint equation, one can obtain the transformation

$$
\begin{Bmatrix} \alpha_e \\ \alpha \end{Bmatrix} = \mathbf{U}^{-1} \begin{Bmatrix} \gamma \\ \alpha \end{Bmatrix}, \tag{6.7}
$$

Table 13

Geometric, aerodynamic, and structural parameters for a uniform composite wing

ELASTIC MODULI:	WING PROPERTIES:
$E_2/E_1 = 0.1$	$\ell/b_R = 6.67$
$G_{12}/E_1 = 0.0373$	$b_R = 1.0$
$\nu_{12} = 0.25$	$\bar{b} = 1.0$
	$a_0 = 2\pi$
	$a_c = 0.5$
	$a = 0.34$

where

$$\mathbf{U}^{-1} = \begin{bmatrix} -\tan\Lambda & \mathbf{I} \\ 0 & \mathbf{I} \end{bmatrix}. \tag{6.8}$$

By applying this transformation in the form of a similarity transformation to Eq. (6.3) while making use of Eq. (6.5), one obtains a reduced eigenvalue problem that can be written as

$$[\mathbf{G}_{22} - (\tan\Lambda)\mathbf{G}_{12}]\{\alpha_e\} = (1/\lambda)\{\alpha_e\}. \tag{6.9}$$

Details on the transformation process used in obtaining Eq. (6.9) are presented in Appendix F. Note that either a similarity transformation or a congruence transformation must be used since these transformations do not affect the eigenvalues.

In order to verify solutions given by Eq. (6.9), divergence eigenvalues were obtained for uniform, forward swept, composite wings with cantilever boundary conditions. Verification was established by comparing the trends of the results with analytical solutions given by Weisshaar [4]. The data used in the analysis are presented in Table 13, and are taken from a uniform, composite wing analyzed by Housner and Stein [51]. These data are also used in a composite wing flutter analysis presented in Chapter 7.

From the material parameters listed in Table 13, angle-ply laminate stiffnesses were calculated for a midplane symmetric composite plate by using the methods given in Appendix C. A special form of these calculations for angle-ply laminates is given in Section 4.4.4 of Jones [25]. Box beam type structures are easily analyzed by carrying out the analyses in terms of an equivalent composite plate. Divergence solutions were investigated for laminates having nondimensional stiffnesses equivalent to an angle-ply laminate with a given number of layers. Since the magnitudes of the composite laminate coupling terms vary with the number of layers, this allows investigation of the effects of coupling stiffness on divergence velocity. The maximum values of coupling are obtained for a laminate with a single layer (i.e., the same as multiple layers with all layers oriented in the same direction). Thus, a single layer angle-ply laminate provides a limiting case solution. As the number of layers increases, the coupling terms decrease and the laminate tends toward quasi-isotropic behavior.

Fig. 9 displays the variation of the nondimensional bending and torsion compliances for a single layer angle-ply laminate as the fiber orientation angle varies. Material properties were taken from Table 13. The orientation angle θ, positive as shown in Fig. C-2, is measured with respect to the laminate reference axis, which in the following problems will be assumed the same as the structural reference axis. For analyzing a composite wing, the structural reference axis is chosen as the midchord of the structural box, since the composite stiffness expressions are developed with respect to this axis. One should note that $\overline{D}^*_{11}$ and $\overline{D}^*_{33}$ are symmetric with respect to $\theta = 0$, whereas the coupling term $\overline{D}^*_{13}$ is antisymmetric in θ. The compliances in Fig. 9 are nondimensionalized as shown in Eqs. (2.30) and (2.32), with the reference stiffness chosen to be D_{11} evaluated at $\theta = 0$.

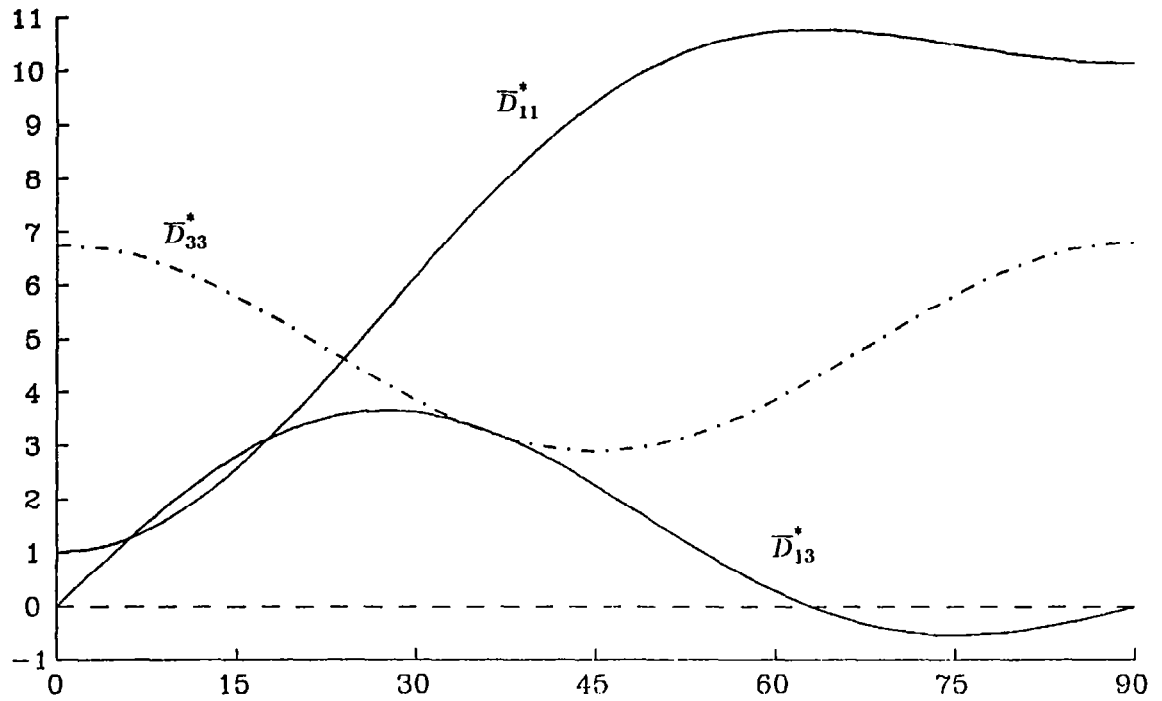

Fig. 9. Nondimensional compliances for a symmetric angle-ply laminate with a single layer

Presented in Fig. 10 are the nondimensional divergence velocities of a uniform, cantilevered, composite wing that is swept forward 30 degrees ($\Lambda = -30°$). Data are taken from Table 13. The nondimensional divergence velocities are plotted as a function of the fiber orientation angle for the equivalent of a midplane symmetric angle-ply laminate. The reference divergence velocity for this figure is the velocity for a one layer laminate with $\theta = -90°$. Three different curves are shown corresponding to coupling stiffnesses equivalent to laminates with one, five, and fifteen layers. As can be seen, the predicted divergence velocities dramatically increase for a range of fiber orientation angles greater than zero. These angles correspond to fibers that are oriented ahead of the structural reference axis. Some of the fiber orientation angles yield negative eigenvalues that give imaginary divergence velocities,

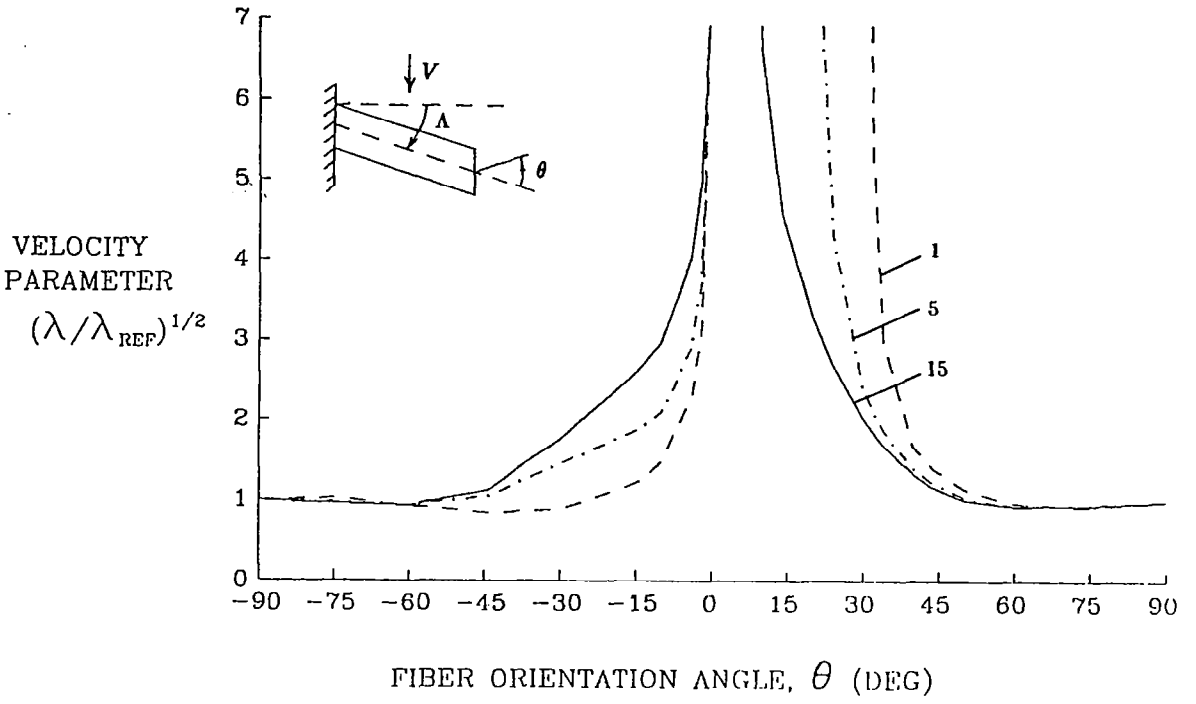

Fig. 10. Nondimensional divergence velocities of a uniform, cantilevered, composite wing—symmetric angle-ply with 1, 5, and 15 layers. ($\Lambda = -30°$, $\lambda_{REF} = \lambda_{(\Lambda=-30°,\theta=-90°)}$)

indicating that divergence does not occur for these fiber angles. The largest range of infinite divergence velocities is exhibited by the single layer equivalent laminate, which possesses the largest value of bending-twist coupling. Although the bending-twist coupling is not the only factor determining the divergence velocity, it is clear that it has a dominant effect. The physical reason underlying the importance of the coupling stiffness is that it can give a lifting surface a washout property, meaning that bending of the surface, and resulting twist, act to alleviate the excessive buildup of aerodynamic loads.

Similar divergence velocity solutions are given in Fig. 11 for a wing that is swept forward 60 degrees ($\Lambda = -60°$). Again, three curves are presented, each

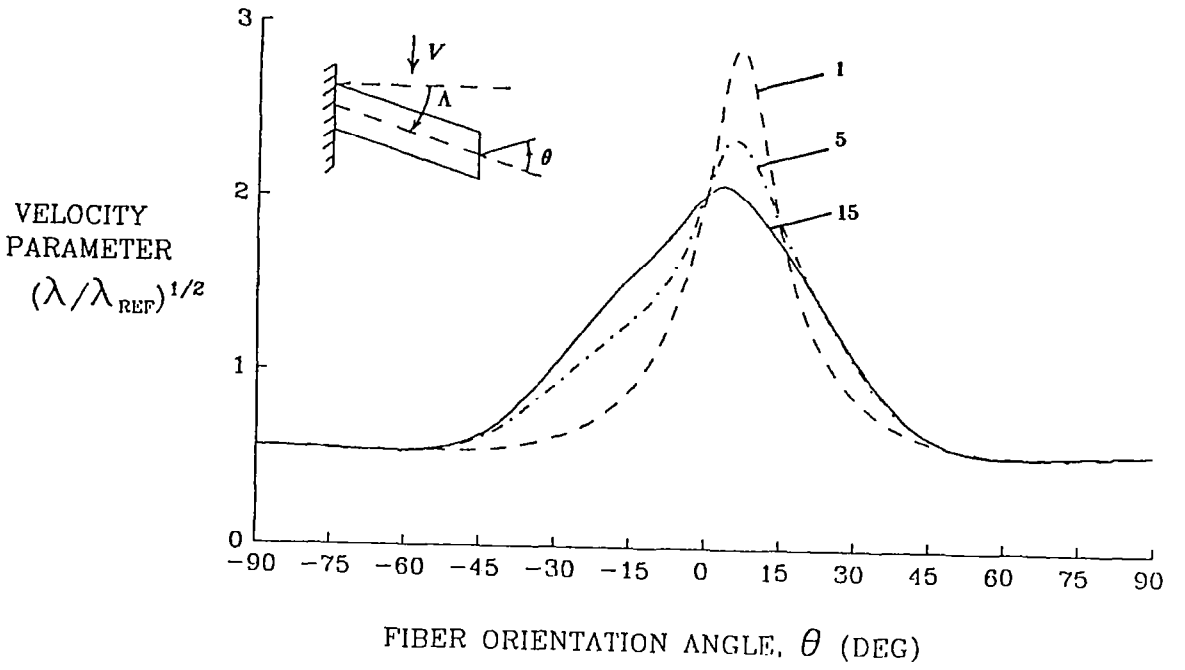

Fig. 11. Nondimensional divergence velocities of a uniform, cantilevered, composite wing—symmetric angle-ply with 1, 5, and 15 layers. ($\Lambda = -60°$, $\lambda_{REF} = \lambda_{(\Lambda=-30°,\theta=-90°)}$)

corresponding to an equivalent angle-ply laminate with a specified number of layers. The reference velocity is the same as that in Fig. 10, which is the divergence velocity for a single layer laminate having a fiber orientation of $\theta = -90°$ and a forward aerodynamic sweep of 30 degrees. For this example, no infinite divergence velocities are predicted since the coupling and bending stiffnesses are not large enough to completely override the aerodynamic loading. The maximum values of divergence velocity still occur at fiber orientation angles slightly ahead of the structural reference axis. An interesting point to note from Fig. 11 is that the result for a laminate with 15 layers, which has only a small amount of coupling stiffness, is nearly symmetric about $\theta = 0$. This indicates that the behavior of a

wing with 60 degrees of forward sweep is also strongly influenced by the bending stiffness. The bending stiffness is symmetric in θ and peaks at $\theta = 0$.

For composite materials that are different from the one on which Figs. 10 and 11 are based, one can expect the locations of the peaks in the divergence velocity to shift slightly. These shifts are possible because other composites may exhibit different ratios of coupling to bending stiffness. The basic trends demonstrated are expected to be valid, however, for any type of unidirectional laminated composite. The trends demonstrated in Figs. 10 and 11 are corroborated by the analytical results presented by Weisshaar [4].

6.2 Aeroelastic Lift of a Forward Swept Composite Wing

Of great interest in aeroelastic design is the equilibrium lift distribution of a flexible wing, especially since aerodynamic efficiency is strongly impacted by the lift distribution. The lift distribution of a flexible wing is also closely tied to maneuver performance as well as to divergence instabilities. That is, the combined bending and twisting of a loaded wing can act either to amplify or to attenuate the loading and the bending moments associated with disturbances about a nominal equilibrium lift condition.

Successful design of forward swept wings hinges upon the ability to "tailor" the lift distribution. Composite materials offer significant advantages in the design and construction of lifting surfaces that are tailored to maintain favorable deformation patterns, and therefore favorable lift distributions, over a range of flight conditions. The following analysis investigates solutions for symmetrical aeroelastic lift of forward swept, cantilevered wings. These wings can be described by the same composite plate-beam model employed in Section 6.1.

The approach adopted in solving for the lift distribution involves specifying

the pitch attitude (angle of attack) of the untwisted, rigid wing. This provides the initial load distribution from which the elastic deformation is determined. The total deformation of the wing is the sum of the rigid wing attitude plus the elastic deformation component. Correspondingly, the total lift distribution of the wing (assuming linear aerodynamics) is the sum of the rigid wing lift plus the elastic lift. A similar approach has been used by Diederich and Foss [3] to study the lift of metallic swept wings, and by Weisshaar [5] to examine the lift of composite wings. Further elaboration on solutions for aeroelastic lift distribution can be found in Chapter 8 of Bisplinghoff, Ashley, and Halfman [45].

Equations that provide the lift distribution solutions for the aforementioned composite plate-beam can be obtained by substituting Eqs. (6.1–6.2) into Eq. (4.26), resulting in

$$\begin{bmatrix} \mathbf{I} - \lambda \mathbf{G}_{11} & -\lambda \mathbf{G}_{12} \\ -\lambda \mathbf{G}_{21} & \mathbf{I} - \lambda \mathbf{G}_{22} \end{bmatrix} \begin{Bmatrix} \gamma \\ \alpha \end{Bmatrix} = \lambda \begin{bmatrix} \mathbf{G}_{11} & \mathbf{G}_{12} \\ \mathbf{G}_{21} & \mathbf{G}_{22} \end{bmatrix} \begin{Bmatrix} \gamma_r \\ \alpha_r \end{Bmatrix} \tag{6.10}$$

where the $\mathbf{G}$ terms are given by Eq. (6.4). The attitude of the rigid wing is specified by γ_r and α_r. Similar to the reduction of the dependent variables in the divergence problem of Section 6.1, the linear system in Eq. (6.10) can be reduced to an effective angle of attack variable, α_e, since neither axial loading nor axial deformation coupling terms are present. By employing the same relationships and the same approach presented in Eqs. (6.5–6.8), Eq. (6.10) reduces to

$$[\mathbf{I} - \overline{\mathbf{G}}]\{\alpha_e\} = \overline{\mathbf{G}}\{\alpha_{e_r}\} \tag{6.11}$$

where

$$\overline{\mathbf{G}} = \lambda[\mathbf{G}_{22} - (\text{`} \tan\Lambda)\mathbf{G}_{12}]\,. \tag{6.12}$$

To verify these results, lift distribution solutions have been obtained from Eq. (6.11) for a uniform, swept-forward composite wing. Material property data for the

analysis were taken from Table 13, and aerodynamic loads were calculated with the aid of simple strip theory aerodynamics. Results are displayed in Fig. 12 for the maximum and minimum values of normalized elastic lift distribution, C_{ℓ_e}/C_{ℓ_r}, as a function of the nondimensional spanwise coordinate $\bar{x}$. A symmetric angle-ply composite with a single layer has been assumed (i.e., all fibers are oriented in the same direction). Since the lift curve slope is assumed constant, the use of strip theory aerodynamics allows the lift distributions to be calculated as the ratio of elastic wing deflections (effective angle of attack) to rigid wing deflections. For solutions obtained in this manner, it is convenient to specify the rigid wing effective angle of attack as a unit value. Also specified prior to the solution of Eq. (6.11) is the nondimensional dynamic pressure parameter λ. The value for this parameter was arbitrarily picked to be one half of the divergence dynamic pressure parameter for a wing having 60 degrees of forward sweep and an angle-ply fiber orientation angle of $\theta = -90°$.

For the wing used in the analysis, it is assumed that all fibers are oriented at an angle θ with respect to the structural reference axis. The results display for each constant wing sweep angle the fiber orientation angle that corresponds to either the maximum load amplification or attenuation that can be achieved by orienting the reinforcing fibers. Hence, these solutions are an indicator of the maximum amount of "tailoring" that can be achieved for a given configuration and material. The designs that fall below the dashed rigid wing reference line in the figure are referred to as load attenuating designs, while those above the reference line correspond to load amplifying designs. It is interesting to note that the maximum amount of lift attenuation, which also corresponds to maximum divergence speed, occurs when the fibers are oriented ahead of the structural reference axis. Those swept-forward wings whose lift distributions fall below the dashed rigid wing reference line are in fact displaying the load alleviating property of an isotropic swept-back wing.

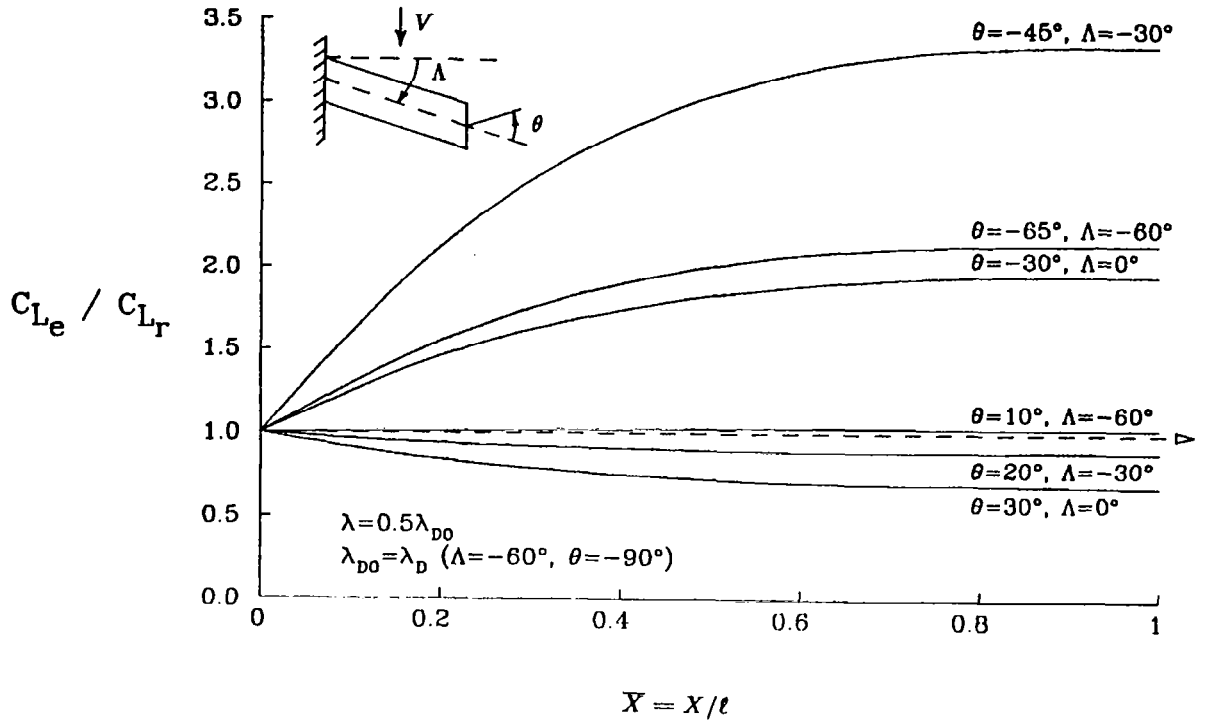

Fig. 12. Limiting elastic lift distributions for a uniform composite wing—symmetric angle-ply with a single layer

These results are verified by an analytical solution developed by Weisshaar [5] for normalized elastic lift distribution of uniform composite wings. A comparison of the analytical solutions with the approximate Jacobi integrating matrix solutions (based on five discretization intervals) shows a maximum deviation from the true lift distribution curves of less than one-tenth of one percent.

Another conclusion that comes from Fig. 12 is that the wing of this example, with 60 degrees of forward sweep, never completely reaches the load attenuating region. This corresponds to the fact that for $\Lambda = -60°$, the wing will always possess a finite divergence velocity. For the other wing sweep angles given in the figure, there exists a fiber orientation angle for which the result is coincident with the rigid wing reference solution. Such designs are referred to as *aero-isoclinic* and have

neither a load attenuating nor load amplifying character.

Chapter 7

Flutter of Isotropic and Composite Wings

DYNAMIC AEROELASTIC BEHAVIOR will now be examined for both isotropic and composite wings having cantilever boundary conditions. The solutions to be pursued in the following problems will yield the airspeeds associated with flutter instabilities. For composite lifting surfaces, it will be shown that the fiber orientation angles have a very strong influence on the points of instability, as well as on the subcritical dynamic response. It should be pointed out that the following investigations are meant only to demonstrate the solution capabilities available with the hybrid state vector approach. A detailed investigation of various types of flutter phenomena is not attempted here since the scope of such a study falls outside the objectives of the present work.

In the sample flutter calculations to be presented, a single formulation of the flutter equations will be used that is appropriate for anisotropic structures; isotropic structures are simply considered as a subset of the anisotropic case. The approach used to obtain the subcritical dynamic response and the flutter points involves tracing out the complex roots loci of the matrix flutter equations. A description of this solution process will be presented in the course of the following analyses.

7.1 Flutter Equations

The general form of the flutter eigenvalue equation to be used was presented in Eq. (4.30). It appears as

$$\left[\mathbf{I} + \mathbf{T}[\mathbf{M}_{FD}s^{*2} + \mathbf{C}_{FD}s^{*} - \mathbf{Q}_{FD}(s^{*},\lambda)]\right]\hat{\mathbf{y}}_{D} = 0 \tag{7.1}$$

where $\mathbf{M}_{FD}$ is the discrete mass matrix for the lifting surface, $\mathbf{C}_{FD}$ is a damping matrix, and $\mathbf{Q}_{FD}$ is an unsteady aerodynamic matrix. Note that Eq. (7.1) is actually the Laplace transform with respect to time of the homogeneous, unsteady aeroelastic equations. It is assumed that the equations have been nondimensionalized such that s^{*} is a nondimensional, complex-valued, Laplace transform variable given by

$$s^{*} = s\ell^{2}\sqrt{\frac{\bar{m}_{R}}{(EI)_{R}}} \tag{7.2}$$

and $\hat{\mathbf{y}}_{D}$ is a nondimensional complex eigenvector. Also note that in the present application λ is a dimensionless dynamic pressure parameter whose definition is given in Appendix D.

Precise forms of the matrix terms in Eq. (7.1) are taken to correspond to the anisotropic plate-beam equations presented in Eq. (2.28). The unsteady aerodynamic matrix, which will be calculated from modified strip theory, is given in Appendix D. The $\mathbf{T}$ matrix has already been presented in Eq. (6.1) for cantilever boundary conditions. It will also be assumed for convenience that the damping terms are zero for the following analyses. In nondimensional form, the mass matrix in Eq. (7.1) can be expressed as

$$\mathbf{M}_{FD} = \begin{bmatrix} 0 & 0 & 0 & 0 \\ 0 & 0 & 0 & 0 \\ 0 & 0 & \grave{\bar{m}}_{ww} & \grave{\bar{m}}_{w\alpha} \\ 0 & 0 & \grave{\bar{m}}_{w\alpha} & \grave{\bar{m}}_{\alpha\alpha} \end{bmatrix} \tag{7.3}$$

where

$$\overline{m}_{ww} = \frac{m}{m_R},$$

$$\overline{m}_{w\alpha} = \overline{m}\left(\frac{b_R}{\ell}\right)\overline{\chi}_\alpha, \tag{7.4}$$

$$\overline{m}_{\alpha\alpha} = \overline{m}\left(\frac{b_R}{\ell}\right)^2 \overline{r}_\alpha^2.$$

The term $\overline{\chi}_\alpha$ represents a section mass static unbalance about the structural reference axis, and $\overline{r}_\alpha$ represents a section dimensionless radius of gyration.

Taking into consideration the zero columns in the mass and aerodynamic matrices, it is readily shown for the case of no damping that the flutter eigenvalue problem can be reduced to

$$\begin{bmatrix} (\mathbf{I}+\mathbf{G}_{22}) & \mathbf{G}_{23} & \mathbf{G}_{24} \\ \mathbf{G}_{32} & (\mathbf{I}+\mathbf{G}_{33}) & \mathbf{G}_{34} \\ \mathbf{G}_{42} & \mathbf{G}_{43} & (\mathbf{I}+\mathbf{G}_{44}) \end{bmatrix} \begin{Bmatrix} \gamma \\ \overline{w} \\ \alpha \end{Bmatrix} = 0, \tag{7.5}$$

where

$$\mathbf{G} = \mathbf{T}[\mathbf{M}_{FD} s^{*2} - \mathbf{Q}_{FD}(s^*, \lambda)]. \tag{7.6}$$

Even further, the first row and first column of Eq. (7.5) can be dropped if the lifting surface has no aerodynamic sweep. Eq. (7.5) can be numerically evaluated for the roots loci of the aeroelastic modes as a function of the dynamic pressure parameter λ, with instability being associated with complex roots s^* having positive real parts.

The procedure used in the present analyses to trace out the complex roots loci was based on a determinant iteration scheme. A determinant iteration method has the advantage of being simple to implement, and furthermore, it is not restricted to solving a particular form of the flutter equations. If desired, the determinant

method can easily solve the flutter equations when the unsteady aerodynamic terms are calculated directly from the Bessel function representation of the generalized Theodorsen function.

Since the roots of the flutter equation correspond to the zeroes of the determinant of the complex-valued matrix in Eq. (7.5), the determinant method simply searches for these zeroes. For a given dynamic pressure and a trial root, the determinant is numerically evaluated from the product of the diagonal terms of the triangular factor that is obtained by applying Gaussian elimination. Muller's method is used to iteratively search for the complex roots of the determinant.

A computer code for determinant iteration was developed directly from routines available in Chapters 2 and 3 of Conte and de Boor [38]. The resulting program worked remarkably well for tracing out the roots loci. Solutions could be started by specifying trial roots along the positive imaginary axis and letting the solutions converge to the free vibration eigenvalues. By incrementing the dynamic pressure and using the roots at the previous dynamic pressure point as iteration starting values, a specified number of branches of the complex roots loci could be simultaneously traced out. Any complex valued roots had their conjugates added to the function deflation in the Muller routine so that only the upper half-plane of the symmetric roots loci was extracted. Zero frequency static divergence roots could also be extracted with determinant iteration.

One point to be aware of is that small sized flutter equations (i.e., not too many degrees of freedom) will usually not encounter problems with determinant evaluation since the range of determinant values tends to be reasonable. For larger problems, one may find it necessary to employ scaled arithmetic in the determinant evaluation in order to prevent overflow or underflow during the computation. Another alternative is to keep the size of the flutter equations small by applying modal superposition to Eq. (7.5). As a result of standard superposition procedures, the flutter matrix

Table 14

Flutter velocities for an unswept, uniform, isotropic wing

Solution	Description	Flutter Velocity km/hr
Ref. [52,53]	Exact Analysis	494
Ref. [51]	25 finite–difference points	483
State Vector	Jacobi I.M., 2 intervals	486
State Vector	Jacobi I.M., 3 intervals	494
State Vector	Jacobi I.M., 4 intervals	494

will be formed by premultiplying the matrix in Eq. (7.5) by the transpose of the modal matrix and postmultiplying it by the untransposed modal matrix.

7.2 Flutter of an Isotropic Wing

Flutter calculations using the state vector approach were verified through comparisons with analytical solutions presented by Goland [52] for an unswept, cantilevered, isotropic wing. (Corrections for Ref. [52] are given in Ref. [53].) The appropriate data for this problem were taken from Ref. 44. Table 14 gives a comparison of numerical flutter results from Eq. (7.5) with those of Goland and with a numerical solution of Housner and Stein [51]. The state vector solutions are based on Jacobi integrating matrices corresponding to two, three, and four collocation intervals, and unsteady aerodynamic calculations employ a rational approximation of the Theodorsen function due to R.T. Jones. Details on the unsteady aerodynamic strip theory can be found in Appendix D.

It is readily seen that the hybrid state vector solutions are quite accurate and converge rapidly to the exact solution as the number of collocation intervals increases. Similar solutions based on Newton integrating matrices also yield highly accurate results that are virtually identical with the Jacobi solutions. The flutter

Table 15

Inertia parameters for the uniform composite wing of Table 13

$\overline{\chi}_\alpha = 0.2$	$\overline{m}_{ww} = 1.0$
$\overline{r}_\alpha = 0.29$	$\overline{m}_{w\alpha} = 0.03$
$\mu = 8.0$	$\overline{m}_{\alpha\alpha} = 0.0065$

solutions for this particular problem depend heavily on the accuracies of the lower frequency coupled bending-torsion modes of free vibration. The high accuracy with which the flutter velocities are determined demonstrates the fact that the integrating matrix solutions contain precise information for these lower modes.

7.3 Flutter of a Composite Wing

Flutter solutions will now be obtained for an unswept, uniform composite wing. The wing geometric, aerodynamic, and structural data to be used in the flutter solutions can be found in Table 13 and Fig. 9 of Section 6.1. (Fig. 9 contains data for a single layer laminate only.) Inertia data are given in Table 15. This data corresponds to a wing that was analyzed by Housner and Stein [51]. The analysis to be given here, however, includes the effect of bending-twist coupling represented by the $\overline{D}^*_{13}$ term. It is assumed that the composite layup is equivalent to a midplane symmetric angle-ply laminate, for which the effective coupling decreases with an increasing number of layers. As in the preceding section, the unsteady aerodynamic loads are calculated from the modified strip theory presented in Appendix D, and the Theodorsen function is calculated from the R.T. Jones rational approximation. No compressibility corrections are applied to the unsteady aerodynamic terms.

Plotted in Fig. 13 is the nondimensional flutter dynamic pressure parameter for the unswept, uniform composite wing as a function of the fiber orientation angle θ. The results are normalized by the flutter dynamic pressure at $\theta = -90°$.

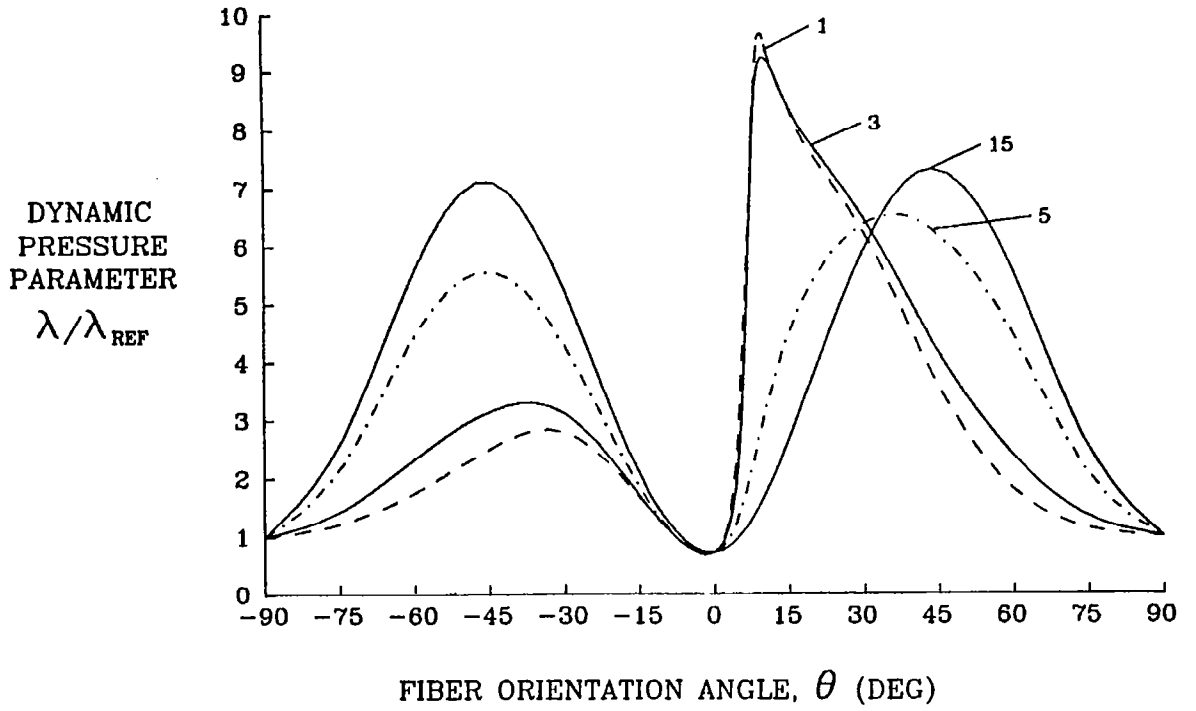

Fig. 13. Effect of fiber orientation on flutter dynamic pressure for an unswept, uniform composite wing—symmetric angle-ply laminate with 1, 3, 5, and 15 layers. ($\lambda_{REF} = \lambda_{(\theta=-90°)}$)

Several curves are displayed corresponding to symmetric angle-ply laminates having 1, 3, 5, and 15 layers. The single layer equivalent laminate possesses the maximum amount of bending twist coupling, while the 15 layer equivalent possesses very little coupling and exhibits essentially quasi-isotropic behavior. It is apparent from Fig. 13 that in the limit of quasi-isotropic behavior, the flutter speed for the unswept wing follows the torsional stiffness variation, with a peak in the flutter dynamic pressure occurring at maximum torsional stiffness corresponding to $\theta = 45°$. These nondimensional results for the 15 layer laminate compare very closely with the quasi-isotropic results given in Fig. 9 of Housner and Stein [51].

In contrast with the quasi-isotropic limit, the behavior of a single layer equivalent symmetric angle-ply laminate demonstrates a limiting case solution involving maximum bending-twist coupling. The asymmetry of the bending-twist coupling term about $\theta = 0°$ is quite apparent from Fig. 13. The sharp peak and the rapid changes in the flutter dynamic pressure for this case are caused by the important participation of the coupling term in the solution. The rapid variation and the sharpness of the peak are quickly diminished when more layers are taken. Since practical composite layups tend more toward quasi-isotropic behavior, it is not anticipated that this single layer limiting case solution will necessarily be attained in practice.

The flutter curves presented in Fig. 13 were obtained directly from Eq. (7.5) by using the previously described root tracking scheme based on determinant iteration. Both Jacobi and Newton integrating matrices for two and three collocation intervals were employed in the flutter calculations. By using the two different interval sizes, the convergence of the flutter solutions as a function of the discretization level could be checked. For the composite wing flutter problem examined here, it was concluded that three intervals gave sufficient convergence, as it did for the case of isotropic wing flutter in Section 7.2. Because of the small number of discretization intervals needed, both the Jacobi and Newton integrating matrix solutions gave the same result. It should also be noted that since solutions were obtained directly from Eq. (7.5), modal superposition was not employed and the question of the number of modes used in the analysis does not arise. For flutter problems in which much more discretization is needed to adequately describe the structure, modal techniques can be applied to keep the flutter solutions within manageable proportions.

To obtain each flutter dynamic pressure, the complex roots loci ($s^* = \sigma^* + j\omega^*$) for that value of fiber orientation angle were traced out beginning with zero dynamic pressure and continuing until one of the branches had roots with positive real parts,

thus indicating a dynamic instability. Figs. 14 and 15 give typical examples of roots loci for two different sets of wing parameters. Fig. 14 gives the roots loci corresponding to the highest peak in the flutter dynamic pressure for the three layer laminate solution plotted in Fig. 13. This peak occurs at a fiber angle of $\theta = 10°$. Fig. 15 gives the roots loci for a single layer equivalent laminate when the mass ratio is taken to be $\mu = 64$ and the fibers are oriented at $\theta = 45°$. For both of these figures only the three lowest root branches are shown. These two figures are indicative of two different types of instability. The instability in Fig. 14 is approached rather slowly as dynamic pressure increases, whereas the instability shown in Fig. 15 is approached very rapidly with a small change in dynamic pressure and involves strong coupling between two of the wing modes.

By tracing each root branch starting with zero dynamic pressure, it was possible to avoid the program logic necessary to detect discontinuities in the flutter speed as θ varies. Such discontinuities were encountered by Housner and Stein [51] for certain values of the mass ratio parameter μ, but not for $\mu = 8$, which was used in obtaining Fig. 13. With the implementation of such detection logic, flutter solutions as a function of θ can be carried out by using the flutter dynamic pressure at an adjacent value of θ as a starting point for the next flutter solution.

The current investigation did not attempt to make a complete examination of the instabilities associated with composite wings. A more thorough study of the instability boundary must involve simultaneous consideration of divergence and flutter and should include the effects of rigid body modes. As indicated by Weisshaar [50], the stability boundary of cantilevered, forward swept composite wings will be determined for a wide range of fiber angles by the low divergence velocities associated with those fiber orientations. Also indicated in Ref. [50] are various changes in the mode of flutter instability as the fiber orientation changes. The presence of these different modes of instability as the wing parameters vary

is worthy of further investigation. It is felt that the solution methods presented here will provide a convenient tool for conducting further research on instability phenomena of composite lifting surfaces.

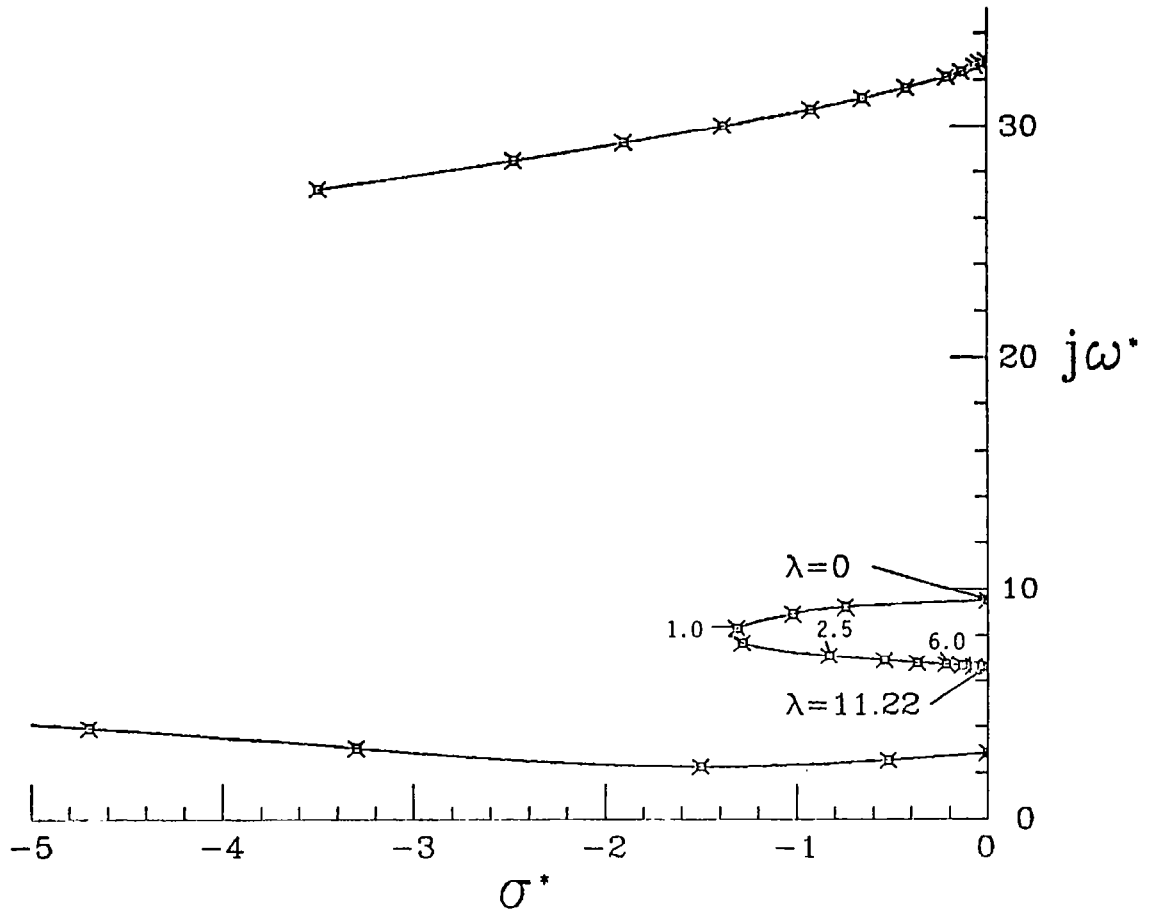

Fig. 14. Roots loci of aeroelastic modes for a uniform composite wing. (Three layer laminate; $\mu = 10$; $\theta = 10°$)

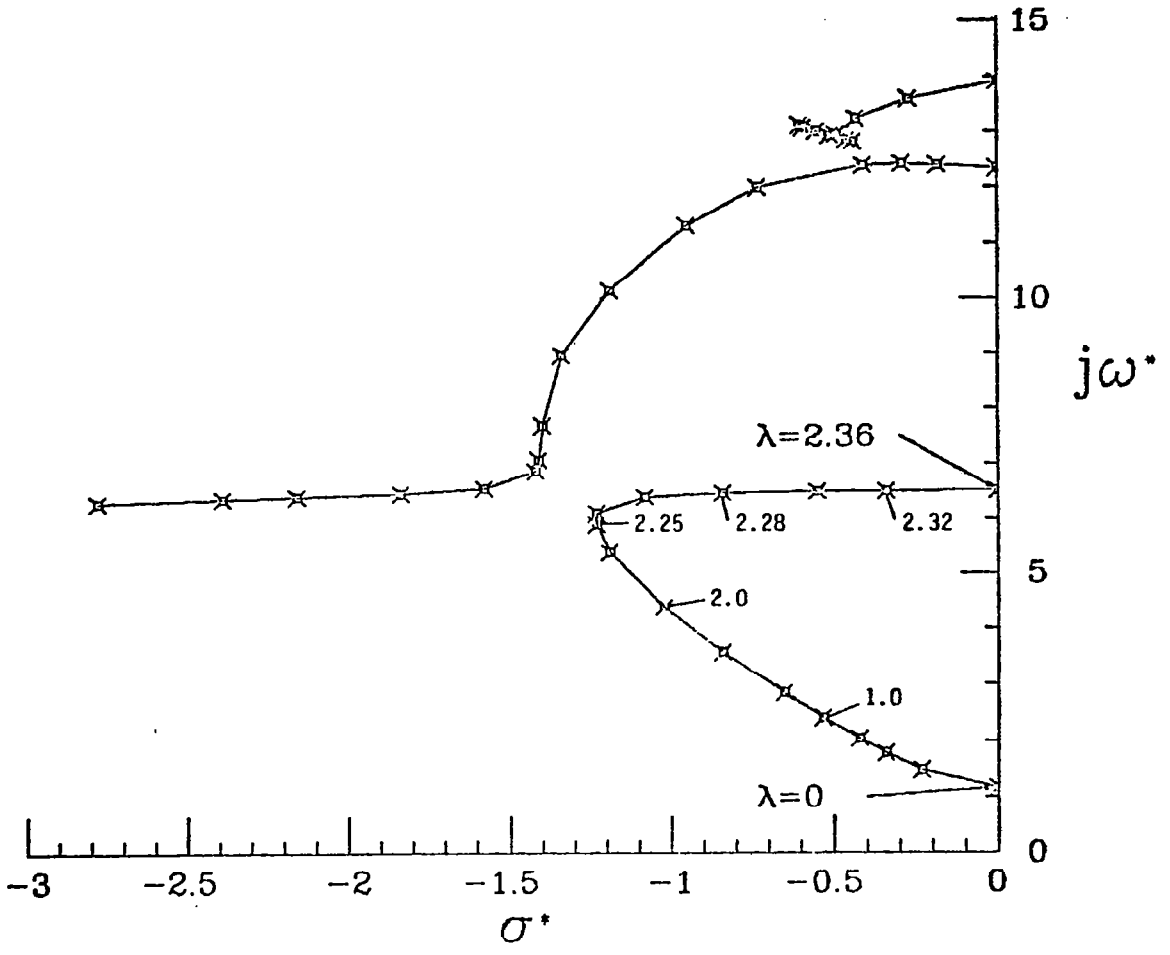

Fig. 15. Roots loci of aeroelastic modes for a uniform composite wing. (Single layer laminate; $\mu = 64$; $\theta = 45°$)

Chapter 8

Concluding Remarks and Recommendations

THE PREVIOUS CHAPTERS describe a hybrid state vector method for solving the differential equations arising in structural dynamics and aeroelasticity. The method proves to be very versatile and can be applied to the solution of any form of ordinary differential equation.

Solutions can be obtained in a consistent fashion for any size problem by working with the state vector form of the differential equations. An integrating matrix method is used to discretize the differential equations, yielding standard linear matrix equations from which one obtains the desired solutions. It is also shown that for simple problems, the integrating matrix can be applied directly to other forms of the differential equations.

It is demonstrated that a convenient form of the state vector equations can be obtained from a variational formulation of the structural equilibrium equations. The equations given by this formulation have properties that are useful for numerical calculations. For structural problems, the state vector equations can be partitioned corresponding to generalized force and displacement variables. By applying matrix partitioning techniques, the solution state vector can be reduced to the displacement state variables only. This reduction process can often be carried out analytically to yield expressions for the direct calculation of the terms in the reduced matrix

equations. For problems in which it might not be convenient to carry out analytical reductions of the equations, the calculations can be performed numerically.

As demonstrated in Chapters 5, 6, and 7, the hybrid state vector method is applicable to a variety of problems and boundary conditions. Results for these problems indicate that high accuracy is easily achievable. By employing high order polynomial approximations, the integrating matrix solutions are capable of providing sufficient accuracy with minimal discretization. The matrix operations required by this solution procedure are straight forward, easily programmable, and allow for efficient problem solution.

A theory of integrating matrices is presented and a calculation procedure is developed for maximum precision integrating matrices that are based on orthogonal polynomials. Discussions are given for several types of integrating matrices and some of their properties. Much flexibility is available in the types of integrating matrices that can be derived and used for special applications. Each type of integrating matrix has its own uniques properties that make it more or less applicable to a particular situation. For the problems examined in this work, the integrating matrices based on Jacobi polynomials have proven to have good convergence properties and are capable of very high accuracy solutions. Newton based integrating matrices, which are convenient for applications requiring evenly spaced grid points, also provide very good accuracies. The convergence of solutions based on Newton matrices, however, tends to be oscillatory in character unless the number of grid points is somewhat larger than the minimum number of points required by a given order of approximating polynomial. Tabulations are presented in Appendix B for both Newton and Jacobi integrating matrices.

Additional work needs to be devoted toward extending the theory of hybrid state vector solutions to two and three dimensional problems. It should prove to be convenient in the development of multidimensional integrating matrices to

introduce the familiar concept of multidimensional shape functions. This concept is routinely employed in finite element analyses. For irregular shaped regions, it is anticipated that a transformation to a simpler domain will be useful in performing the integrations. That is, integrating matrices are more easily developed for these simpler domains. Again, this concept is very much similar to practices currently in use for isoparametric finite element solutions. It is also possible to extend the present method to two dimensional problems by applying separation of variables, thus allowing reduction of the partial differential equations to ordinary differential equations. For multidimensional problems in general, it should prove worthwhile to investigate the use of integration methods that are especially suited to multidimensional integration.

Other types of integrating matrices should be investigated for special types of problems. For instance, semi-infinite boundary value problems should easily yield to numerical solution by integrating matrix. In this connection, it would be worthwhile to examine the prospect of developing integrating matrices from the orthogonal polynomials that are normally used for quadratures on semi-infinite domains.

Further studies are also warranted for applications of the hybrid state vector method to nonlinear problems. For materially nonlinear structures in particular, it appears that the Reissner variational formulation (written in terms of the hybrid state vector) may offer important advantages for numerical solution by integrating matrices and is deserving of a more thorough investigation. In the presence of nonlinearities, the hybrid state vector formulation, in conjunction with integrating matrices, provides a very convenient method for obtaining a compact set of nonlinear algebraic equations that describe the solution of the nonlinear problem.

Finally, there are many questions yet to be answered concerning the flutter of composite wings. Some of the more important questions are mentioned in Chapter 7. The present examination does not attempt to address all of these problems, but

rather forms the foundation for further parameter studies of wing flutter. Most certainly, the answers to some of these problems will be very useful in preliminary aeroelastic design.

Appendix A

Weighting Matrices and Shape Functions for Jacobi Polynomials

The following presents a summary of the calculation procedures for Jacobi integrating matrices. Jacobi integrating matrices are developed from Lagrange interpolating polynomials that can be written in terms of the normalized Jacobi polynomials $p_n^{(1,1)}(x)$. Included in this formulation is a detailed description of the integration methods required to calculate the Jacobi weighting matrices. In addition, the interpolating polynomials are presented in the form of shape functions (basis functions). Discussions on shape functions can be found in Zienkiewicz [54] and Gallagher [55].

First, a distinction must be made between the notation in Chapter 3 and the notation appearing in this appendix. In Chapter 3, n denotes the number of subintervals in the interval of integration, with $n+1$ being the total number of grid points on the interval. In this appendix, however, n refers to the number of grid points in the *interior* of the interval of integration (i.e., excluding end points). This notational change prevents undesirable complication of subscripts and limits and allows the use of an accepted notation for Jacobi polynomials. Since the notational change is confined entirely to the calculations in this appendix, no confusion should arise. It should be noted that whenever n is used as a subscript in a polynomial, it denotes the degree of the polynomial; however, the degree is the same as the number of interior grid points.

All of the integrations and interpolations will be written for the normalized

interval $[-1,1]$, and the subscript k will designate the quadrature points on this interval. The quadrature points x_k are fixed grid point locations that are determined by the zeroes of the appropriate Jacobi polynomial. These quadrature points are the same as the abscissas for Lobatto integration, which can be found, for instance, on page 920 of Abramowitz and Stegun [40]. Appendix B lists these abscissas for each Jacobi integrating matrix. Note too, that a distinction will be made between the unnormalized Jacobi polynomials $P_n^{(1,1)}(x)$ and the normalized polynomials $p_n^{(1,1)}(x)$. These polynomials are a special case of the general Jacobi polynomial

$$p_n^{(\alpha,\beta)}(x) = \sqrt{\delta_n}\, P_n^{(\alpha,\beta)}(x) \tag{A.1}$$

where the normalizing factor δ_n is

$$\delta_n = \frac{(\alpha+\beta+2n+1)n!\,\Gamma(\alpha+\beta+n+1)}{2^{\alpha+\beta+1}\Gamma(\alpha+n+1)\Gamma(\beta+n+1)}. \tag{A.2}$$

For $\alpha = \beta = 1$, the normalizing factor can be reduced to

$$\delta_n = \frac{(2n+3)(n+2)}{8(n+1)}. \tag{A.3}$$

Some more preliminaries on Jacobi polynomials are necessary before discussing shape functions and integrating matrices. First, the Jacobi polynomials $P_n^{(1,1)}(x)$ can be calculated recursively via the formula

$$P_n^{(1,1)}(x) = (n+1)r_0(x) \tag{A.4}$$

with

$$r_{m-1}(x) = 1 + \frac{(n+1-m)(n+2+m)}{2m(m+1)}(x-1)r_m(x). \tag{A.5}$$

The recursive calculation is repeated for $m = n, n-1, \ldots, 2, 1$, beginning with $r_n(x) = 1$. By means of Eqs. (A.4–A.5) one can show that

$$P_0^{(1,1)}(x) = 1 \tag{A.6}$$

and

$$P_n^{(1,1)}(1) = (n+1). \tag{A.7}$$

Using identities listed on page 777 of Abramowitz and Stegun [40], one also finds that

$$P_n^{(1,1)}(-1) = (-1)^n P_n^{(1,1)}(1) = (-1)^n (n+1), \tag{A.8}$$

and from the differential relations given on page 783 of Ref. [40], a useful derivative term is expressible in the form

$$P_n^{(1,1)\prime}(x_k) = \frac{n+1}{1-x_k^2} P_{n-1}^{(1,1)}(x_k). \tag{A.9}$$

From the recursion relations given in Eqs. (A.4–A.5), the following series expansion of $P_n^{(1,1)}(x)$ was developed for use in integrations:

$$P_n^{(1,1)}(x) = (n+1)\left[1 + \sum_{m=1}^{n} e_m^n (x-1)^m\right] \tag{A.10}$$

where

$$e_m^n = \prod_{k=1}^{m} \left(\frac{(n+1-k)(n+2+k)}{2k(k+1)}\right). \tag{A.11}$$

Note that the summation on the right-hand side of Eq. (A.10) vanishes whenever $n < 1$. One final definition that's needed in the following discussion is the definition for the leading coefficient of an orthonormal polynomial. For the normalized Jacobi

polynomials with $\alpha = \beta = 1$, the leading coefficient, a_n (i.e., the coefficient of the highest order term x^n) can be expressed as

$$a_n = \sqrt{\delta_n}\,\frac{(2n+2)!}{2^n n!(n+2)!}. \tag{A.12}$$

Turning now to interpolation, it is assumed that a sufficiently smooth function $f(x)$ can be reasonably approximated by a Lagrange interpolating polynomial. If the end points of the interval $[-1,1]$ are included in the interpolation, then an approximation to $f(x)$ can be expressed as

$$f(x) \approx \sum_{k=1}^{n} \frac{p_n^{(1,1)}(x)(x^2-1)}{(x-x_k)p_n^{(1,1)\prime}(x_k)(x_k^2-1)} f(x_k) + \sum_{j=1}^{2} \frac{p_n^{(1,1)}(x)(x^2-1)}{(x-d_j)p_n^{(1,1)}(d_j)(2d_j)} f(d_j) \tag{A.13}$$

where the end points of the interval are $d_1 = -1$ and $d_2 = 1$. This particular form of the Lagrange interpolating polynomial is convenient for use with orthogonal functions.

The interpolation given by Eq. (A.13) can be equivalently written in terms of shape functions, $N(x)$, as

$$f(x) \approx \lfloor N_{-1}(x) \;\; N_k(x) \;\; N_{+1}(x) \rfloor \{f\} \tag{A.14}$$

where

$$\{f\} = \{f(-1) \;\; f(x_k) \;\; f(+1)\}^T. \tag{A.15}$$

If interpolation is to be performed for multiple points, then the left hand side of Eq. (A.14) becomes a column vector and the shape function terms are written in the form of a rectangular matrix rather than a row matrix.

The shape functions, which provide a convenient way of expressing Eq. (A.13), can be simplified by applying Eqs. (A.6–A.8). As a result of this simplification, the

end point shape functions appear as

$$N_{-1}(x) = \frac{(-1)^{n+1}}{2(n+1)}(x-1)P_n^{(1,1)}(x) \tag{A.16}$$

and

$$N_{+1}(x) = \frac{1}{2(n+1)}(x+1)P_n^{(1,1)}(x). \tag{A.17}$$

For internal points x_k on the interval $[-1,1]$ the shape functions are

$$N_k(x) = \frac{p_n^{(1,1)}(x)\vartheta(x)}{(x-x_k)p_n^{(1,1)\prime}(x_k)(x_k^2-1)} \tag{A.18}$$

where the weighting function $\vartheta(x) = x^2 - 1$. This weighting function is the same as mentioned in Section 3.1. Note too, that the prime in the denominator of Eq. (A.18) indicates differentiation with respect to x. To facilitate further manipulation of the shape functions, the superscript $(1,1)$ will be dropped in the remainder of this appendix. That is, $p_n^{(1,1)}(x)$ and $P_n^{(1,1)}(x)$ will now be referred to simply as $p_n(x)$ and $P_n(x)$.

Unfortunately, Eq. (A.18) is very inconvenient for numerical calculations. The Christoffel-Darboux identity, however, proves useful in reducing the interior point shape functions to a much more desirable form (see, for example, Krylov [39], p. 103). By using the fact that $P_n(x_k) = 0$ when evaluated at its zero points, x_k, a useful form of the Christoffel-Darboux identity can be written as

$$\sum_{s=0}^{n-1} p_s(x)p_s(x_k) = \frac{-a_n}{a_{n+1}}\frac{p_n(x)p_{n+1}(x_k)}{x-x_k}. \tag{A.19}$$

If Eq. (A.19) is first multiplied through by $\vartheta(x) = x^2 - 1$, then some rearranging gives

$$\frac{p_n(x)\vartheta(x)}{x-x_k} = \frac{a_n B_k(x)}{a_{n-1}P_{n-1}(x_k)}, \tag{A.20}$$

where

$$B_k(x) = \sum_{s=0}^{n-1} \delta_s P_s(x_k) \vartheta(x) P_s(x). \tag{A.21}$$

To write Eq. (A.20) in its present form, use was made of the standard recurrence relation for orthonormal polynomials, which allows one to obtain the equality

$$\frac{-a_{n+1}}{a_n P_{n+1}(x_k)} = \frac{a_n}{a_{n-1} P_{n-1}(x_k)}. \tag{A.22}$$

By substituting Eq. (A.20) into Eq. (A.18), one finally obtains a convenient form for the shape functions

$$N_k(x) = \frac{-8 B_k(x)}{(n+1)(n+2)\big(P_{n-1}(x_k)\big)^2} \tag{A.23}$$

where Eq. (A.3), Eq. (A.9), and Eq. (A.12) have been employed to arrive at Eq. (A.23). The final form of the shape functions are represented by Eq. (A.16), Eq. (A.17), and Eq. (A.23). With the aid of the recursion relations given by Eqs. (A.4–A.5), the shape functions, used in conjunction with Eq. (A.14), provide a convenient way of numerically performing interpolations. These interpolation expressions also provide the foundation for calculation of the Jacobi weighting matrices.

It is useful to note that the interpolations can be carried out in matrix notation after defining a matrix of shape function values. For example, if one chooses a number of fixed points $x = x_j$, $(j = 1, \ldots, t)$ at which to interpolate, then the $t \times n$ matrix $[N_{j,k}]$, for the interior point shape functions, is given by

$$[N_{j,k}] = [N_k(x_j)] = \frac{-8}{(n+1)(n+2)} [B_{j,k}] [\grave{} P_{n-1}^2(x_k)]^{-1} \tag{A.24}$$

where the $t \times n$ matrix $[B_{j,k}]$ is written as

$$[B_{j,k}] = [R_{j,s}][\delta_s P_{s,k}]. \tag{A.25}$$

The matrix product on the right-hand side of Eq. (A.25) performs the same summation as the right-hand side of Eq. (A.21). $[\mathcal{R}_{j,s}]$ is a $t \times n$ matrix given by

$$[\mathcal{R}_{j,s}] = [(x_j^2 - 1)P_s(x_j)] \tag{A.26}$$

and $[\delta_s P_{s,k}]$ is an $n \times n$ matrix calculated as

$$[\delta_s P_{s,k}] = [\delta_s P_s(x_k)]\,. \tag{A.27}$$

In addition to $[\mathcal{N}_{j,k}]$, the following column vectors arise from evaluating the end point shape functions via Eqs. (A.16–A.17):

$$\{\mathcal{N}_{-j}\} = \{\mathcal{N}_{-1}(x_j)\}\,, \tag{A.28}$$

$$\{\mathcal{N}_{+j}\} = \{\mathcal{N}_{+1}(x_j)\}\,. \tag{A.29}$$

Finally, by collecting Eqs. (A.24), (A.28), and (A.29), one obtains the complete shape function matrix in the form

$$\mathcal{N} = [\,\{\mathcal{N}_{-j}\}\,|\,[\mathcal{N}_{j,k}]\,|\,\{\mathcal{N}_{+j}\}\,]\,. \tag{A.30}$$

This matrix of shape function values can now be used for function interpolation in the manner indicated by Eq. (A.14).

Having obtained expressions for the interpolation of $f(x)$, the next step is to calculate the weighting matrices from these approximations. But first, a convenient notation must be agreed upon for the subintervals over which the integrations will be performed. In Section 3.1, it was convenient to label subintervals by grid points. That is, a particular subinterval was referred to by $[x_i, x_{i+1}]$, where the subscripts i and $i+1$ designated the two consecutive grid points on that subinterval. In discussing

the integrations required for Jacobi weighting matrices, however, it will greatly simplify the notation to refer to the same subinterval by $[x_j, x_{j+}]$ $(j = 1, \ldots, n+1)$, where j denotes a particular interval rather than a grid point.

The elements in a Jacobi weighting matrix can be determined by integrating the approximate expression for $f(x)$ given in Eq. (A.14). These integrations, which will be carried out over subintervals, are written in the general form

$$\int_{x_j}^{x_{j+}} f(x)\,dx = \int_{x_j}^{x_{j+}} g(x)\vartheta(x)\,dx\,. \tag{A.31}$$

As mentioned in Chapter 3, a maximum precision quadrature will result only if $g(x)$ is orthogonal to $\vartheta(x)$ over the total interval of integration. The total interval of integration here is the normalized interval $[-1, 1]$. Since the weighting function that arises during interpolation is $\vartheta(x) = x^2 - 1$, the Jacobi polynomials are the proper choice for the orthogonal function.

Equation (A.14) is now substituted into Eq. (A.31). When the shape function definitions in Eq. (A.16), (A.17), and (A.23) are taken into account, one can define the integrals

$$D_{-j} = \int_{x_j}^{x_{j+}} N_{-1}(x)\,dx = \frac{(-1)^{n+1}}{2(n+1)} \int_{x_j}^{x_{j+}} (x-1)P_n(x)\,dx \tag{A.32}$$

and

$$D_{+j} = \int_{x_j}^{x_{j+}} N_{+1}(x)\,dx = \frac{1}{2(n+1)} \int_{x_j}^{x_{j+}} (x+1)P_n(x)\,dx \tag{A.33}$$

and finally,

$$C_{j,k} = \int_{x_j}^{x_{j+}} N_k(x)\,dx = \frac{-8}{(n+1)(n+2)\big(P_{n-1}(x_k)\big)^2} \int_{x_j}^{x_{j+}} B_k(x)\,dx. \tag{A.34}$$

In order to isolate the integral portion of the terms in Eqs. (A.32–A.33), it is convenient to rewrite these equations as

$$D_{-j} = \frac{(-1)^{n+1}}{2(n+1)} Q_{-j} \tag{A.35}$$

and

$$D_{+j} = \frac{1}{2(n+1)} Q_{+j} \tag{A.36}$$

where

$$Q_{-j} = \int_{x_j}^{x_{j+}} (x-1) P_n(x)\, dx \tag{A.37}$$

and

$$Q_{+j} = \int_{x_j}^{x_{j+}} (x+1) P_n(x)\, dx. \tag{A.38}$$

With the aid of Eq. (A.21), it is possible to recast Eq. (A.34) in a similar manner to obtain

$$C_{j,k} = \frac{-8 B^*_{j,k}}{(n+1)(n+2)\big(P_{n-1}(x_k)\big)^2} \tag{A.39}$$

where

$$B^*_{j,k} = \sum_{s=0}^{n-1} \delta_s P_s(x_k) R^*_{j,s} \tag{A.40}$$

and

$$R^*_{j,s} = \int_{x_j}^{x_{j+}} (x^2-1) P_s(x)\, dx. \tag{A.41}$$

The next step in calculating the weighting matrices requires the development of expressions for the integrals in Eqs. (A.37), (A.38), and (A.41). Appropriate expressions for these integrals are derived with the help of Eqs. (A.10–A.11), which will allow term by term integration. Therefore, substitution of Eq. (A.10) for $P_n(x)$ in Eq. (A.37) yields the integration

$$Q_{-j} = (n+1)\left[\int_{x_j}^{x_{j+}} (x-1)\, dx + \sum_{m=1}^{n} e^n_m \int_{x_j}^{x_{j+}} (x-1)^{m+1}\, dx\right]. \tag{A.42}$$

Carrying out this integration provides the result

$$\mathcal{Q}_{-j} = (n+1)\left[\frac{1}{2}(x_{j+}^2 - x_j^2) - (x_{j+} - x_j) + \sum_{m=1}^{n} e_m^n \left\{\frac{1}{m+2}[(x_{j+}-1)^{m+2} - (x_j - 1)^{m+2}]\right\}\right] \tag{A.43}$$

A similar operation applied to Eq. (A.38) yields the integrals

$$\mathcal{Q}_{+j} = (n+1)\left[\int_{x_j}^{x_{j+}} (x+1)\,dx + \sum_{m=1}^{n} e_m^n \int_{x_j}^{x_{j+}} [(x-1)^m + x(x-1)^m]\,dx\right] \tag{A.44}$$

with the final result of the integration being

$$\mathcal{Q}_{+j} = (n+1)\left[\frac{1}{2}(x_{j+}^2 - x_j^2) + (x_{j+} - x_j) + \sum_{m=1}^{n} e_m^n \left\{\frac{2}{m+1}[(x_{j+}-1)^{m+1} - (x_j-1)^{m+1}] + \frac{1}{m+2}[(x_{j+}-1)^{m+2} - (x_j-1)^{m+2}]\right\}\right] \tag{A.45}$$

Proceeding with a similar approach for Eq. (A.41) gives

$$\mathcal{R}_{j,s}^{*} = (n+1)\left[\int_{x_j}^{x_{j+}} (x^2-1)\,dx + \sum_{m=1}^{s} e_m^s \int_{x_j}^{x_{j+}} [(x-1)^{m+1} + x(x-1)^{m+1}]\,dx\right] \tag{A.46}$$

for which the integrated result is

$$\mathcal{R}_{j,s}^{*} = (s+1)\left[\frac{1}{3}(x_{j+}^3 - x_j^3) - (x_{j+} - x_j) + \sum_{m=1}^{s} e_m^s \left\{\frac{2}{m+2}[(x_{j+}-1)^{m+2} - (x_j-1)^{m+2}] + \frac{1}{m+3}[(x_{j+}-1)^{m+3} - (x_j-1)^{m+3}]\right\}\right] \tag{A.47}$$

It is important to note that $0 \leq s \leq n-1$ as required by Eq. (A.21); however, the summation appearing on the right-hand side of Eq. (A.47) vanishes whenever $s < 1$.

The Jacobi weighting matrices can now be constructed from the values for $\mathcal{D}_{-j}$, $\mathcal{D}_{+j}$, and $\mathcal{C}_{j,k}$. Numerical calculation of these values makes use of Eqs. (A.35–A.36)

and Eqs. (A.39–A.40) in conjunction with Eqs. (A.43), (A.45), and (A.47). Note that D_{-j} and D_{+j} actually form column vectors with a dimension equal to the number of discretization subintervals. Similarly, the elements $C_{j,k}$ form a rectangular matrix with a row dimension equal to the number of discretization subintervals and a column dimension equal to the number of internal grid points, where the number of internal grid points is one less than the number of subintervals. Analogous to Eqs. (A.24–A.25), one finds that the matrix $[C_{j,k}]$ can be computed from

$$[C_{j,k}] = \frac{-8}{(n+1)(n+2)}[B^*_{j,k}][\grave{} P^2_{n-1}(x_k)]^{-1} \tag{A.48}$$

where the $(n+1) \times n$ matrix $[B^*_{j,k}]$ is

$$[B^*_{j,k}] = [R^*_{j,s}][\delta_s P_{s,k}]. \tag{A.49}$$

The second matrix on the right of Eq. (A.49) is the same as Eq. (A.27). And finally, with these definitions, the Jacobi weighting matrix is constructed in the form

$$\mathcal{W}_{n+1} = \begin{bmatrix} 0 & \cdots & 0 \\ \{D_{-j}\} & [C_{j,k}] & \{D_{+j}\} \end{bmatrix} \tag{A.50}$$

where, as mentioned in Section 3.1, the first row contains only zeroes. Considering the definition of n in this appendix, the dimension of $\mathcal{W}_{n+1}$ is $(n+2) \times (n+2)$.

Appendix B

Tables of Integrating Matrices

The integrating matrix L was defined by Eq. (3.11) as

$$\mathsf{L} = \mathcal{S}\mathcal{W}_n.$$

This definition applies to all of the integrating matrices given in this appendix.

Jacobi Integrating Matrices

The following Jacobi weighting matrices are for the normalized interval $[-1, 1]$, and can be transformed to the interval $[0, 1]$ by multiplying by the factor $1/2$. The coordinate values x, which denote grid points on $[-1, 1]$, are listed above the horizontal bar in each matrix. Equivalent grid points t on $[0, 1]$ are given by the linear transformation $t = 0.5(1+x)$. For the Jacobi weighting matrices, the subscript n refers to the number of discretization intervals, with the integration being exact for all polynomials of degree $\leq 2n-1$.

$$\mathcal{W}_2 = \begin{bmatrix} -1.00000000 & .00000000 & 1.00000000 \\ \hline .00000000 & .00000000 & .00000000 \\ .41666667 & .66666666 & -.08333333 \\ -.08333333 & .66666666 & .41666667 \end{bmatrix} \tag{B.1}$$

$$\mathcal{W}_3 = \begin{bmatrix} -1.00000000 & -.44721360 & .44721360 & 1.00000000 \\ \hline .00000000 & .00000000 & .00000000 & .00000000 \\ .22060113 & .37939886 & -.06781473 & .02060113 \\ -.07453560 & .52174919 & .52174919 & -.07453560 \\ .02060113 & -.06781473 & .37939886 & .22060113 \end{bmatrix} \tag{B.2}$$

$$\mathcal{W}_4 = \begin{bmatrix} -1.00000000 & -.65465367 & .00000000 & .65465367 & 1.00000000 \\ .00000000 & .00000000 & .00000000 & .00000000 & .00000000 \\ .13545686 & .23948954 & -.04347144 & .02127165 & -.00740028 \\ -.05420686 & .36687883 & .39902700 & -.08319557 & .02615028 \\ .02615028 & -.08319557 & .39902700 & .36687883 & -.05420686 \\ -.00740028 & .02127165 & -.04347144 & .23948954 & .13545686 \end{bmatrix} \qquad (B.3)$$

$$\mathcal{W}_5 = \begin{bmatrix} -1.00000000 & -.76505532 & -.28523152 & .28523152 & .76505532 & 1.00000000 \\ .00000000 & .00000000 & .00000000 & .00000000 & .00000000 & .00000000 \\ .09135961 & .16373565 & -.02974921 & .01525535 & -.00894356 & .00328685 \\ -.03954284 & .26394600 & .29767068 & -.06326350 & .03255895 & -.01154547 \\ .02310851 & -.07282206 & .33494505 & .33494505 & -.07282206 & .02310851 \\ -.01154547 & .03255895 & -.06326350 & .29767068 & .26394600 & -.03954284 \\ .00328685 & -.00894356 & .01525535 & -.02974921 & .16373565 & .09135961 \end{bmatrix}$$

$(B.4)$

$$\mathcal{W}_6 = \begin{bmatrix} -1.00000000 & -.83022390 & -.46884879 & .00000000 & .46884879 & .83022390 & 1.00000000 \\ .00000000 & .00000000 & .00000000 & .00000000 & .00000000 & .00000000 & .00000000 \\ .06569253 & .11864577 & -.02153719 & .01119518 & -.00697786 & .00443419 & -.00167654 \\ -.02968808 & .19675645 & .22624682 & -.04815170 & .02613302 & -.01579792 & .00587650 \\ .01905508 & -.05982575 & .27026169 & .28076604 & -.06238108 & .03261326 & -.01164044 \\ -.01164044 & .03261326 & -.06238108 & .28076604 & .27026169 & -.05982575 & .01905508 \\ .00587650 & -.01579792 & .02613302 & -.04815170 & .22624682 & .19675645 & -.02968808 \\ -.00167654 & .00443419 & -.00697786 & .01119518 & -.02153719 & .11864577 & .06569253 \end{bmatrix}$$

(B.5)

$$\mathcal{W}_7 = \begin{bmatrix} -1.00000000 & -.87174015 & -.59170018 & -.20929922 & .20929922 & .59170018 & .87174015 & 1.00000000 \\ .00000000 & .00000000 & .00000000 & .00000000 & .00000000 & .00000000 & .00000000 & .00000000 \\ .04947503 & .08978532 & -.01628154 & .00850816 & -.00540841 & .00369077 & -.00245244 & .00094295 \\ -.02295759 & .15151413 & .17627681 & -.03746983 & .02067231 & -.01335611 & .00866234 & -.00330210 \\ .01555127 & -.04873911 & .21808803 & .23145357 & -.05153854 & .02849936 & -.01742762 & .00651400 \\ -.01050927 & .02936159 & -.05579463 & .24624152 & .24624152 & -.05579463 & .02936159 & -.01050927 \\ .00651400 & -.01742762 & .02849936 & -.05153854 & .23145357 & .21808803 & -.04873911 & .01555127 \\ -.00330210 & .00866234 & -.01335611 & .02067231 & -.03746983 & .17627681 & .15151413 & -.02295759 \\ .00094295 & -.00245244 & .00369077 & -.00540841 & .00850816 & -.01628154 & .08978532 & .04947503 \end{bmatrix} \quad \text{(B.6)}$$

$$\mathcal{W}_8 = \begin{bmatrix} -1.00000000 & -.89975800 & -.67718628 & -.36311746 & .00000000 & .36311746 & .67718628 & .89975800 & 1.00000000 \\ .00000000 & .00000000 & .00000000 & .00000000 & .00000000 & .00000000 & .00000000 & .00000000 & .00000000 \\ .03858768 & .07025101 & -.01272820 & .00666755 & -.00427369 & .00298860 & -.00214812 & .00146755 & -.00057039 \\ -.01821952 & .11992193 & .14059219 & -.02983902 & .01657357 & -.01095025 & .00765877 & -.00516256 & .00199655 \\ .01277058 & -.03998597 & .17790013 & .19134243 & -.04256122 & .02396286 & -.01570330 & .01027426 & -.00393093 \\ -.00915870 & .02555263 & -.04839968 & .21134521 & .21602098 & -.04908886 & .02736692 & -.01682355 & .00630252 \\ .00630252 & -.01682355 & .02736692 & -.04908886 & .21602098 & .21134521 & -.04839968 & .02555263 & -.00915870 \\ -.00393093 & .01027426 & -.01570330 & .02396286 & -.04256122 & .19134243 & .17790013 & -.03998597 & .01277058 \\ .00199655 & -.00516256 & .00765877 & -.01095025 & .01657357 & -.02983902 & .14059219 & .11992193 & -.01821952 \\ -.00057039 & .00146755 & -.00214812 & .00298860 & -.00427369 & .00666755 & -.01272820 & .07025101 & .03858768 \end{bmatrix}$$

(B.7)

$$W_9 = \begin{bmatrix}
-1.00000000 & -.91953391 & -.73877386 & -.47792495 & -.16527896 & .16527896 & .47792495 & .73877386 & .91953391 & 1.00000000 \\
.00000000 & .00000000 & .00000000 & .00000000 & .00000000 & .00000000 & .00000000 & .00000000 & .00000000 & .00000000 \\
.03093030 & .05643594 & -.01021815 & .00535941 & -.00344925 & .00243838 & -.00180282 & .00133952 & -.00093228 & .00036504 \\
-.01478117 & .09711306 & .11445424 & -.02425882 & .01351771 & -.00901930 & .00647953 & -.00474040 & .00327262 & -.00127744 \\
.01060291 & -.03317994 & .14707011 & .15961048 & -.03544673 & .02011031 & -.01349794 & .00954557 & -.00647836 & .00251255 \\
-.00790229 & .02203034 & -.04165330 & .18070787 & .18731172 & -.04253068 & .02416459 & -.01594323 & .01047691 & -.00401595 \\
.00578828 & -.01543233 & .02503502 & -.04471961 & .19460760 & .19460760 & -.04471961 & .02503502 & -.01543233 & .00578828 \\
-.00401595 & .01047691 & -.01594323 & .02416459 & -.04253068 & .18731172 & .18070787 & -.04165330 & .02203034 & -.00790229 \\
.00251255 & -.00647836 & .00954557 & -.01349794 & .02011031 & -.03544673 & .15961048 & .14707011 & -.03317994 & .01060291 \\
-.00127744 & .00327262 & -.00474040 & .00647953 & -.00901930 & .01351771 & -.02425882 & .11445424 & .09711306 & -.01478117 \\
.00036504 & -.00093228 & .00133952 & -.00180282 & .00243838 & -.00344925 & .00535941 & -.01021815 & .05643594 & .03093030
\end{bmatrix} \tag{B.8}$$

Newton Integrating Matrices

The following weighting matrices are repeated from Ref. [27]. For the Newton weighting matrices, the subscript n denotes the degree of the assumed polynomial upon which the integrating matrix is based. The parameter h is the step size.

$$\mathcal{W}_1 = \frac{h}{2}\begin{bmatrix} 0 & 0 & 0 & \dots & 0 \\ 1 & 1 & 0 & \dots & 0 \\ 0 & 1 & 1 & \dots & 0 \\ \vdots & & \ddots & & \vdots \\ 0 & \dots & 0 & 1 & 1 \end{bmatrix} \tag{B.9}$$

$$\mathcal{W}_2 = \frac{h}{12}\begin{bmatrix} 0 & 0 & 0 & 0 & & \dots & 0 \\ 5 & 8 & -1 & 0 & & \dots & 0 \\ 0 & 5 & 8 & -1 & & \dots & 0 \\ \vdots & & & \ddots & & & \vdots \\ 0 & \dots & & 5 & 8 & -1 & 0 \\ 0 & \dots & & 0 & 5 & 8 & -1 \\ 0 & \dots & & 0 & -1 & 8 & 5 \end{bmatrix} \tag{B.10}$$

$$\mathcal{W}_3 = \frac{h}{24}\begin{bmatrix} 0 & 0 & 0 & 0 & 0 & & & \dots & 0 \\ 9 & 19 & -5 & 1 & 0 & & & \dots & 0 \\ -1 & 13 & 13 & -1 & 0 & & & \dots & 0 \\ 0 & -1 & 13 & 13 & -1 & & & \dots & 0 \\ \vdots & & & & \ddots & & & & \vdots \\ 0 & \dots & & & -1 & 13 & 13 & -1 & 0 \\ 0 & \dots & & & 0 & -1 & 13 & 13 & -1 \\ 0 & \dots & & & 0 & 1 & -5 & 19 & 9 \end{bmatrix} \tag{B.11}$$

$$W_4 = \frac{h}{720}\begin{bmatrix} 0 & 0 & 0 & 0 & 0 & 0 & & & & \dots & 0 \\ 251 & 646 & -264 & 106 & -19 & 0 & & & & \dots & 0 \\ -19 & 346 & 456 & -74 & 11 & 0 & & & & \dots & 0 \\ 0 & -19 & 346 & 456 & -74 & 11 & & & & \dots & 0 \\ \vdots & & & & & \ddots & & & & & \vdots \\ 0 & \dots & & & & -19 & 346 & 456 & -74 & 11 & 0 \\ 0 & \dots & & & & 0 & -19 & 346 & 456 & -74 & 11 \\ 0 & \dots & & & & 0 & 11 & -74 & 456 & 346 & -19 \\ 0 & \dots & & & & 0 & -19 & 106 & -264 & 646 & 251 \end{bmatrix}$$

(*B*.12)

$$W_5 = \frac{h}{1440}\begin{bmatrix} 0 & 0 & 0 & 0 & 0 & 0 & 0 & & & \dots & 0 \\ 475 & 1427 & -798 & 482 & -173 & 27 & 0 & & & \dots & 0 \\ -27 & 637 & 1022 & -258 & 77 & -11 & 0 & & & \dots & 0 \\ 11 & -93 & 802 & 802 & -93 & 11 & 0 & & & \dots & 0 \\ 0 & 11 & -93 & 802 & 802 & -93 & 11 & & & \dots & 0 \\ \vdots & & & & & & \ddots & & & & \vdots \\ 0 & \dots & & & 11 & -93 & 802 & 802 & -93 & 11 & 0 \\ 0 & \dots & & & 0 & 11 & -93 & 802 & 802 & -93 & 11 \\ 0 & \dots & & & 0 & -11 & 77 & -258 & 1022 & 637 & -27 \\ 0 & \dots & & & 0 & 27 & -173 & 482 & -798 & 1427 & 475 \end{bmatrix}$$

(*B*.13)

$$\mathcal{W}_6 = \frac{h}{60480}\begin{bmatrix}
0 & 0 & 0 & 0 & 0 & 0 & 0 & 0 & \cdots & 0 \\
19087 & 65112 & -46461 & 37504 & -20211 & 6312 & -863 & 0 & \cdots & 0 \\
-863 & 25128 & 46989 & -16256 & 7299 & -2088 & 271 & 0 & \cdots & 0 \\
271 & -2760 & 30819 & 37504 & -6771 & 1608 & -191 & 0 & \cdots & 0 \\
0 & 271 & -2760 & 30819 & 37504 & -6771 & 1608 & -191 & \cdots & 0 \\
\vdots & & & & & & & \ddots & & \vdots \\
0 & \cdots & & 271 & -2760 & 30819 & 37504 & -6771 & 1608 & -191 & 0 \\
0 & \cdots & & 0 & 271 & -2760 & 30819 & 37504 & -6771 & 1608 & -191 \\
0 & \cdots & & 0 & -191 & 1608 & -6771 & 37504 & 30819 & -2760 & 271 \\
0 & \cdots & & 0 & 271 & -2088 & 7299 & -16256 & 46989 & 25128 & -863 \\
0 & \cdots & & 0 & -863 & 6312 & -20211 & 37504 & -46461 & 65112 & 19087
\end{bmatrix} \tag{B.14}$$

$$\mathcal{W}_7 = \frac{h}{120960}\begin{bmatrix}
0 & 0 & 0 & 0 & 0 & 0 & 0 & 0 & 0 & \cdots & 0 \\
36799 & 139849 & -121797 & 123133 & -88547 & 41499 & -11351 & 1375 & 0 & \cdots & 0 \\
-1375 & 47799 & 101349 & -44797 & 26883 & -11547 & 2999 & -351 & 0 & \cdots & 0 \\
351 & -4183 & 57627 & 81693 & -20227 & 7227 & -1719 & 191 & 0 & \cdots & 0 \\
-191 & 1879 & -9531 & 68323 & 68323 & -9531 & 1879 & -191 & 0 & \cdots & 0 \\
0 & -191 & 1879 & -9531 & 68323 & 68323 & -9531 & 1879 & -191 & \cdots & 0 \\
\vdots & & & & & & & & \ddots & & \vdots \\
0 & \cdots & -191 & 1879 & -9531 & 68323 & 68323 & -9531 & 1879 & -191 & 0 \\
0 & \cdots & 0 & -191 & 1879 & -9531 & 68323 & 68323 & -9531 & 1879 & -191 \\
0 & \cdots & 0 & 191 & -1719 & 7227 & -20227 & 81693 & 57627 & -4183 & 351 \\
0 & \cdots & 0 & -351 & 2999 & -11547 & 26883 & -44797 & 101349 & 47799 & -1375 \\
0 & \cdots & 0 & 1375 & -11351 & 41499 & -88547 & 123133 & -121797 & 139849 & 36799
\end{bmatrix} \tag{B.15}$$

A Sample Gauss-Legendre Integrating Matrix

The Gauss-Legendre integrating matrix presented here is an example of an integrating matrix that does not use end point nodes. Obviously, such matrices cannot be used for intervals where boundary conditions must be applied at the end points; instead, their intended use is for interior integration regions. As pointed out in Section 3.2, the merging process, which forms *global* weighting matrices from the summation of *local* weighting matrices, allows one to combine weighting matrices with and without endpoint nodes.

Gauss-Legendre integrating matrices, which are based upon Legendre polynomials, are related to Gauss-Legendre quadrature. These matrices are also a close relative of the Jacobi integrating matrices since Legendre polynomials prove to be a special case of the more general Jacobi polynomials with $\alpha = \beta = 0$. In fact, the general calculation procedure in Appendix A for Jacobi weighting matrices, when adapted to Legendre polynomials, can be used for the Gauss-Legendre weighting matrices. Note, however, that the Gauss-Legendre matrices, because of the lack of end points, are rectangular rather than square. To make the Gauss-Legendre matrices "conform" to other matrices with end points, the first and last columns of the matrix are "padded" with zeroes as shown in the example below; this padding allows the definition of consistent merging rules as noted in Section 3.2.

The weighting matrix below, with two internal grid points, is for the normalized interval $[-1, 1]$; it can be transformed to $[0, 1]$ by multiplying by the factor $1/2$. Similar to the Jacobi matrices, the coordinate values x, which denote grid points on $[-1, 1]$, are listed above the horizontal bar in the matrix. The grid points t on $[0, 1]$ can be obtained with the linear transformation $t = 0.5(1 + x)$. The subscript n refers to the number of discretization intervals, with the integration being exact for all polynomials of degree $\leq 2n - 3$.

$$\mathcal{W}_3 = \begin{bmatrix} & -.57735027 & .57735027 & \\ \hline .00000000 & .00000000 & .00000000 & .00000000 \\ .00000000 & -.07735027 & .50000000 & .00000000 \\ .00000000 & .57735027 & .57735027 & .00000000 \\ .00000000 & .50000000 & -.07735027 & .00000000 \end{bmatrix} \qquad (B.2)$$

Appendix C

Composite Laminate Constitutive Equations

The behavior of multi-ply laminated composites and composite skin box-beams can be predicted by developing relationships in the laminate axes between the applied loads and the resulting deflections. To develop such relationships, one begins with the stress-strain behavior of a single lamina of an orthotropic material. The lamina behavior is subsequently transformed from principal axes of the lamina to the reference axes for the multi-ply laminate. By then applying the assumptions of thin plate theory, expressions are developed from the properties of the constituent laminae relating force and moment resultants acting on the plate to midplane strains and plate curvatures. These expressions are the laminate constitutive equations. The following is intended only as a brief description of the process for obtaining the constitutive equations. More detailed presentations of these developments are given by Jones [25] and Ashton, Halpin, and Petit [56].

Assuming a state of plane stress, the simplified stress-strain relationships for a lamina of orthotropic material can be written as

$$\begin{Bmatrix} \sigma_1 \\ \sigma_2 \\ \tau_{12} \end{Bmatrix}_k = \begin{bmatrix} Q_{11} & Q_{12} & 0 \\ Q_{12} & Q_{22} & 0 \\ 0 & 0 & Q_{66} \end{bmatrix}_k \begin{Bmatrix} \epsilon_1 \\ \epsilon_2 \\ \gamma_{12} \end{Bmatrix}_k \qquad (C.1)$$

where

$$
\begin{aligned}
Q_{11} &= \frac{E_1}{1-\nu_{12}\nu_{21}} \\
Q_{12} &= \frac{\nu_{12}E_2}{1-\nu_{12}\nu_{21}} = \frac{\nu_{21}E_1}{1-\nu_{12}\nu_{21}} \\
Q_{22} &= \frac{E_2}{1-\nu_{12}\nu_{21}} \\
Q_{66} &= G_{12}\,,
\end{aligned}
\tag{C.2}
$$

and the subscript k denotes the kth layer in the laminate. The terms Q_{ij}, which are referred to as reduced stiffnesses, are defined in the lamina principle axes (see Fig. C-1).

If θ is defined as the angle between the x-axis and the 1-axis (see Fig. C-2), then a transformation of both stress and strain components in Eq. (C.1) leads to the following stress-strain equations for the lamina in the laminate axis system:

$$
\begin{Bmatrix} \sigma_x \\ \sigma_y \\ \tau_{xy} \end{Bmatrix}_k = \begin{bmatrix} \overline{Q}_{11} & \overline{Q}_{12} & \overline{Q}_{16} \\ \overline{Q}_{12} & \overline{Q}_{22} & \overline{Q}_{26} \\ \overline{Q}_{16} & \overline{Q}_{26} & \overline{Q}_{66} \end{bmatrix}_k \begin{Bmatrix} \epsilon_x \\ \epsilon_y \\ \gamma_{xy} \end{Bmatrix}_k \tag{C.3}
$$

where the $\overline{Q}_{ij}$ are the transformed reduced stiffnesses, which have the definitions

$$
\begin{aligned}
\overline{Q}_{11} &= Q_{11}\cos^4\theta + 2(Q_{12}+2Q_{66})\sin^2\theta\cos^2\theta + Q_{22}\sin^4\theta \\
\overline{Q}_{12} &= (Q_{11}+Q_{22}-4Q_{66})\sin^2\theta\cos^2\theta + Q_{12}(\sin^4\theta+\cos^4\theta) \\
\overline{Q}_{22} &= Q_{11}\sin^4\theta + 2(Q_{12}+2Q_{66})\sin^2\theta\cos^2\theta + Q_{22}\cos^4\theta \\
\overline{Q}_{16} &= (Q_{11}-Q_{12}-2Q_{66})\sin\theta\cos^3\theta + (Q_{12}-Q_{22}+2Q_{66})\sin^3\theta\cos\theta \\
\overline{Q}_{26} &= (Q_{11}-Q_{12}-2Q_{66})\sin^3\theta\cos\theta + (Q_{12}-Q_{22}+2Q_{66})\sin\theta\cos^3\theta \\
\overline{Q}_{66} &= (Q_{11}+Q_{22}-2Q_{12}-2Q_{66})\sin^2\theta\cos^2\theta + Q_{66}(\sin^4\theta+\cos^4\theta)\,.
\end{aligned}
\tag{C.4}
$$

A convenient form exists for calculating the transformed reduced stiffnesses in terms of stiffness invariants. This invariant form, which was first developed by Tsai

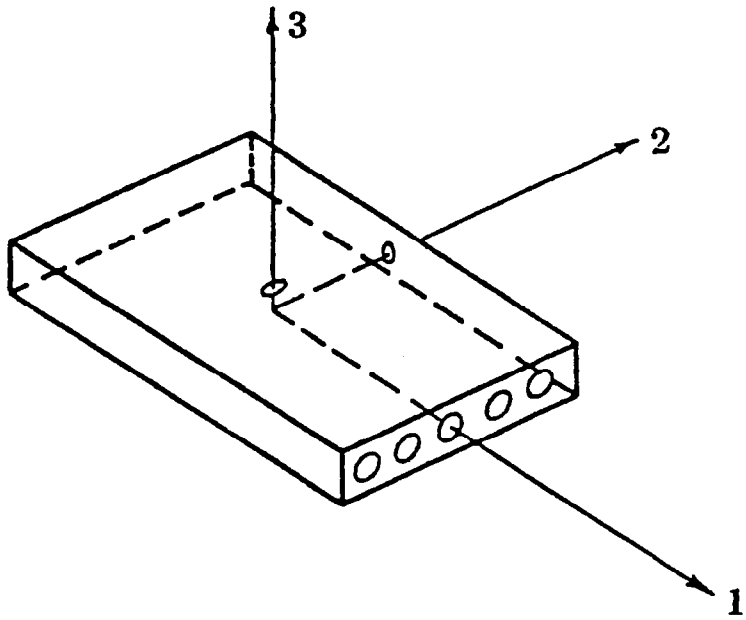

Fig. C-1. Lamina axis system (1,2,3)

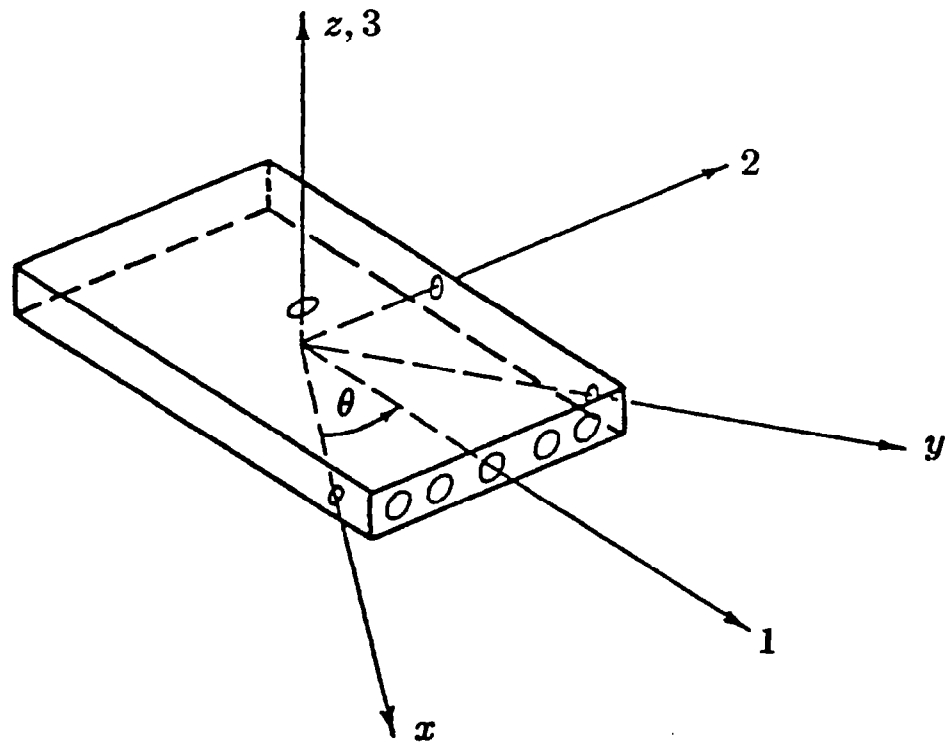

Fig. C-2. Laminate axis system (x, y, z)

and Pagano [57], is written as

$$\begin{aligned}
\overline{Q}_{11} &= U_1 + U_2 \cos 2\theta + U_3 \cos 4\theta \\
\overline{Q}_{12} &= U_4 + U_3 \cos 4\theta \\
\overline{Q}_{22} &= U_1 - U_2 \cos 2\theta + U_3 \cos 4\theta \\
\overline{Q}_{16} &= \frac{1}{2} U_2 \sin 2\theta + U_3 \sin 4\theta \\
\overline{Q}_{26} &= \frac{1}{2} U_2 \sin 2\theta - U_3 \sin 4\theta \\
\overline{Q}_{66} &= U_5 - U_3 \cos 4\theta
\end{aligned} \tag{C.5}$$

where the stiffness invariants are

$$\begin{aligned}
U_1 &= \frac{1}{8}(3Q_{11} + 3Q_{22} + 2Q_{12} + 4Q_{66}) \\
U_2 &= \frac{1}{2}(Q_{11} - Q_{22}) \\
U_3 &= \frac{1}{8}(Q_{11} + Q_{22} - 2Q_{12} - 4Q_{66}) \\
U_4 &= \frac{1}{8}(Q_{11} + Q_{22} + 6Q_{12} - 4Q_{66}) \\
U_5 &= \frac{1}{8}(Q_{11} + Q_{22} - 2Q_{12} + 4Q_{66}).
\end{aligned} \tag{C.6}$$

With the foregoing knowledge of the behavior of a single layer, classical lamination theory for thin plates can now be used to determine the behavior of the laminate, or laminated box-beam. Classical lamination theory embodies a collection of stress and deformation assumptions which constitute the familiar Kirchhoff hypothesis for plates. Under these assumptions, the strains for any point in the laminate can be written in terms of geometrical midplane displacements u_0, v_0, and

w_0 as

$$\epsilon_x = \frac{\partial u_0}{\partial x} - z\frac{\partial^2 w_0}{\partial x^2},$$

$$\epsilon_y = \frac{\partial v_0}{\partial y} - z\frac{\partial^2 w_0}{\partial y^2}, \tag{C.7}$$

$$\gamma_{xy} = \frac{\partial u_0}{\partial y} + \frac{\partial v_0}{\partial x} - 2z\frac{\partial^2 w_0}{\partial x \partial y}.$$

Furthermore, the laminate strains given by Eq. (C.7) are equivalently expressed in terms of the midplane strains and plate curvatures as

$$\begin{Bmatrix} \epsilon_x \\ \epsilon_y \\ \gamma_{xy} \end{Bmatrix} = \begin{Bmatrix} \epsilon_x^0 \\ \epsilon_y^0 \\ \gamma_{xy}^0 \end{Bmatrix} + z\begin{Bmatrix} \kappa_x \\ \kappa_y \\ \kappa_{xy} \end{Bmatrix} \tag{C.8}$$

If we now define the vectors

$$\begin{aligned} \boldsymbol{\sigma} &= \{\sigma_x \quad \sigma_y \quad \tau_{xy}\}^T, \\ \boldsymbol{\epsilon}^0 &= \{\epsilon_x^0 \quad \epsilon_y^0 \quad \gamma_{xy}^0\}^T, \\ \boldsymbol{\kappa} &= \{\kappa_x \quad \kappa_y \quad \kappa_{xy}\}^T, \end{aligned} \tag{C.9}$$

then, with the aid of Eq. (C.8), the kth layer stress-strain relationships in Eq. (C.3) can be expressed in the form

$$\boldsymbol{\sigma}_k = [\overline{Q}]_k \boldsymbol{\epsilon}^0 + z[\overline{Q}]_k \boldsymbol{\kappa}. \tag{C.10}$$

Force and moment resultants offer a convenient way of expressing the relationships between internal and external loads of a laminated plate. With this in mind, it is convenient to make use of a force resultant vector $\mathbf{n}$ and a moment resultant

vector **m** which appear as

$$\mathbf{n} = \{N_x \quad N_y \quad N_{xy}\}^T, \qquad \mathbf{m} = \{M_x \quad M_y \quad M_{xy}\}^T . \tag{C.11}$$

By assuming that the plate (or box-beam) has total thickness t and a number of layers NL, the force and moment resultants (i.e., force and moment per unit width) are defined by integrating the stresses in each lamina over the thickness, that is,

$$\begin{Bmatrix} \mathbf{n} \\ \mathbf{m} \end{Bmatrix} = \int_{-t/2}^{t/2} \begin{Bmatrix} \sigma_k \\ \sigma_k z \end{Bmatrix} dz = \sum_{k=1}^{NL} \int_{z_{k-1}}^{z_k} \begin{Bmatrix} \sigma_k \\ \sigma_k z \end{Bmatrix} dz . \tag{C.12}$$

By substituting Eq. (C.10) into Eq. (C.12) and noting that $[\overline{Q}]$, ϵ^0, and κ are not functions of z, one obtains the force and moment resultant expressions

$$\mathbf{n} = \sum_{k=1}^{NL} [\overline{Q}]_k \left\{ \epsilon^0 \int_{z_{k-1}}^{z_k} dz + \kappa \int_{z_{k-1}}^{z_k} z\, dz \right\} \tag{C.13}$$

and

$$\mathbf{m} = \sum_{k=1}^{NL} [\overline{Q}]_k \left\{ \epsilon^0 \int_{z_{k-1}}^{z_k} z\, dz + \kappa \int_{z_{k-1}}^{z_k} z^2\, dz \right\} . \tag{C.14}$$

After carrying out the integrations, Eqs. (C.13–C.14) can be written as

$$\begin{Bmatrix} N_x \\ N_y \\ N_{xy} \\ M_x \\ M_y \\ M_{xy} \end{Bmatrix} = \begin{bmatrix} A_{11} & A_{12} & A_{16} & B_{11} & B_{12} & B_{16} \\ A_{12} & A_{22} & A_{26} & B_{12} & B_{22} & B_{26} \\ A_{16} & A_{26} & A_{66} & B_{16} & B_{26} & B_{66} \\ B_{11} & B_{12} & B_{16} & D_{11} & D_{12} & D_{16} \\ B_{12} & B_{22} & B_{26} & D_{12} & D_{22} & D_{26} \\ B_{16} & B_{26} & B_{66} & D_{16} & D_{26} & D_{66} \end{bmatrix} \begin{Bmatrix} \epsilon_x^0 \\ \epsilon_y^0 \\ \gamma_{xy}^0 \\ \kappa_x \\ \kappa_y \\ \kappa_{xy} \end{Bmatrix} \tag{C.15}$$

where

$$A_{ij} = \sum_{k=1}^{NL} (\overline{Q}_{ij})_k \, (z_k - z_{k-1})$$

$$B_{ij} = \frac{1}{2} \sum_{k=1}^{NL} (\overline{Q}_{ij})_k \, (z_k^2 - z_{k-1}^2) \qquad (C.16)$$

$$D_{ij} = \frac{1}{3} \sum_{k=1}^{NL} (\overline{Q}_{ij})_k \, (z_k^3 - z_{k-1}^3)$$

In Eqs. (C.15) and (C.16), the A_{ij} are extensional stiffnesses, the B_{ij} are coupling stiffnesses, and the D_{ij} are bending stiffnesses. For those laminates with layers arranged symmetrically about the geometric midplane of the plate, the B_{ij} terms will be zero.

The integrating matrix approach requires knowledge of the compliance terms rather than the stiffness terms. The compliance terms are obtained by simply inverting the (6 × 6) matrix of stiffness terms appearing in Eq. (C.15). In symbolic form, the composite compliance relationship can be written as

$$\begin{Bmatrix} \epsilon^0 \\ \kappa \end{Bmatrix} = \begin{bmatrix} \mathbf{A^*} & \mathbf{B^*} \\ \mathbf{B^*} & \mathbf{D^*} \end{bmatrix} \begin{Bmatrix} \mathbf{n} \\ \mathbf{m} \end{Bmatrix}. \qquad (C.17)$$

In Eq. (C.17), the subscripts of the terms in the (3×3) submatrices will be designated by $i, j = 1, 2, 3$, rather than $i, j = 1, 2, 6$.

Appendix D

Modified Strip Theory Aerodynamics

The following nondimensional unsteady aerodynamic loads have evolved from the modified strip theory developed by Yates [58,59]. These Laplace transformed aerodynamic loads, which are valid for arbitrary motion, are made applicable to the Laplace domain by inclusion of either a generalized Theodorsen's function or an appropriate rational approximation as discussed by Edwards [60–62]. The loads presented here are intended for use with the Laplace transformed flutter equations (cf., Eqs. (2.21) and (4.30)), and correspond to those load terms required by Eq. (2.28). The nondimensionalization of the aerodynamic loads is the same as that indicated for the p's in Eq. (2.31).

As in the theory presented by Yates, these aerodynamics employ a variable section lift-curve slope $a_0(\bar{x})$ instead of 2π, a variable section aerodynamic center $a_c(\bar{x})$ instead of -0.5 (the quarter-chord), and a variable section structural reference axis location $a(\bar{x})$. The Theodorsen function can be modified by a factor which accounts for compressibility effects on the magnitude of the lift and pitching moment. For more details on the modifications accompanying a particular planform and Mach number, see the above references by Yates. It should be noted that for incompressible flow over untapered wings having a lift-curve slope of 2π and an aerodynamic center at the quarter-chord, the aerodynamics given here reduce to the elementary strip theory used by Barmby, Cunningham, and Garrick [63].

The nondimensional Laplace transformed aerodynamic loads providing lift and pitching moment per unit span can be conveniently calculated with the aid of an

aerodynamic influence matrix $\mathbf{Q}_{FD}(s^*, \lambda)$. The terms appearing in $\mathbf{Q}_{FD}$ are given by

$$\hat{L}_w(s^*, \lambda) = \frac{\ell}{b_R}\left\{-\pi\beta^2 s^{*2} - \mathrm{RC}(\bar{s})a_0\sqrt{\lambda}\,\beta s^*\right\}$$

$$\hat{L}_\alpha(s^*, \lambda) = \bar{b}\left\{\pi a\beta^2 s^{*2} - \pi\sqrt{\lambda}\,\beta s^* - \mathrm{RC}(\bar{s})a_0(a_d - a)\sqrt{\lambda}\,\beta s^* - \mathrm{RC}(\bar{s})a_0\lambda\right\}$$

$$\hat{L}_\gamma(s^*, \lambda) = \bar{b}\left\{\pi\sqrt{\lambda}\,\beta s^* + \mathrm{RC}(\bar{s})a_0\lambda\right\}\tan\Lambda$$

$$\hat{L}_\tau(s^*, \lambda) = \bar{b}^2\frac{b_R}{\ell}\left\{\pi a\sqrt{\lambda}\,\beta s^* - \mathrm{RC}(\bar{s})a_0(a_d - a)\lambda\right\}\tan\Lambda$$

$$\hat{M}_w(s^*, \lambda) = \bar{b}\left\{\pi a\beta^2 s^{*2} + \mathrm{RC}(\bar{s})a_0(a - a_c)\sqrt{\lambda}\,\beta s^*\right\}$$

$$\hat{M}_\alpha(s^*, \lambda) = \bar{b}^2\frac{b_R}{\ell}\left\{-\pi\left(\tfrac{1}{8} + a^2\right)\beta^2 s^{*2} - \pi(a_d - a)\sqrt{\lambda}\,\beta s^* + \mathrm{RC}(\bar{s})a_0(a - a_c)(a_d - a)\sqrt{\lambda}\,\beta s^* + \mathrm{RC}(\bar{s})a_0(a - a_c)\lambda\right\}$$

$$\hat{M}_\gamma(s^*, \lambda) = \bar{b}^2\frac{b_R}{\ell}\left\{-\pi a\sqrt{\lambda}\,\beta s^* - \mathrm{RC}(\bar{s})a_0(a - a_c)\lambda\right\}\tan\Lambda$$

$$\hat{M}_\tau(s^*, \lambda) = \bar{b}^3\left(\frac{b_R}{\ell}\right)^2\left\{-\pi\left(\tfrac{1}{8} + a^2\right)\sqrt{\lambda}\,\beta s^* + \mathrm{RC}(\bar{s})a_0(a - a_c)(a_d - a)\lambda\right\}\tan\Lambda\,.$$

(*D*.1)

From the terms in Eq. (D.1), the aerodynamic matrix $\mathbf{Q}_{FD}(s^*, \lambda)$ is constructed in the form

$$\mathbf{Q}_{FD}(s^*, \lambda) = \begin{bmatrix} 0 & 0 & 0 & 0 \\ 0 & 0 & 0 & 0 \\ 0 & \grave{\hat{L}}_\gamma & \grave{\hat{L}}_w & \hat{L}_{\alpha,\tau} \\ 0 & \grave{\hat{M}}_\gamma & \grave{\hat{M}}_w & \hat{M}_{\alpha,\tau} \end{bmatrix} \qquad (D.2)$$

where

$$\hat{L}_{\alpha,\tau} = \grave{\hat{L}}_\alpha + \grave{\hat{L}}_\tau D \qquad (D.3)$$

and

$$\hat{\boldsymbol{M}}_{\alpha,\tau} = \grave{} \hat{\boldsymbol{M}}_{\alpha} + \grave{} \hat{\boldsymbol{M}}_{\tau} \boldsymbol{D}, \tag{D.4}$$

with $\boldsymbol{D}$ being a differentiating matrix. (Note that the subscript τ is used as a reference to the variable, $\tau = \frac{\partial \alpha}{\partial \bar{x}}$.) For moderate angles of wing aerodynamic sweep and large aspect ratio, the last term on the right-hand side of Eqs. (D.3–D.4) is negligible compared to the remaining term.

The following definitions apply to the foregoing equations, in which λ is a dimensionless dynamic pressure parameter and s^* is a dimensionless Laplace variable:

$$\begin{aligned}
s^* &= s\ell^2 \sqrt{\frac{m_R}{(EI)_R}} \\
\bar{s} &= \frac{sb}{V^*} = \frac{\beta s^*}{\sqrt{\lambda}} \\
\lambda &= \frac{\rho b_R \ell^3 V^{*2}}{(EI)_R} \\
V^* &= V \cos \Lambda \\
\mu &= \frac{m_R}{\pi \rho b_R^2} \\
\beta &= \bar{b} \sqrt{\frac{b_R}{\pi \mu \ell}} \\
\bar{b} &= \frac{b}{b_R} .
\end{aligned} \tag{D.5}$$

The aerodynamic downwash point a_d is calculated from

$$a_d = \frac{a_0}{2\pi} + a_c . \tag{D.6}$$

A convenient rational approximation to the Theodorsen function, attributed to

R.T. Jones, is given by

$$C(\bar{s}) = \frac{0.5\bar{s}^2 + 0.2808\bar{s} + 0.01365}{\bar{s}^2 + 0.3455\bar{s} + 0.01365} . \qquad (D.7)$$

As discussed in Yates [58], for higher Mach numbers M, $C(\bar{s})$ can be empirically corrected for compressibility effects by scaling by a factor $R(\bar{s}, M)$, which is determined from a ratio of the magnitudes of compressible and incompressible circulation functions.

Appendix E

Solutions for Problems with Concentrated Loads

Concentrated loads present a special type of discontinuity that can be treated with the help of delta functions. To include the possibility of delta functions in the integrating matrix approach, it is first necessary to extend the developments of Section 3.1 for the integrating matrices of continuous integrands. Once delta functions have been included in the formulation of integrating matrices, the solution methods presented in Chapter 4 can be expanded to accommodate concentrated loads.

Instead of considering a simple continuous function $f(x)$, as was done in Section 3.1, it is now necessary to consider a function of the form

$$\overline{f}(x) = f(x) + p_i^+ \delta(x - x_i) \tag{E.1}$$

where p_i^+ gives the magnitude of the delta function (concentrated load) at the point $x = x_i$. Taking the integral of Eq. (E.1) over the subinterval $[x_i, x_{i+1}]$, with the delta function located at x_{i+1}, yields

$$\begin{aligned} \int_{x_i}^{x_{i+1}} \overline{f}(x)\,dx &= \int_{x_i}^{x_{i+1}} f(x)\,dx + p_{i+1}^+ \int_{x_i}^{x_{i+1}} \delta(x - x_{i+1})\,dx \\ &= \int_{x_i}^{x_{i+1}} f(x)\,dx + p_{i+1}^+ . \end{aligned} \tag{E.2}$$

By using the definitions for $\{\mathcal{F}\}$ and $\{f\}$ given in Eqs. (3.5) and (3.6) and including

the definition of the column vector

$$\{p^+\} = (p_0^+,\ p_1^+, \ldots,\ p_N^+)^T, \tag{E.3}$$

one can express the set of all integrals given by Eq. (E.2) as

$$\{\mathcal{F}\} = \mathcal{W}_n\{f\} + \{p^+\}. \tag{E.4}$$

This result is analogous to Eq. (3.7); note, however, that the first term in $\{\mathcal{F}\}$ is zero only if p_0^+ is zero. As in Section 3.1, Eq. (E.4) can be premultiplied by the summing matrix $\mathcal{S}$ to yield the integrating matrix relationship

$$\{\overline{\mathcal{F}}\} = \mathsf{L}\{f\} + \mathcal{S}\{p^+\} \tag{E.5}$$

where the integrating matrix L is the same as defined in Eq. (3.11). Thus, from Eq. (E.5) it is clear that the "integrating matrix" for delta functions is simply the summing matrix $\mathcal{S}$.

The foregoing results can be applied to solving problems as discussed in Section 4.1. Consider, for example, the discretized equations given in Eq. (4.2). After including the concentrated loads, the equation can be written in the form

$$\tilde{\mathbf{y}}' = \tilde{\mathbf{Z}}\tilde{\mathbf{y}} - \lambda(\tilde{\mathbf{A}} + \tilde{\mathbf{A}}^+\delta(x - x_i))\tilde{\mathbf{y}} - (\tilde{\mathbf{a}}_r + \tilde{\mathbf{a}}_r^+\delta(x - x_i)). \tag{E.6}$$

Applying the integrating matrices then yields

$$\tilde{\mathbf{y}} = \tilde{\mathsf{L}}(\tilde{\mathbf{Z}}\tilde{\mathbf{y}} - \lambda\tilde{\mathbf{A}}\tilde{\mathbf{y}} - \tilde{\mathbf{a}}_r) - \tilde{\mathcal{S}}(\lambda\tilde{\mathbf{A}}^+\tilde{\mathbf{y}} + \tilde{\mathbf{a}}_r^+) + \tilde{\mathbf{k}}. \tag{E.7}$$

This result compares with that of Eq. (4.3). Note that the global summing matrix $\tilde{\mathcal{S}}$ will be composed of diagonal blocks of dimension $(N+1)\times(N+1)$, which corresponds to $\tilde{\mathsf{L}}$ in Eq. (4.4).

If one now solves for $\tilde{\mathbf{k}}$, the equivalent of Eq. (4.9) is obtained. Thus,

$$\tilde{\mathbf{k}} = -\tilde{\mathbf{B}}[\tilde{\mathbf{L}}(\tilde{\mathbf{Z}}\tilde{\mathbf{y}} - \lambda\tilde{\mathbf{A}}\tilde{\mathbf{y}} - \tilde{\mathbf{a}}_r) - \tilde{\mathbf{S}}(\lambda\tilde{\mathbf{A}}^+\tilde{\mathbf{y}} + \tilde{\mathbf{a}}_r^+)] - \tilde{\mathbf{B}}_{nh}\tilde{\mathbf{y}}. \qquad (E.8)$$

After substituting Eq. (E.8) into Eq. (E.7), grouping similar terms, and then rearranging, one has the result

$$[\mathbf{H} - \lambda(\mathbf{F}\tilde{\mathbf{A}} + \mathbf{F}^+\tilde{\mathbf{A}}^+)]\tilde{\mathbf{y}} = \mathbf{f} \qquad (E.9)$$

where

$$\mathbf{H} = \mathbf{I} + \tilde{\mathbf{B}}_{nh} + \mathbf{F}\tilde{\mathbf{Z}} \qquad (E.10)$$

$$\mathbf{F} = [\tilde{\mathbf{B}} - \mathbf{I}]\tilde{\mathbf{L}}, \qquad \mathbf{F}^+ = [\tilde{\mathbf{B}} - \mathbf{I}]\tilde{\mathbf{S}} \qquad (E.11)$$

$$\mathbf{f} = \mathbf{F}\tilde{\mathbf{a}}_r + \mathbf{F}^+\tilde{\mathbf{a}}_r^+ . \qquad (E.12)$$

It is clear that these equations are simply an extension of Eqs. (4.10–4.13).

Carrying the analysis one step further, the reduced nonhomogeneous linear system in Eq. (4.26), for $\mathbf{H}_{FD} = 0$, appears as

$$[\mathbf{I} - \lambda(\mathbf{T}\mathbf{A}_{FD} + \mathbf{T}^+\mathbf{A}_{FD}^+)]\tilde{\mathbf{y}}_D = \mathbf{T}\tilde{\mathbf{a}}_{r_F} + \mathbf{T}^+\tilde{\mathbf{a}}_{r_F}^+ \qquad (E.13)$$

where

$$\mathbf{T} = -\mathbf{H}_{DD}^{-1}\mathbf{H}_{DF}\mathbf{H}_{FF}^{-1}\mathbf{F}_{FF} \qquad (E.14)$$

and

$$\mathbf{T}^+ = -\mathbf{H}_{DD}^{-1}\mathbf{H}_{DF}\mathbf{H}_{FF}^{-1}\mathbf{F}_{FF}^+ . \qquad (E.15)$$

Similarly, the reduced eigenvalue problem can be written as

$$[(\mathbf{T}\mathbf{A}_{FD} + \mathbf{T}^+\mathbf{A}_{FD}^+) - (1/\lambda)\mathbf{I}]\tilde{\mathbf{y}}_D = 0 . \qquad (E.16)$$

Appendix F

Constraint Equations

Auxiliary constraint equations can be used in specific instances to reduce the degrees of freedom required for a numerical solution. To carry out reductions on matrix equations, it is convenient to think in terms of partitioned matrices, where the variables to be eliminated are placed in a partition of the solution vector, and all matrices appearing in the matrix equation are partitioned accordingly. The constraint equations are then used to obtain a transformation of variables

$$\mathbf{y} = \mathbf{U}\mathbf{y}^* \tag{F.1}$$

where $\mathbf{y}$ is a vector containing the original variables, $\mathbf{y}^*$ is a vector of transformed variables, and $\mathbf{U}$ is a transformation matrix. It is assumed initially that $\mathbf{U}$ is a square matrix that possesses an inverse, but as noted below, one can make use of other types of transformations that are characterized by rectangular transformation matrices.

Consider first a partitioned system of linear equations

$$\begin{bmatrix} \mathbf{G}_{11} & \mathbf{G}_{12} \\ \mathbf{G}_{21} & \mathbf{G}_{22} \end{bmatrix} \begin{Bmatrix} \mathbf{y}_1 \\ \mathbf{y}_2 \end{Bmatrix} = \begin{Bmatrix} \mathbf{f}_1 \\ \mathbf{f}_2 \end{Bmatrix}. \tag{F.2}$$

Equation (F.1) can be substituted into Eq. (F.2), and the resulting matrix equation premultiplied by $\mathbf{U}^{-1}$. If $\mathbf{U}$ does in fact represent an elimination of variables, then $\mathbf{G}$ will be transformed by this similarity transformation into a block triangular form

such that

$$\begin{bmatrix} \mathbf{G}'_{11} & \mathbf{0} \\ \mathbf{G}'_{21} & \mathbf{I} \end{bmatrix} \begin{Bmatrix} \mathbf{y}_1^* \\ \mathbf{y}_2^* \end{Bmatrix} = \begin{Bmatrix} \mathbf{f}_1^* \\ \mathbf{f}_2^* \end{Bmatrix} \tag{F.3}$$

where $\mathbf{y}_2^*$ contains the eliminated variables and $\mathbf{f}^* = \mathbf{U}^{-1}\mathbf{f}$. The reduced linear system is obtained directly from Eq. (F.3) as

$$\mathbf{G}'_{11}\mathbf{y}_1^* = \mathbf{f}_1^*. \tag{F.4}$$

An identical approach can be followed for the eigenvalue problem given by

$$\begin{bmatrix} \mathbf{G}_{11} & \mathbf{G}_{12} \\ \mathbf{G}_{21} & \mathbf{G}_{22} \end{bmatrix} \begin{Bmatrix} \mathbf{y}_1 \\ \mathbf{y}_2 \end{Bmatrix} = \lambda \begin{Bmatrix} \mathbf{y}_1 \\ \mathbf{y}_2 \end{Bmatrix}. \tag{F.5}$$

The similarity transformation in this situation yields the equations

$$\begin{bmatrix} \mathbf{G}'_{11} & \mathbf{0} \\ \mathbf{G}'_{21} & \mathbf{0} \end{bmatrix} \begin{Bmatrix} \mathbf{y}_1^* \\ \mathbf{y}_2^* \end{Bmatrix} = \lambda \begin{Bmatrix} \mathbf{y}_1^* \\ \mathbf{y}_2^* \end{Bmatrix} \tag{F.6}$$

from which the reduced eigenvalue problem is

$$[\mathbf{G}'_{11} - \lambda\mathbf{I}]\mathbf{y}_1^* = \mathbf{0}. \tag{F.7}$$

For those problems for which $\mathbf{U}$ is a square, invertable matrix, the foregoing reduction process is carried out as presented. On the other hand, it is also possible to use a transformation that involves a rectangular transformation matrix. In this situation, the above procedure requires a congruence transformation rather than a similarity transformation. To convert the resulting eigenvalue problem to standard form requires the inversion of the matrix product $\mathbf{U}^T\mathbf{U}$. Unless this product results in a diagonal matrix, or otherwise has some special form, the best numerical approach makes use of singular value decomposition and the pseudoinverse. Discussions on this subject can be found in Strang [64] and Atkinson [65].

Appendix G

Calculation of Transition and Influence Matrices

Integrating matrices offer a convenient method for numerically calculating transition matrix solutions of two-point boundary problems. For structural solutions, the transition matrix can also be applied to the development of stiffness influence matrices. In formulating eigenvalue problems, the direct integrating matrix approach presented in Chapter 4 is to be preferred for its simplicity and numerical efficiency. Nevertheless, it is possible to use the transition matrix concept to advantage in certain types of numerical calculations. A detailed description of transition (also known as transfer or transmission) matrix methods in structural mechanics is presented by Pestel and Leckie [66]. A brief, but useful account of the method can also be found in Chapter 10 of McGuire and Gallagher [20]. In addition, the reader can refer to Chapter 7 of Boyce and DiPrima [67] for a general review of fundamental matrices and the role they play in the solution of linear differential equations. For useful applications and properties of transition matrices, one should consult Appendix A4 of Bryson and Ho [21] and Chapter 9 of Kailath [68].

The calculation of a transition matrix begins with the integrated version of the homogeneous state vector equations. These equations can be obtained from Eq. (4.3) by dropping the nonhomogeneous term $\tilde{\mathbf{L}}\tilde{\mathbf{a}}_r$, thus yielding

$$\tilde{\mathbf{y}} = \tilde{\mathbf{L}}\tilde{\mathbf{Z}}\tilde{\mathbf{y}} - \lambda\tilde{\mathbf{L}}\tilde{\mathbf{A}}\tilde{\mathbf{y}} + \tilde{\mathbf{k}}. \qquad (G.1)$$

It will be assumed that the ordering of the components of the global state vector is

the same as that used in the derivations presented in Section 4.1. As will be recalled, the global state vector is arranged such that it can be partitioned into generalized force and generalized displacement subsets, and the discrete set of values for a particular variable are grouped together. (An alternate ordering scheme that can be used for transition matrix derivation involves consecutively placing each local state vector into the global state vector. This ordering scheme, however, requires one to use a modified definition of the global integrating matrix. The modified integrating matrix is obtained by expanding each element of $\mathbf{L}$ into a diagonal submatrix, with the element value repeated in each of the diagonal terms of the submatrix.)

As the next step in calculating the transition matrix, choose the constant of integration to be equal to the local state vector at the end point $x = 0$. This means that the global constant vector of integration can be written as

$$\tilde{\mathbf{k}} = \mathbf{B}\mathbf{y}_0 = \begin{bmatrix} \mathbf{B}_{FF} & \mathbf{B}_{FD} \\ \mathbf{B}_{DF} & \mathbf{B}_{DD} \end{bmatrix} \begin{Bmatrix} \mathbf{y}_{F_0} \\ \mathbf{y}_{D_0} \end{Bmatrix} \tag{G.2}$$

where $\mathbf{B}$ will be termed a selection matrix since it selects the component of the local state vector to be placed in each component of $\tilde{\mathbf{k}}$. $\mathbf{B}$ consists primarily of zeroes, but has appropriately placed unit terms. For clarity, it is worth noting that if NS is the number of state variables and $(N+1)$ is the number of grid points, then the dimension of $\mathbf{y}_0$ will be NS and the dimensions of $\mathbf{B}$ will be NS$(N+1)\times$NS.

If one now combines Eq. (G.1) with Eq. (G.2) the result is

$$\mathbf{H}\tilde{\mathbf{y}} = \mathbf{B}\mathbf{y}_0 = \tilde{\mathbf{k}} \tag{G.3}$$

where

$$\mathbf{H} = \mathbf{I} - \tilde{\mathbf{L}}\tilde{\mathbf{Z}} + \lambda\tilde{\mathbf{L}}\tilde{\mathbf{A}}. \tag{G.4}$$

The corresponding partitioned form of Eq. (G.3) appears as

$$\begin{bmatrix} \mathbf{H}_{FF} & \mathbf{H}_{FD} \\ \mathbf{H}_{DF} & \mathbf{H}_{DD} \end{bmatrix} \begin{Bmatrix} \tilde{\mathbf{y}}_F \\ \tilde{\mathbf{y}}_D \end{Bmatrix} = \begin{bmatrix} \mathbf{B}_{FF} & \mathbf{B}_{FD} \\ \mathbf{B}_{DF} & \mathbf{B}_{DD} \end{bmatrix} \begin{Bmatrix} \mathbf{y}_{F_0} \\ \mathbf{y}_{D_0} \end{Bmatrix}. \tag{G.5}$$

In a straight forward manner, Eq. (G.5) can be solved by partitions, which yields

$$\begin{Bmatrix} \tilde{\mathbf{y}}_F \\ \tilde{\mathbf{y}}_D \end{Bmatrix} = \begin{bmatrix} \boldsymbol{\Upsilon}_{FF} & \boldsymbol{\Upsilon}_{FD} \\ \boldsymbol{\Upsilon}_{DF} & \boldsymbol{\Upsilon}_{DD} \end{bmatrix} \begin{Bmatrix} \mathbf{y}_{F_0} \\ \mathbf{y}_{D_0} \end{Bmatrix} \tag{G.6}$$

where

$$\begin{aligned} \boldsymbol{\Upsilon}_{FF} &= \mathbf{H}_{FF}^{-1}[\boldsymbol{\Xi}_{FF} - \mathbf{H}_{FD}\boldsymbol{\Upsilon}_{DF}] \\ \boldsymbol{\Upsilon}_{FD} &= \mathbf{H}_{FF}^{-1}[\boldsymbol{\Xi}_{FD} - \mathbf{H}_{FD}\boldsymbol{\Upsilon}_{DD}] \\ \boldsymbol{\Upsilon}_{DF} &= [\mathbf{H}_{DD} - \mathbf{H}_{DF}\mathbf{H}_{FF}^{-1}\mathbf{H}_{FD}]^{-1}[\boldsymbol{\Xi}_{DF} - \mathbf{H}_{DF}\mathbf{H}_{FF}^{-1}\boldsymbol{\Xi}_{FF}] \\ \boldsymbol{\Upsilon}_{DD} &= [\mathbf{H}_{DD} - \mathbf{H}_{DF}\mathbf{H}_{FF}^{-1}\mathbf{H}_{FD}]^{-1}[\boldsymbol{\Xi}_{DD} - \mathbf{H}_{DF}\mathbf{H}_{FF}^{-1}\boldsymbol{\Xi}_{FD}]. \end{aligned} \tag{G.7}$$

By definition, the transition (transfer) matrix transforms the state vector at one point into the state vector at another point. Considering the transition matrix between the state vector at $x = 0$ and the state vector at the ith grid point, one can write the general transition matrix relationship as

$$\begin{Bmatrix} \mathbf{y}_{F_i} \\ \mathbf{y}_{D_i} \end{Bmatrix} = \begin{bmatrix} \boldsymbol{\Phi}_{FF_i} & \boldsymbol{\Phi}_{FD_i} \\ \boldsymbol{\Phi}_{DF_i} & \boldsymbol{\Phi}_{DD_i} \end{bmatrix} \begin{Bmatrix} \mathbf{y}_{F_0} \\ \mathbf{y}_{D_0} \end{Bmatrix}. \tag{G.8}$$

At the same time, it is possible to write another expression for the local state vector appearing on the left-hand side of Eq. (G.8). This expression, which makes use of another selection matrix, $\boldsymbol{\Gamma}_i$, transforms the global state vector into the local vector at the ith point. The expression is written as

$$\begin{Bmatrix} \mathbf{y}_{F_i} \\ \mathbf{y}_{D_i} \end{Bmatrix} = \begin{bmatrix} \boldsymbol{\Gamma}_i & \mathbf{0} \\ \mathbf{0} & \boldsymbol{\Gamma}_i \end{bmatrix} \begin{Bmatrix} \tilde{\mathbf{y}}_F \\ \tilde{\mathbf{y}}_D \end{Bmatrix}. \tag{G.9}$$

By substituting the result for the global state vector from Eq. (G.6) into Eq. (G.9), and then comparing with Eq. (G.8), one finds that the transition matrix for the ith grid point is given by

$$\boldsymbol{\Phi}_i = \begin{bmatrix} \boldsymbol{\Gamma}_i\boldsymbol{\Upsilon}_{FF} & \boldsymbol{\Gamma}_i\boldsymbol{\Upsilon}_{FD} \\ \boldsymbol{\Gamma}_i\boldsymbol{\Upsilon}_{DF} & \boldsymbol{\Gamma}_i\boldsymbol{\Upsilon}_{DD} \end{bmatrix}. \tag{G.10}$$

This equation, in conjunction with Eq. (G.7), provides a method for calculating the transition matrix.

The foregoing results for transition matrices can be applied in calculating a stiffness influence matrix. For the influence matrix calculation, the load terms multiplied by λ in Eq. (G.1) are set to zero; for certain problems this can mean that $\mathbf{H}_{FD}$ in Eqs. (G.5) and (G.7) will be zero. The strategy in developing a stiffness influence matrix from a transition matrix is to obtain a force-displacement relationship between degrees of freedom at each end of the normalized interval $[0,1]$. By definition, the matrix that relates the force degrees of freedom to the displacement degrees of freedom will be the influence matrix.

By making use of Eq. (G.8), and taking into account the properties of a normalized transition matrix, one can write the expression

$$\begin{Bmatrix} \mathbf{y}_D(0) \\ \mathbf{y}_D(1) \end{Bmatrix} = \begin{bmatrix} \boldsymbol{\Phi}_{DF}(0) & \boldsymbol{\Phi}_{DD}(0) \\ \boldsymbol{\Phi}_{DF}(1) & \boldsymbol{\Phi}_{DD}(1) \end{bmatrix} \begin{Bmatrix} \mathbf{y}_{F_0} \\ \mathbf{y}_{D_0} \end{Bmatrix} = \begin{bmatrix} \mathbf{0} & \mathbf{I} \\ \boldsymbol{\Phi}_{DF}(1) & \boldsymbol{\Phi}_{DD}(1) \end{bmatrix} \begin{Bmatrix} \mathbf{y}_{F_0} \\ \mathbf{y}_{D_0} \end{Bmatrix}. \qquad (G.11)$$

Solving for the constant vector on the far right-hand side of Eq. (G.11) gives

$$\begin{Bmatrix} \mathbf{y}_{F_0} \\ \mathbf{y}_{D_0} \end{Bmatrix} = \begin{bmatrix} -\boldsymbol{\Phi}_{DF}^{-1}(1)\boldsymbol{\Phi}_{DD}(1) & \boldsymbol{\Phi}_{DF}^{-1}(1) \\ \mathbf{I} & \mathbf{0} \end{bmatrix} \begin{Bmatrix} \mathbf{y}_D(0) \\ \mathbf{y}_D(1) \end{Bmatrix}. \qquad (G.12)$$

Similar to Eq. (G.11), an expression can be written for the forces at the endpoints. This expression appears as

$$\begin{Bmatrix} \mathbf{y}_F(0) \\ -\mathbf{y}_F(1) \end{Bmatrix} = \begin{bmatrix} \boldsymbol{\Phi}_{FF}(0) & \boldsymbol{\Phi}_{FD}(0) \\ -\boldsymbol{\Phi}_{FF}(1) & -\boldsymbol{\Phi}_{FD}(1) \end{bmatrix} \begin{Bmatrix} \mathbf{y}_{F_0} \\ \mathbf{y}_{D_0} \end{Bmatrix} = \begin{bmatrix} \mathbf{I} & \mathbf{0} \\ -\boldsymbol{\Phi}_{FF}(1) & -\boldsymbol{\Phi}_{FD}(1) \end{bmatrix} \begin{Bmatrix} \mathbf{y}_{F_0} \\ \mathbf{y}_{D_0} \end{Bmatrix}. \qquad (G.13)$$

Substituting the constant vector from Eq. (G.12) into Eq. (G.13) yields

$$\begin{Bmatrix} \mathbf{y}_F(0) \\ -\mathbf{y}_F(1) \end{Bmatrix} = \begin{bmatrix} \mathbf{K}'_{00} & \mathbf{K}'_{01} \\ \mathbf{K}'_{10} & \mathbf{K}'_{11} \end{bmatrix} \begin{Bmatrix} \mathbf{y}_D(0) \\ \mathbf{y}_D(1) \end{Bmatrix} \qquad (G.14)$$

where the stiffness influence matrix $\mathbf{K}'$ is given by

$$\mathbf{K}' = \begin{bmatrix} -\boldsymbol{\Phi}_{DF}^{-1}(1)\boldsymbol{\Phi}_{DD}(1) & \boldsymbol{\Phi}_{DF}^{-1}(1) \\ \boldsymbol{\Phi}_{FF}(1)\boldsymbol{\Phi}_{DF}^{-1}(1)\boldsymbol{\Phi}_{DD}(1) - \boldsymbol{\Phi}_{FD}(1) & -\boldsymbol{\Phi}_{FF}(1)\boldsymbol{\Phi}_{DF}^{-1}(1) \end{bmatrix}. \qquad (G.15)$$

Provided that certain conditions are met by the transition matrix, it can be shown that $\mathbf{K}'$ is a symmetric matrix. To demonstrate this fact requires knowledge of the transition matrix for the adjoint system of homogeneous differential equations, where the adjoint equations are obtained by substituting $-\mathbf{Z}^T$ for $\mathbf{Z}$ in Eq. (G.1). The transition matrices of the original and adjoint systems share the identity

$$\boldsymbol{\Phi}_A^T \boldsymbol{\Phi} = \mathbf{I}. \qquad (G.16)$$

where $\boldsymbol{\Phi}_A$ is the transition matrix for the adjoint system. Normally, one would obtain $\boldsymbol{\Phi}_A$ by solving the adjoint differential equations, but for symplectic systems (see Section 2.1) the adjoint transition matrix can be obtained directly from the original transition matrix through the relationship

$$\boldsymbol{\Phi}_A^T = \boldsymbol{\Phi}^{-1} = \mathbf{J}^T \boldsymbol{\Phi}^T \mathbf{J} \qquad (G.17)$$

where $\mathbf{J}$ is as defined in Chapter 2 (see Bryson and Ho [21], p.157). With the aid of this relationship, it can be shown that if the numerically calculated transition matrices satisfy Eq. (G.16), then $\mathbf{K}' - \mathbf{K}'^T = 0$, which shows that $\mathbf{K}'$ is symmetric. It should be noted, however, that sample numerical calculations seem to indicate that the discretization level determines how accurately the numerically calculated transition matrices match the identity in Eq. (G.16). The satisfaction of Eq. (G.16) possibly might serve as an indicator of sufficient discretization, but at the present time this has not been verified and thus remains an object for further study.

A final item to be noted about transition matrix solutions is that calculations for nonhomogeneous linear problems can be simplified considerably if they are symplectic. That is, by making use of integrating matrices and by applying the relationship in Eq. (G.17), one finds that the usual variation of parameters solution for the state vector equations can be written in a conveniently calculable form.

References

[1] Gimmestad, D., "An Aeroelastic Optimization Procedure for Composite High Aspect Ratio Wings," AIAA/ASME/ASCE/AHS 20th Structures, Structural Dynamics, and Materials Conf., Vol. I, St. Louis, Mo., April 1979, pp. 79–86.

[2] Diederich, F.W., and Budiansky, B., "Divergence of Swept Wings," NACA TN 1680, August 1948.

[3] Diederich, F.W., and Foss, K.A., "Charts and Approximate Formulas for the Estimation of Aeroelastic Effects on the Loading of Swept and Unswept Wings," NACA Report 1140, 1953. (Supercedes NACA TN 2608.)

[4] Weisshaar, T.A., "Aeroelastic Stability and Performance Characteristics of Aircraft with Advanced Composite Sweptforward Wing Structures," AFFDL-TR-78-116, September 1978.

[5] Weisshaar, T.A., "Forward Swept Wing Static Aeroelasticity," AFFDL-TR-79-3087, June 1979.

[6] Lehman, L.L., "A Hybrid State Vector Approach to Aeroelastic Analysis with Application to Composite Lifting Surfaces," AIAA/ASME/ASCE/AHS 22nd Structures, Structural Dynamics and Materials Conference, Vol. II, Atlanta, Ga., April 1981, pp. 821–831.

[7] Noor, A.K., Stephens, W.B., and Fulton, R.E., "An Improved Numerical Process for Solution of Solid Mechanics Problems," *Computers and Structures,* Vol. 3, 1973, pp. 1397–1437.

[8] Noor, A.K., and Stephens, W.B., "Mixed Finite-Difference Scheme for Free-Vibration Analysis of Noncircular Cylinders," NASA TN D-7107, February 1973.

[9] Noor, A.K., and Stephens, W.B., "Comparison of Finite-Difference Schemes for Analysis of Shells of Revolution," NASA TN D-7337, December 1973.

[10] Stroud, R.C, and Mayers, J., "Dynamic Response of Rapidly Heated Plate Elements," *AIAA Journal,* Vol. 9, No. 1, January 1971, pp. 76–83.

[11] Steele, C.R., "Asymptotic Solutions Without Special Functions for Steep and Shallow Shells," *Mechanics Today,* Vol. 5, 1980, pp. 483–494.

[12] Steele, C.R., Ranjan, G.V., and Pulliam, T.H., "Computer Analysis of Shells of Revolution Using Asymptotic Results," AIAA/ASME/ASCE/AHS 20th Structures, Structural Dynamics and Materials Conf., Vol. I, St. Louis, Mo., April 1979, pp. 162–170.

[13] Steele, C.R. and Barry, K.E., "Asymptotic Integration Methods Applied to Rotating Beams," *Journal of Applied Mechanics,* Vol. 47, No. 4, December 1980, pp. 884–890.

[14] Nemat-Nasser, S., "General Variational Methods for Waves in Elastic Composites," *Journal of Elasticity,* Vol. 2, No. 2, June 1972, pp. 73–90.

[15] Nemat-Nasser, S., "On Variational Methods in Finite and Incremental Elastic Deformation Problems With Discontinuous Fields," *Quarterly of Applied Mathematics,* July 1972, pp. 143–156.

[16] Reissner, E., "Variational Methods and Boundary Conditions in Shell Theory," *Studies in Optimization, Proceedings of the Symposium on Optimization,* Vol. 1, Society for Industrial and Applied Mathematics, Philadelphia, Pa., 1970, pp. 78–94.

[17] Reissner, E., "On a Variational Theorem in Elasticity," *Journal of Mathematics and Physics,* Vol. 29, 1950, pp. 27–52.

[18] Nimmer, R.P., and Mayers, J., "Limit Point Buckling Loads of Axially Compressed, Circular Cylindrical Shells—The Effect of Nonlinear Material Behavior," *Journal of Applied Mechanics,* Vol. 46, No. 2, June 1979, pp. 386–392.

[19] Anderson, R.E., and Mayers, J., "Effects of Nonlinear Material Behavior on Postbuckling Stiffness of Laminated Composite Plates," AIAA Paper No. 79-1806, August 1979.

[20] McGuire, W., and Gallagher, R.H., *Matrix Structural Analysis,* Wiley, New York, 1979, pp. 362–369.

[21] Bryson, A.E., and Ho, Y.-C., *Applied Optimal Control,* Hemisphere Publishing Corp., Washington, D.C., 1975.

[22] Love, A.E.H., *A Treatise on the Mathematical Theory of Elasticity,* 4th. ed., Dover, New York, 1944, pp. 381–398.

[23] Ojalvo, I.U., and Newman, M., "Buckling of Naturally Curved and Twisted Beams," *ASCE Journal of the Engineering Mechanics Division,* Vol. 94, No. EM5, October 1968, pp. 1067–1087.

[24] Nitzsche, F., "Aeroelastic Analysis of a Troposkien-Type Wind Turbine Blade," *Proceedings of the International Colloquium on Wind Energy,* Brighton U.K., August 1981, pp. 255–260.

[25] Jones, R.M., *Mechanics of Composite Materials,* McGraw-Hill, New York, 1975.

[26] Vakhitov, M.B., "Integrating Matrices as a Means of Numerical Solution of Differential Equations in Structural Mechanics," *Izvestiya VUZ. Aviatsionnaya Tekhnika,* Vol. 9, No. 3, 1966, pp. 50–61 (English: *Soviet Aeronautics,* Vol. 9, No. 3, 1966, pp. 27–33).

[27] Hunter, W.F., "Integrating-Matrix Method for Determining the Natural Vibration Characteristics of Propeller Blades," NASA TN D-6064, December 1970.

[28] Spector, J., "Integral Series Solution for Uncoupled Vibrations of Nonuniform Bars," Master of Applied Mechanics Thesis, University of Virginia, May 1952, pp. 77–80.

[29] White, W.F.,Jr., and Malatino, R.E., "A Numerical Method for Determining the Natural Vibration Characteristics of Rotating Nonuniform Cantilever Blades," NASA TM X-72751, October 1975.

[30] Kvaternik, R.G., White, W.F.,Jr., and Kaza, K.R.V., "Nonlinear Flap-Lag-Axial Equations of a Rotating Beam with Arbitrary Precone Angle," AIAA Paper No. 78-491, AIAA/ASME 19th Structures, Structural Dynamics and Materials Conf., Bethesda, Md., April 1978, pp. 214–227.

[31] White, W.F.,Jr., Kvaternik, R.G., and Kaza, K.R.V., "Buckling of Rotating Beams," *International Journal of Mechanical Sciences,* Vol. 21, 1979, pp. 739–745.

[32] Vakhitov, M.B., and Grankin, Y.G., "Bending Calculation of Axisymmetric Circular Plates of Variable Stiffness," *Izvestiya VUZ. Aviatsionnaya Tekhnika,* Vol. 16, No. 4, 1973, pp. 35–41 (English: *Soviet Aeronautics,* Vol. 16, No. 4, 1973, pp. 26–30).

[33] Levashov, P.D., "Determination of the Deflections and Stresses in a Low-Aspect-Ratio Wing by the Displacement Method," *Izvestiya VUZ. Aviatsionnaya Tekhnika,* Vol. 16, No. 2, 1973, pp. 34–39 (English: *Soviet Aeronautics,* Vol. 16, No. 2, 1973, pp. 27–31).

[34] Levashov, P.D., "Numerical Solution for Determining Deflections and Stresses in a Monolithic Wing by the Generalized Ritz Method," *Izvestiya VUZ. Aviatsionnaya Tekhnika,* Vol. 16, No. 4, 1973, pp. 42–48 (English: *Soviet Aeronautics,* Vol. 16, No. 3, 1973, pp. 31–35).

[35] Levashov, P.D., "Influence of Differentiation and Integration Matrix Structure on Stiffness Matrix Accuracy," *Izvestiya VUZ. Aviatsionnaya Tekhnika,* Vol. 20, No. 4, 1977, pp. 126–128 (English: *Soviet Aeronautics,* Vol. 20, No. 4, 1977, pp. 101–103).

[36] Lakin, W.D., "Integrating Matrices for Arbitrarily Spaced Grid Points," NASA CR-159172, November 1979.

[37] Schneider, H., and Reddy, P.B., "Spline Method for Nonlinear Optimal Thrust Vector Controls for Atmospheric Interceptor Guidance," *AIAA Journal,* Vol. 15, No. 4, April 1977, pp. 449–450.

[38] Conte, S.D., and de Boor, C., *Elementary Numerical Analysis, An Algorithmic Approach,* 2nd ed., McGraw-Hill, New York, 1972.

[39] Krylov, V.I., *Approximate Calculation of Integrals,* (translated by A.H. Stroud), MacMillan, New York, 1962.

[40] Abramowitz, M., and Stegun, I.A. (ed.), *Handbook of Mathematical Functions,* Dover, New York, 1965.

[41] Collatz, L., *The Numerical Treatment of Differential Equations,* Springer-Verlag, Berlin, 1960.

[42] Meirovitch, L., *Analytical Methods in Vibrations,* MacMillan, New York, 1967, pp. 156–160.

[43] Przemieniecki, J.S., *Theory of Matrix Structural Analysis,* McGraw-Hill, New York, 1968.

[44] Smith, B.T., *et al., Matrix Eigensystem Routines: EISPACK Guide,* Springer-Verlag, New York, 1974.

[45] Bisplinghoff, R. L., Ashley, H., and Halfman, R. L., *Aeroelasticity,* Addison-Wesley, Reading, Mass., 1955.

[46] Hildebrand, F.B., and Reissner, E., "The Influence of the Aerodynamic Span Effect on the Magnitude of the Torsional Divergence Velocity and on the Shape of the Corresponding Deflection Mode," N.A.C.A. T.N. 926, February, 1944.

[47] Hodges, D.H., "Direct Solutions for Sturm-Liouville Systems with Discontinuous Coefficients," *AIAA Journal,* Vol. 17, No. 8, August 1979, pp. 924–926..

[48] Hodges, D.H., and Rutkowski, M.J., "Free-Vibration Analysis of Rotating Beams by a Variable-Order Finite-Element Method," AIAA/ASME/ASCE/AHS 22nd Structures, Structural Dynamics and Materials Conference, Vol. 2, Atlanta, Ga., April 1981, pp. 444–453.

[49] Peters, D.A., and Hodges, D.H., "In-Plane Vibration and Buckling of a Rotating Beam Clamped Off the Axis of Rotation," *Journal of Applied Mechanics,* Vol. 102, No. 2, June 1980, pp. 398–402.

[50] Weisshaar, T.A., "The Influence of Aeroelasticity on Swept Composite Wings," AFWAL-TR-80-3137, Vol. 1, November 1980.

[51] Housner, J.M., and Stein, M. "Flutter Analysis of Swept-wing Subsonic Aircraft with Parameter Studies of Composite Wings," NASA TN D-7539, September 1974.

[52] Goland, M., "The Flutter of a Uniform Cantilever Wing," *Journal of Applied Mechanics,* Vol. 12, No. 4, December 1945, pp. A-197–A-208.

[53] Goland, M., and Luke, Y.L., "The Flutter of a Uniform Wing with Tip Weights," *Journal of Applied Mechanics,* Vol. 15, No. 1, March 1948, pp. 13–20.

[54] Zienkiewicz, O.C., *The Finite Element Method,* 3rd. ed., McGraw-Hill, London, 1977.

[55] Gallagher, R. H., *Finite Element Analysis Fundamentals,* Prentice-Hall, Englewood Cliffs, New Jersey, 1975.

[56] Ashton, J.E., Halpin, J.C., and Petit, P.H., *Primer on Composite Materials: Analysis,* Technomic, Stamford, Conn., 1969.

[57] Tsai, S.W., Halpin, J.C., and Pagano, N.J., *Composite Materials Workshop,* Technomic, Stamford, Conn., 1968, pp. 233–253.

[58] Yates, E.C.,Jr., "Calculation of Flutter Characteristics for Finite-Span Swept or Unswept Wings at Subsonic or Supersonic Speeds by a Modified Strip Analysis," NACA RM L57L10, 1958.

[59] Yates, E.C.,Jr., "Flutter and Unsteady Lift Theory. Performance and Dynamics of Aerospace Vehicles," NASA SP-258, 1971, pp. 289–374.

[60] Edwards, J.W., "Unsteady Aerodynamic Modeling and Active Aeroelastic Control," SUDAAR 504, Stanford University, February 1977. (Available as NASA CR-148019.)

[61] Edwards, J.W., Ashley, H., and Breakwell, J.V., "Unsteady Aerodynamic Modeling for Arbitrary Motions," AIAA Paper No. 77-451, March 1977.

[62] Edwards, J.W., "Applications of Laplace Transform Methods to Airfoil Motion and Stability Calculations," AIAA/ASME/ASCE/AHS 20th Structures, Structural Dynamics and Materials Conf., Vol. II, St. Louis, Mo., April 1979, pp. 465–481.

[63] Barmby, J.G., Cunningham, H.J., and Garrick, I.E., "Study of Effects of Sweep on the Flutter of Cantilever Wings," NACA Report 1014, 1951. (Supercedes NACA TN 2121.)

[64] Strang, G., *Linear Algebra and its Applications,* Academic Press, New York, 1976, pp. 130–137.

[65] Atkinson, K.E., *An Introduction to Numerical Analysis,* Wiley, New York, 1978, pp. 408–410.

[66] Pestel, E.C., and Leckie, F.A., *Matrix Methods in Elastomechanics,* McGraw-Hill, New York, 1963.

[67] Boyce, W.E., and DiPrima, R.C., *Elementary Differential Equations and Boundary Value Problems,* 2nd. ed., Wiley, New York, 1969.

[68] Kailath, T., *Linear Systems,* Prentice-Hall, Englewood Cliffs, New Jersey, 1980.

1. Report No.	2. Government Accession No.	3. Recipient's Catalog No.
NASA CR-3591		

4. Title and Subtitle	5. Report Date
HYBRID STATE VECTOR METHODS FOR STRUCTURAL DYNAMIC AND AEROELASTIC BOUNDARY VALUE PROBLEMS	August 1982
	6. Performing Organization Code

7. Author(s)	8. Performing Organization Report No.
Larry Lee Lehman	
	10. Work Unit No.

9. Performing Organization Name and Address	11. Contract or Grant No.
Stanford University Dept. of Aeronautics and Astronautics Stanford, CA 94305	NGL-05-020-243
	13. Type of Report and Period Covered
12. Sponsoring Agency Name and Address	Contractor Report
National Aeronautics and Space Adminstration Washington, D.C. 20546	14. Sponsoring Agency Code 505-33-53-01

15. Supplementary Notes
Adapted from Ph.D. Dissertation, February 1982
Langley Technical Monitor: Robert V. Doggett, Jr.
Topical Report

16. Abstract

A computational technique is developed that is suitable for performing preliminary design aeroelastic and structural dynamic analyses of large aspect ratio lifting surfaces. The method proves to be quite general and can be adapted to solving various two-point boundary value problems.

The solution method, which is applicable to both fixed and rotating wing configurations, is based upon a formulation of the structural equilibrium equations in terms of a hybrid state vector containing generalized force and displacement variables. A mixed variational formulation is presented that conveniently yields a useful form for these state vector differential equations. Solutions to these equations are obtained by employing an integrating matrix method. The application of an integrating matrix provides a discretization of the differential equations that only requires solutions of standard linear matrix systems. It is demonstrated that matrix partitioning can be used to reduce the order of the required solutions. Results are presented for several example problems in structural dynamics and aeroelasticity to verify the technique and to demonstrate its use. These problems examine various types of loading and boundary conditions and include aeroelastic analyses of lifting surfaces constructed from anisotropic composite materials.

Integrating matrices, which provide a powerful tool for solving differential equations, are discussed in detail, and methods are given for their calculation. A derivation and calculation procedure is presented for a new type of maximum accuracy integrating matrix based upon orthogonal polynomials.

17. Key Words (Suggested by Author(s))	18. Distribution Statement
Aeroelasticity Structural Dynamics State Vector Boundary Value Integrating Matrices	Unclassified-Unlimited Subject Category 02

19. Security Classif. (of this report)	20. Security Classif. (of this page)	21. No. of Pages	22. Price
Unclassified	Unclassified	198	A09

For sale by the National Technical Information Service, Springfield, Virginia 22161

NASA-Langley, 1982